KINETICS AND MECHANISMS OF THE PRECIPITATION OF LAYERED FE(II)-HYDROXIDES DURING FE(II) SORPTION ONTO COMMON SOIL MINERALS

by

YING ZHU

A Dissertation submitted to the

Graduate School – Newark

Rutgers, The State University of New Jersey

in partial fulfillment of the requirements

for the degree of

Doctor of Philosophy

Graduate Program in

Environmental Science

written under the direction of

Professor Evert Elzinga

and approved by

_____

_____

_____

_____

Newark, New Jersey

May, 2017

ABSTRACT OF THE DISSERTATION

KINETICS AND MECHANISMS OF THE PRECIPITATION OF LAYERED FE(II)-HYDROXIDES DURING FE(II) SORPTION ONTO COMMON SOIL MINERALS

By Ying Zhu

Dissertation Director:

Evert Elzinga

This dissertation studies the formation kinetics and thermodynamics of secondary Fe(II) precipitates during aqueous Fe(II) sorption onto Al and/or Si containing minerals under various lab-based anoxic model systems. In Chapter 2, sorption of Fe(II) in anoxic aqueous suspensions of γ-Al_2O_3, smectitic clay and amorphous silica was studied under various pH values. In Chapter 3 and 4, the impacts of As and organic compounds on Fe(II) sorption kinetics and mechanisms onto γ-Al_2O_3 and/or clay were investigated at pH 7.5. Uv-Vis spectroscopy and ICP-OES were employed to determine the aqueous concentrations of Fe, As and Si in the supernatants sampled during the macroscopic batch experiments, while the XAS was applied to characterize the solid-phase Fe and As sorption products.

The Fe(II)-Al(III)-LDH formed at pH $\geq$ 7.0 during Fe(II) sorption onto γ-Al_2O_3, and at pH 7.0 and 7.5 during Fe(II) sorption onto clay. The poorly crystalline trioctahedral Fe(II)-phyllosilicates formed at pH $\geq$ 7.5 during Fe(II) sorption onto

amorphous silica, and at pH 8.0 during Fe(II) sorption onto clay. Greater sorption rate and extent were observed with increasing pH. Significantly slower Fe(II) sorption kinetics in clay systems compared to γ-Al_2O_3 and SiO_2 is due to the relatively low dissolution of substrate-derived Al and Si.

While As(III) did not interfere with the Fe(II)-Al(III)-LDH formation and Fe(II) sorption kinetics onto γ-Al_2O_3 at pH 7.5, the presence of As(V) slowed down the Fe(II)-Al(III)-LDH formation at low As(V) concentrations, and fully shut it down at high As(V) concentrations, leading to the formation of Fe(II) surface complexes instead. The inhibitive effects of As(V) is attributed to the interference of adsorbed As(V) with the Al needed for Fe(II)-Al(III)-LDH formation. On the other hand, the presence of Fe(II) did not affect the sorption kinetics and mechanisms of As(III) onto γ-Al_2O_3, however enhanced As(V) sorption rate and extent and did not change the As(V) adsorption mode onto γ-Al_2O_3.

The presence of humic substances (HS) generally hindered the formation of Fe(II)-Al(III)-LDH during Fe(II) sorption onto γ-Al_2O_3 and clay substrates at pH 7.5. In Fe(II) reacted γ-Al_2O_3 systems, HS slowed down the formation kinetics of Fe(II)-Al(III)-LDH precipitate. Larger inhibitive impacts of HS were observed when it cosorbed with Fe(II) onto γ-Al_2O_3 than when it pre-coated onto γ-Al_2O_3 before Fe(II) sorption. In Fe(II) reacted clay systems, humic acid (HA) coating on clay primarily altered the main Fe(II) sorption product from Fe(II)-Al(III)-LDH into poorly crystalline Fe(II)-phyllosilicate. The effects of HS on Fe(II) sorption onto mineral sorbents were associated with Al dissolution capability from mineral substrates, HS formation of organo-Al complexes and

HS masking on mineral surfaces limiting the Al and/or Si needed to form secondary Fe(II) precipitates.

The results from this work suggest substantial complexity in the composition and structure of Fe(II) sorption products, and the occurrence of which may represent significant pathways for Fe(II) sequestration under reducing geochemical environments. This work develops our understanding of the fate and transport of Fe(II) under anoxic and suboxic environments such as natural riparian soils and sediments.

ACKNOWLEDGEMENTS

Along my Ph.D. journey, I have been supported, encouraged and helped by many people. I would like to thank them all for their generosity and contribution to the development and completion of this dissertation work.

Primarily, I would like to express my heartful gratitude to my advisor Prof. Evert Elzinga, for his tremendous academic support throughout my Ph.D. study. He guided me through every step of my research in the field of geochemistry. He is such a patient, humble and knowledgeable scholar, who has inspired me in many ways. I also would like to thank my committee members: Professors Lisa Axe, Nathan Yee, Ashaki Rouff and Kristina Keating for their valuable time, suggestions and comments.

I would like to sincerely thank all the faculty, staff and students in the Department of Earth and Environmental Sciences at Rutgers University – Newark. I am honored to be an integral member of this friendly and productive department. Special thanks to Dr. Alexander Gates for admitting me into the program and offering the teaching assistantship, Ms. Liz Morrin, Professors Adam Kustka, Yuan Gao, Lee Slater and Dimitris Ntarlagiannis for providing me with advices and supporting my research in various ways. Many thanks go to my fellow graduate students Joshua Lefkowitz, Lu Wang, Chi Zhang, Jianqiong Zhan and Guojie Xu for being my friends and supporters.

Lastly, I am deeply grateful to my parents for their endless love and constant support. They have always cared about me and trusted every decision I have made. And most importantly, I want to mention Zhongjie Yu, my loving and supportive husband, my

best friend, who has accompanied me through this journey. I am thankful to have a family and share the great and the difficult moments of life with him.

Chapter 2:

This work was supported by National Science Foundation grant EAR-1226581. We thank Matt Siebecker (U. of Delaware) for help with the WT analyses, the beamline scientists at X11A (NSLS) and 12-BMB (APS) for assistance with data collection, and three anonymous reviewers for helpful comments.

Chapter 3:

This work was supported by National Science Foundation grant EAR-1226581. We thank the beamline scientists at 12-BMB (APS) and X11A (NSLS) for assistance with data collection, and Daniel Giammar and three anonymous reviewers for helpful review comments.

TABLE OF CONTENTS

LIST OF TABLES

LIST OF FIGURES

Chapter 1: Introduction

1.1 Background and Overview

1.1.1 Occurrence of ferrous iron in suboxic and anoxic geochemical environments

Iron (Fe) is the fourth most abundant element in the Earth's crust and an essential nutrient for plants and microorganisms.[1] The biogeochemical cycle of iron is closely correlated with the cycling of carbon, nitrogen, phosphorus and sulfur, and affects the fate of trace elements in aqueous geochemical environments.[2] Ferrous iron refers to the divalent iron (Fe(II)) species, which is the reduced form of iron, and exists to a significant extent as aqueous dissolved species in the natural environment.[2,3] In suboxic and anoxic soils and sediments, such as wetlands and riparian zone, Fe(II) is released to solution at mM level by microbially mediated reduction of Fe(III)-bearing minerals and dissolved Fe(III)-organic complexes as alternative terminal electron acceptors.[4,5]

The geochemical fate of released Fe(II) is at least partially controlled by sorption reactions at mineral-water interface. Previous studies focus on the Fe(II) sorption processes onto various Fe(III) based minerals.[6–16] Interfacial Electron transfer between adsorbed Fe(II) and structural Fe(III) has been observed at iron oxide-water interfaces, resulting in modification of crystal morphology of Fe(III)-bearing minerals.[7,8,11–14] In addition, Fe(II) plays a catalytic role in ferrihydrite conversion into more stable Fe(II) oxides.[15,16] However, sorption mechanisms of aqueous Fe(II) onto mineral substrates without structural Fe are not well understood. A recent work demonstrated the formation of Fe(II)-Al(III) layered double hydroxides (LDHs) during mM level Fe(II) sorption onto Al-oxide at near neutral pH typical of anoxic soil conditions.[17]

1.1.2 Precipitates of Me(II) layered hydroxides as divalent ion sequestration pathway onto mineral substrates

The secondary precipitates of Me(II)-hydroxide, Me(II)-Al(III)-LDH and Me(II)-phyllosilicate formed during Me(II) sorption reactions onto mineral substrates. [17–31] Several studies have shown the formation of Me(II)-Al(III)-LDH during divalent Ni, Co, Zn and Fe sorption onto Al-oxides and Al-bearing phyllosilicates at near neutral pH values in lab-based model systems.[17–30] Additionally, the presence of Ni(II)-Al(III)-LDH and Zn(II)-Al(III)-LDH was also identified in contaminated whole soils.[26,32–37] The formed LDH phases consist of brucite($Mg(OH)_2$)-like octahedral mixed metal-hydroxide layers showing net positive charge due to the partial substitution of divalent metal ions by trivalent Al ions, which is balanced by interlayer anions (Figure 1.1).[38] Formation of LDH phases was observed within a reaction scale of minutes comparable to adsorption reactions, suggesting the formation of such phase is thermodynamically and kinetically favored under typical soil conditions.[17,21,32,39,40] In addition, the solubility of Me(II)-Al(III)-LDH precipitates is lower than that of pure Me(II)-hydroxides and surface metal complexes.[22,24,26,41]

The formation of Me(II)-phyllosilicates has been reported during Me(II) sorption onto amorphous silica (SiO_2) and quartz at near neutral to alkaline pH,[20,42,43] or as a result of aging effects of Me(II)-Al(III)-LDH upon Me(II) sorption onto clay substrates which involves the substitution of interlayer anions by polymerized Si tetrahedral.[19,26,40,44,45] Compared with Me(II)-Al(III)-LDH, the phyllosilicate phase is thermodynamically more stable.[26,45] Therefore, proper identification of the surface precipitate formation is of great

importance to understand the solubility, mobility and bioavailability of the divalent metal ions.

Several key factors were identified in previous studies to determine the form and kinetic of Me(II) sorption products on mineral substrates, such as the type of mineral sorbents, pH, the presence of organic compounds and foreign metal(loid). The type of mineral substrates controls the solubility and availability of Al and Si required for Me(II)-Al(III)-LDH and/or Me(II)-phyllosilicate formation,[19,21,28,32,39,40,44–46] and the abundance and reactivity of mineral surface sites that may compete with precipitation by forming mononuclear Me(II) adsorption complexes.[25,27,47] The formation of Me(II)-Al(III)-LDH phases is kinetically and thermodynamically favored with the presence of more soluble Al-containing minerals.[21,39,46] The dissolved Si may stabilize the LDH structure by substituting interlayer anions, leading to the formation of phyllosilicate phases.[19,42–45] In addition, the formation of Me(II) precipitates is promoted at higher pH.[25,28] Furthermore, the presence of organic compounds has been shown to slow down or inhibit the Me(II)-Al(III)-LDH formation during Me(II) sorption onto Al-bearing substrates at neutral to alkaline pH, [31,48–51] and the presence of foreign metal cations may incorporate into the octahedral layer of LDH and modify its stability and solubility.[34]

1.1.3 Secondary Fe(II) precipitate as main Fe(II) sorption mode

Elzinga 2012 reported the formation of Fe(II)-Al(III)-LDH phases during reaction of Fe(II) with aluminum oxide at pH 7.5 at initial Fe(II) concentration from 1 mM to 3 mM under anoxic conditions.[17] This finding implies that these phases may act as an important sink of Fe(II) under suboxic and anoxic geochemical environments, and potentially affect the fate of other chemical species. However, the formation kinetics, mechanisms and

thermodynamics of the Fe(II)-Al(III)-LDH phases and related secondary Fe(II) precipitate phases are not well understood. This work aims to study the key factors impacting Fe(II) layered hydroxides formation onto mineral substrates, and the interaction of other chemical elements with the Fe(II) sorptive reactions onto mineral sorbents.

1.2 Motivation and Hypotheses

The objective of this work is to improve our understanding of iron geochemistry under suboxic and anoxic environments, by investigating kinetics and mechanisms of aqueous Fe(II) sorption onto mineral sorbents under various reaction conditions. This work addresses the overall hypothesis that secondary Fe(II) precipitates such as Fe(II)-Al(III)-LDH are overlooked secondary minerals in anoxic geochemical systems, and affect the cycling of Fe as well as the geochemical fate of other elements in the heterogeneous soil environments. The specific research hypotheses are:

1. Secondary Fe(II) precipitates form extensively and rapidly during aqueous Fe(II) sorption onto clay and metal-oxide substrates under anoxic geochemical conditions. System pH, substrate type and reaction time control the type and stability of the formed precipitates.
2. Arsenic interacts with iron(II) during cosorption onto Al-oxide by mutually changing sorption kinetics and mechanisms. The effects of arsenic during the cosorptive reaction depend on As speciation and concentration.
3. The presence of humic substances limits the growth of Fe(II)-Al(III)-LDH under reaction conditions where the formation of such phase is originally favored. The

effects of humic substances vary by the type of mineral substrates, and composition, concentration and addition sequence of humic substances.

1.3 Organization of the Dissertation

In Chapter 2, the kinetics and formation of layered Fe(II) hydroxides upon aqueous Fe(II) sorption onto clay, Al-oxide and amorphous SiO_2 substrates under various pH were studied. In Chapter 3, the interaction of As(III)/As(V) with Fe(II) during cosorption onto Al-oxide at pH 7.5 was examined. In Chapter 4, the effects of humic substances on Fe(II) sorption kinetics and mechanisms onto Al-oxide and clay at pH 7.5 were investigated.

1.4 Acknowledgement of Previous Publications

(1) The contents of Chapter 2 were previously published in the article *Formation of layered Fe(II)-hydroxides during Fe(II) sorption onto clay and metal-oxide substrates*, in volume 48, issue 9 of Environmental Science and Technology (2014). This work can be cited as: Zhu, Y.; Elzinga, E. J. Formation of layered Fe(II)-hydroxides during Fe(II) sorption onto clay and metal-oxide substrates. *Environ. Sci. Technol.* **2014,** 48, 4937−4945. The contents were reformatted in this thesis to meet the doctoral dissertation style guide of Rutgers University.

(2) The contents of Chapter 3 were previously published in the article *Macroscopic and spectroscopic assessment of the cosorption of Fe(II) with As(III) and As(V) on Al-oxide*, in volume 49, issue 22 of Environmental Science and Technology (2015). This work can be cited as: Zhu, Y.; Elzinga, E. J. Macroscopic and spectroscopic assessment of the cosorption of Fe(II) with As(III) and As(V) on Al-oxide. *Environ. Sci. Technol.* **2015,** 49, 13369−13377. The contents were reformatted in this thesis to meet the doctoral dissertation style guide of Rutgers University.

1.5 Figures

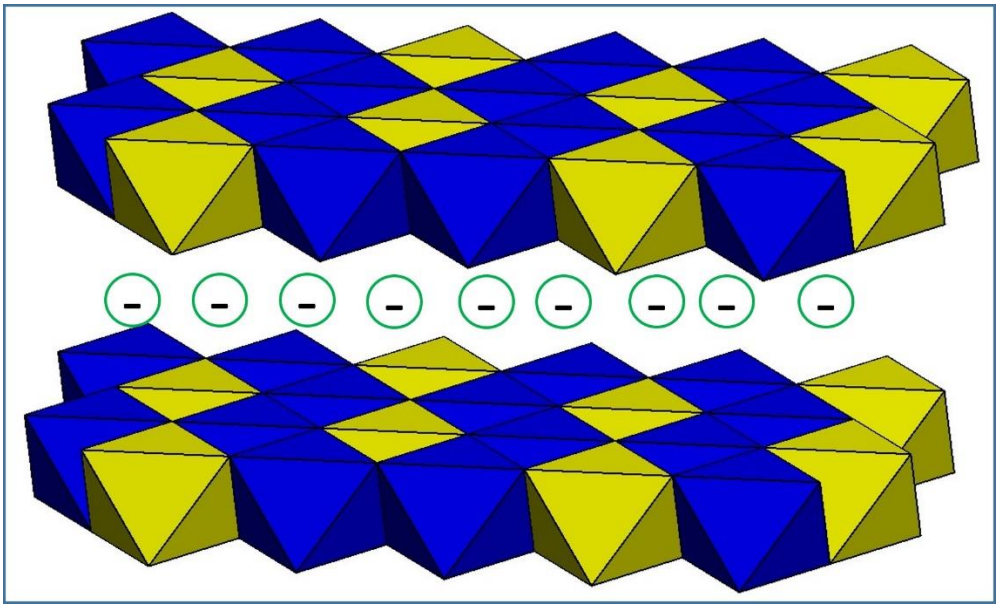

Figure 1.1. Mineralogical structure of Me(II)-Al(III)-LDH

Blue and yellow octahedra represent Me(II) and Al(III) cations in octahedral coordination, respectively. The green circles represent the anions intercalated in the interlayer to balance the net positive charge of the octahedral metal-hydroxide sheets.

Chapter 2: Formation of Layered Fe(II)-Hydroxides during Fe(II) Sorption onto Clay and Metal-Oxide Substrates

Abstract

Sorption of Fe(II) in anoxic aqueous suspensions of γ-Al_2O_3, smectitic clay and amorphous silica was studied as a function of pH (5.0-10.0) and reaction time (up to 110 days), using batch experiments complemented with synchrotron X-ray absorption spectroscopic analyses. Formation of secondary Fe(II) precipitates was observed at pH > 7 in all systems, with the rate of precipitation and the types of precipitates formed varying with pH and substrate type. Sorption of Fe(II) on γ-Al_2O_3 at pH ≥ 7.0 and onto clay at pH 7.0 and 7.5 led to formation of Fe(II)-Al(III) layered double hydroxides, whereas poorly crystalline tri-octahedral Fe(II)-phyllosilicates formed in the amorphous SiO_2 suspensions at pH > 7.5 and in the clay suspensions at pH 8.0. The rate and extent of Fe(II) sorption increased with pH, underscoring the importance of pH in regulating precipitate formation. Notably slower Fe(II) precipitation in the clay suspensions compared to γ-Al_2O_3 and SiO_2 is attributed to relatively low availability of substrate-derived Al and Si. Our findings demonstrate that sorbent type, pH and reaction time are important factors affecting precipitation of secondary Fe(II) minerals in anoxic environments, and suggest substantial complexity in the type and reactivity of Fe(II) sorption products that may form.

2.1 Introduction

Sorption reactions at mineral-water interfaces greatly impact metal speciation, mobility and bioavailability in aqueous geochemical systems such as soils and sediments, and have therefore attracted much attention in studies concerned with the environmental

behavior and fate of metal pollutants. Clay and metal-oxides are major sinks for metal sequestration able to sorb metals through various mechanisms including surface adsorption and precipitation reactions.[17–22,40,41,46,52–54] Metal precipitation is considered a particularly effective way of removing metal ions from solution as it is capable of sequestering substantial quantities of metals in relatively stable form.[18,19,21,22,40]

Recent studies have shown that Ni(II), Co(II), Zn(II) readily form secondary Me(II)-Al(III)-layered double hydroxide (LDH) precipitates during sorption with Al-oxides and Al-bearing phyllosilicates at near-neutral pH values.[18–30,40] These phases consist of metal cations arranged in tri-octahedral (brucite-type) metal-hydroxide sheets where partial substitution of Al(III) for Me(II) generates a net positive layer charge which is neutralized by interlayer anions.[38] Precipitation of such phases has been observed during sorption of Ni(II), Zn(II) and Co(II) on various clay mineral and metal oxide surfaces in laboratory model systems,[18–22,24,25,27–30,40] and recent research has identified Ni(II)-Al(III)-LDH and Zn(II)-Al(III)-LDH in field and laboratory contaminated whole soils,[26,32–37] suggesting an important role for these phases in regulating Zn and Ni solubility and mobility in contaminated soils.

Studies addressing the formation of Ni(II)-, Zn(II)-, and Co(II)-Al(III)-LDH phases during sorption onto Al-bearing mineral substrates have identified several key factors that determine the favorability and kinetics of precipitation and the composition of the resulting precipitate phases. The types of mineral sorbents present is of major importance, as these control the solubility and availability of Al required for Me(II)-Al(III)-LDH precipitation,[19,21,28,32,38–40,46] as well the availability and solubility of Si, which may stabilize the LDH structure by substituting for interlayer anions,[19,44,45] and the

abundance and reactivity of mineral surface sites that may compete with Me(II)-Al(III)-LDH precipitation by forming mononuclear Me(II) adsorption complexes.[25,27,47] Solution pH, a "master variable" in a broad array of geochemical processes,[2] plays a major role in controlling LDH precipitation as well, with formation of these phases promoted at higher pH values.[25,28] Additional factors that have been demonstrated to impact LDH precipitation during metal sorption are the presence of dissolved organics, which may interfere with LDH formation,[31,49] and the presence of foreign metal cations which may substitute in the octahedral sheets and modify LDH stability and solubility.[34]

The current study focuses on the precipitation of Fe(II)-LDH phases, for which there have been far fewer studies compared to Ni(II), Zn(II) and Co(II). We recently demonstrated formation of Fe(II)-Al(III)-LDH during Fe(II) sorption onto Al-oxide at pH 7.5 and mM level Fe(II) solution concentrations.[17] Here, we studied the effect of pH and reaction time on the formation of these Fe(II) minerals, and assessed precipitation of related Fe(II) phases during sorption of Fe(II) onto clay and amorphous silica sorbents. The results of this study provide insights as to the importance of layered Fe(II) hydroxide phases in controlling Fe(II) solubility and reactivity in anoxic geochemical aqueous environments.

2.2 Materials and Methods

2.2.1 Mineral sorbents

The sorbents used for this study were (i) γ-Al_2O_3 (Alfa Aesar, catalogue #39812); (ii) synthetic mica-montmorillonite, obtained as Syn-1 from the Clay Minerals Repository[55]; and (iii) amorphous silica (Alfa Aesar, catalogue # 42737). All three substrates had negligible structural Fe, allowing X-ray absorption spectroscopy (XAS) measurements of

sorbed Fe without interference. The γ-Al_2O_3 and amorphous SiO_2 sorbents were used with no further treatment, while the clay was fractionated by sedimentation to obtain the < 1 μm size fraction, which was saturated with Na^+, dialyzed to remove excess salts, and freeze dried. The N_2-BET surface areas were 124.6 m^2 g^{-1}, 70.5 m^2 g^{-1}, and 84.2 m^2 g^{-1} for the clay, γ-Al_2O_3, and SiO_2 sorbents, respectively.[56]

2.2.2 Batch experiments

All sorption experiments were conducted under strictly anoxic conditions using established protocols[17] described in Appendix 1. Two main types of batch experiments were conducted: pH edge experiments, where the main variable was pH, and kinetic studies, characterizing effects of reaction time. Anoxic sorbent suspensions of 5.0 g L^{-1} were prepared at pH 5-10, with pH stabilized using 50 mM MES (pKa=6.1), HEPES (pKa=7.5), EPPS (pKa=8.0) or CHES (pKa=9.5) buffer dissolved in the electrolyte. Ionic strength was set at 0.1 M with NaCl after accounting for the buffer speciation at the pH of interest and the addition of titrant NaOH. Following hydration (24 h), Fe(II) was introduced at an initial concentration of 2.7 mM through addition of acidified 1.0 M $FeCl_2$ stock. Blank samples were run as well and consisted of identical solutions as used for the sorption samples but without mineral sorbent added. Samples for the pH edge experiments were collected after 1 week of reaction, while for the kinetic studies samples were taken regularly over the course of a 3 month time period. For the clay and amorphous SiO_2 systems, control samples consisting of mineral suspensions with no Fe(II) added were run in parallel to the Fe(II)-spiked samples. Slight drifting of suspension pH (< 0.21 pH units) to lower values was observed in the pH 7.5 and 8.0 sorption experiments, which exhibited the most extensive Fe(II) sorption.

Sampling of the γ-Al_2O_3 and SiO_2 suspensions involved syringe filtration of 5.0 mL suspension aliquots through a 0.22 μm nitrocellulose membrane inside the glovebox. Filtrates were collected in a polyethylene tube containing a small aliquot of concentrated HCl. Clay suspensions could not be filtered, and were centrifuged instead. A 5.0 mL suspension aliquot was sealed in an airtight centrifuge tube inside the glovebox and then taken outside for centrifugation at 122,823 *g* for 6 minutes. The centrifuged suspension was transferred back inside the glovebox where the supernatant was filtered through a 0.22 μm nitrocellulose membrane. Supernatants were analyzed for dissolved Fe(II) using the ferrozine method,[57] and sorption was calculated as the difference between the initial and remaining Fe(II) solution concentrations. Supernatants from the clay and SiO_2 experiments were further analyzed for dissolved silica by ICP-OES.

2.2.3 XAS studies

XAS samples were prepared with the same methods described above for the isotherm and kinetic samples, following the protocols of Elzinga.[17] A total of 20 samples were analyzed, which differed in pH (6.5- 8.0), substrate type (γ-Al_2O_3, amorphous SiO_2, clay, or no sorbent), and sorption time (2 h - 15 mo), while ionic strength (0.1 M total Na), the pH buffer concentration (50 mM), initial [Fe(II)] (2.7 mM), and the suspension density (5.0 g L^{-1}) were equal for all samples. Details are described in Appendix 1.

Synchrotron Fe *K*-edge (7112 eV) XAS spectra were recorded on beamline X-11A of the National Synchrotron Light Source at Brookhaven National Laboratory, and beamline 12-BMB of the Advanced Photon Source at Argonne National Laboratory, using procedures described in Appendix 1. The following reference Fe compounds were analyzed as well: (1) goethite (α-$Fe^{III}OOH$); (2) hematite ($Fe^{III}_2O_3$); (3) magnetite

($Fe^{III}_2Fe^{II}O_4$); (4) Fe(II)-Fe(III)-hydroxychloride green rust; (5) nikischerite ($NaFe^{II}_6Al_3(SO_4)_2(OH)_{18}(H_2O)_{12}$); (6) white rust (β-$Fe(OH)_2$) and (7) aqueous Fe^{2+}. EXAFS data processing and fitting were performed with WINXAS3.1[58] in conjunction with Feff 7.0[59] and ARTEMIS[60]. Wavelet transform (WT) analyses were performed using the Igor Pro script developed by Funke et al.[61] Details on the reference compounds and EXAFS data analyses are provided in Appendix 1.

2.3 Results and Discussion

2.3.1 Macroscopic batch experiments

Figure 2.1 presents the pH edges of Fe(II) sorption in the γ-Al_2O_3, clay, and amorphous SiO_2 suspensions following 7 d of reaction, and compares these to the pH-dependent removal of aqueous Fe(II) in the blank samples, which contained no sorbent. Iron(II) sorption increases steeply at pH > 7 in the mineral suspensions, whereas in the control samples, removal of aqueous Fe(II) from solution occurs at pH > 8.2 but is negligible at lower pH values (Figure 2.1). The 1.0-1.5 pH unit shift to lower values observed for the pH edges of γ-Al_2O_3, clay and SiO_2 relative to the blank samples demonstrates the importance of the mineral sorbents in mediating Fe(II) removal from solution through sorption processes.

Figure 2.2 shows the kinetics of Fe(II) sorption in the γ-Al_2O_3, clay, and amorphous SiO_2 suspensions at pH 6.0-8.0 and reaction times up to 110 days. Sorption of Fe(II) in these systems increases with increasing pH consistent with the pH edge data of Figure 2.1. The kinetic sorption patterns vary distinctly with pH. At pH 6.0 and 6.5, the two lowest pH values studied here, Fe(II) sorption on all three sorbents reaches equilibrium relatively fast with no or minor further Fe(II) uptake occurring after the first

time point of sampling (≈1 h). At pH 7.5 and 8.0, the Fe(II) sorption kinetics are biphasic, with an initial step of rapid Fe(II) sorption during the first hours of reaction followed by a slower sorption stage continuing for days to weeks (Figure 2.2). At pH 7.0, the kinetic sorption trends differ for the three sorbents, with Fe(II) sorption in the γ-Al_2O_3 suspension continuing for 6-8 weeks, while Fe(II) sorption on amorphous silica reaches equilibrium within hours (Figure 2.2). For the clay, Fe(II) sorption appears to achieve equilibrium within just a few days at pH 7.0 (Figure 2.2b); however, spectroscopic analysis of long-term samples (presented below) indicate slow Fe(II) sorption continuing for months in the clay suspension at this pH. Of note is that all Fe(II)-γAl_2O_3 systems presented in Figure 2.2 reach apparent equilibrium within the 100 day experimental reaction time frame, with solution [Fe(II)] stabilizing after approximately 15, 30, and 55 days at pH 8.0, 7.5 and 7.0, respectively (Figure 2.2a). In contrast, Fe(II) sorption in the clay suspension is still ongoing after 72 days at both pH 7.5 and 8.0 (Figure 2.2b), while for amorphous SiO_2, Fe(II) sorption stabilizes after approximately 10 days at pH 8.0, and after approximately 80 days at pH 7.5 (Figure 2.2c). The equilibration times of Fe(II) sorption at neutral to alkaline pH are thus controlled both by sorbent type and solution pH, with sorption equilibrium attained faster at higher pH values, and faster on γ-Al_2O_3 and amorphous SiO_2 than on the clay substrate at equivalent pH.

The biphasic Fe(II) sorption kinetics observed at pH ≥ 7.0 (Figure 2.2) are quite common for metal sorption onto mineral phases,[6,22,23,30,39,41,62–64] and attributed to initial fast metal adsorption to readily accessible surface sites, followed by a slow reaction stage which may involve diffusion, coordination to sites of lower reactivity, and/or precipitation.[52] We have recently demonstrated precipitation of Fe(II)-Al(IIII)-layered

double hydroxides (LDHs) during Fe(II) sorption onto γ-Al_2O_3 at pH 7.5,[17] suggesting that formation of secondary Fe(II)-Al(III)-LDH or related phases may be involved in the slow continuous Fe(II) uptake observed at neutral and alkaline pH in the sorption systems characterized here. The influence of sorbent type, pH and reaction time on Fe(II) sorption products formed is assessed below based on results from Fe *K*-edge EXAFS spectroscopy.

2.3.2 XAS data

The EXAFS data of the sorption and reference samples are presented in Figure 2.3, with Figure 2.3a showing the raw and fitted k^3-weighted χ functions and Figure 2.3b the radial structure functions (RSFs) obtained from Fourier transformation of the raw χ data. The EXAFS data fit results are summarized in Table 2.1. The Fe *K* near-edge spectra of the sorption samples (Figure A1.1) showed no evidence for the presence of Fe(III), which is consistent with our previous work,[17] and rules out Fe(II) oxidation and precipitation of Fe(III) phases (e.g. green rust or Fe(III)-(hydr)oxides) under the experimental conditions and protocols applied here, as further confirmed by the EXAFS fitting results presented below.

The EXAFS data of the sorption samples vary strongly with pH. For all samples, a peak is observed at ~1.6 Å (uncorrected for phase shift) in the RSFs (Figure 2.3b), representing the first-shell O ligands surrounding sorbed Fe. The shell is fitted with 5.2-6.2 O atoms at a radial distance of 2.10-2.14 Å (Table 2.1), consistent with an octahedral arrangement of the O atoms around central Fe(II), as in the Fe(II)(aq), nikischerite, and β-$Fe(OH)_2$ reference compounds[17,65–68] (Table 2.1). For the samples reacted at pH ≥ 7.0, a second peak is observed in the RSFs at ~2.8 Å (uncorrected for phase shift) which is due

to second-neighbor Fe backscatterers and indicates the formation of Fe(II) precipitates. The Fe(II) phases formed in the sorption samples are different from those formed in the blank samples, where precipitation of β-$Fe(OH)_2$ occurs at pH > 8.2 (Figure 2.3; Table 2.1) in agreement with thermodynamic calculations in MINEQL+[69] predicting supersaturation of β-$Fe(OH)_2$ at these pH values. The RSFs of the sorption samples reacted at pH ≤ 6.5 for the γ-Al_2O_3 substrate and pH < 7.0 for clay show no evidence for the presence of second-neighbor atomic backscatterers, suggesting formation of mononuclear Fe(II) adsorption complexes under these conditions (Figure 2.3b). The absence of second-shell Al and/or Si associated with the substrate surfaces may indicate formation of outer-sphere Fe(II) complexes, but may also be due to the difficulty of resolving the weak signal of (light) Al and Si given the relatively high noise level of the EXAFS data obtained for these low-loading samples (Figure 2.3), prohibiting assessment of the exact coordination of the Fe(II) surface complexes.

The EXAFS data and fitting results of the Fe(II)-γAl_2O_3 sorption samples reacted at pH 7.0-8.0 (Figure 2.3, Table 2.1) show that Fe(II)-Al(III)-LDH is the main Fe(II) sorption product in these samples. The k^3-weighted χ spectra of these sorption samples are remarkably similar to that of the nikischerite reference (Figure 2.3a; Figure A1.2), indicating that the Fe(II)-Al(III)-LDH phases formed have octahedral Fe(II) sheets that are structurally very similar to the nikischerite reference and vary little with pH. The second shell at R = 2.5 Å in the RSFs of these samples (Figure 2.3b) is fitted with Fe and Al neighbors located at a radial distance of 3.14 Å from central Fe (Table 2.1), in agreement with crystallographic data of nikischerite.[66] This much shorter Fe-Fe distance in Fe(II)-Al(III)-LDH compared to β-$Fe(OH)_2$ (R=3.26 Å; Table 2.1) is due to structural

contraction resulting from substitution of Al^{3+} for Fe^{2+} in the octahedral $Fe(OH)_2$ sheets. The structure of Fe(II)-Al(III)-LDH is illustrated in Figure A1.3.

Wavelet transform (WT) analyses of the second coordination shell of the sorption samples and Fe reference compounds are presented in Figure 2.4. The analyses successfully resolve the Al and Fe atoms in the second coordination shell of central Fe in Fe(II)-Al(III)-LDH, as shown by the two distinct k maxima at R = 2.5 Å in the WT plots of the Fe(II)-γAl_2O_3 sorption samples and the nikischerite reference (Figure 2.4a, d), with the lower k maximum representing (light) Al and the higher k representing (heavier) Fe second shell neighbors.[61] In contrast, second shell scattering in β-$Fe(OH)_2$ and green rust, which are constituted of octahedral hydroxide sheets containing only Fe cations, is dominated by Fe neighbors, as demonstrated by the strong k maximum of 8-9 $Å^{-1}$ at R=2.5 Å in the WT plots of these compounds (Figure 2.4b, c). A small scattering contribution with a lower k maximum is seen in the WT plot of green rust as well at a distance similar to that of Fe-Fe, (Figure 2.4c). The origin of this contribution is not clear; possible sources may include scattering from adsorbed salt ions or from interlayer water molecules coordinated to the surface by hydrogen bonding,[70,71] but require further study. Despite this ambiguity, the distinct differences in the WT results of the Fe(II)-Al(III)-LDH versus β-$Fe(OH)_2$ and green rust in terms of second shell composition (Figure 2.4) demonstrate the utility of WT analyses in distinguishing between these structurally comparable compounds and in assisting EXAFS data interpretation of the sorption samples.

The EXAFS data of the Fe(II) sorption products formed in the amorphous SiO_2 suspensions at pH 7.5 and 8.0 (Figure 2.3, Table 2.1) demonstrate formation of Fe(II)

precipitates with a composition and structure different than the Fe(II)-Al(III)-LDH phases formed in the γ-Al_2O_3 suspensions, as expected given the absence in the SiO_2 suspensions of Al^{3+} required to induce formation of Fe(II)-Al(III)-LDH. We rule out precipitation of β-$Fe(OH)_2$ based on the Fe-Fe distance of 3.22-3.23 Å, which is notably shorter than in β-$Fe(OH)_2$ (R=3.26 Å; Table 2.1). Moreover, WT analyses of the Fe(II)-SiO_2 sorption spectra indicate the presence of two different types of second shell atomic neighbors in the second coordination sphere of central Fe(II) in the precipitates formed, which is inconsistent with $Fe(OH)_2$ or green rust precipitation (Figure 2.4). In addition, the pH 7.5 and 8.0 Fe(II)-SiO_2 sorption samples exhibit distinct depletion of dissolved Si relative to control samples consisting of amorphous SiO_2 suspensions that were identical to the sorption samples but without added Fe(II) (Figure A1.4), suggesting association of Si with the secondary Fe(II) phases formed. Combined, these observations lead us to conclude that precipitation of Fe(II)-phyllosilicate phases occurs in the pH 7.5 and 8.0 Fe(II)-SiO_2 sorption samples, with structural features similar to minnesotaite (a 2:1 hydrous iron silicate) and greenalite (1:1). These ferrous phyllosilicates consist of brucitic $Fe(OH)_2$ sheets coordinated to one or two tetrahedral Si sheets through corner-sharing linking of O atoms along the basal planes,[72–74] to build tri-octahedral Fe(II)-phyllosilicates where central Fe is surrounded by second neighbor Fe and Si at similar distance (Figure A1.3). The Fe-Fe and Fe-Si radial distances in minnesotaite and greenalite (3.20-3.23 Å and ~3.30 Å, respectively,[72–74]) are similar to the distances observed in our sorption samples (Table 2.1), with a Fe-Fe distance contracted relative to β-$Fe(OH)_2$ to adjust the octahedral and tetrahedral sheets in layer silicates.[72,75,76] The Fe(II)-phyllosilicates present in the sorption samples are likely to be poorly crystalline

with partially polymerized Si tetrahedral layers, as has been suggested for the tri-octahedral Co(II)- and Ni(II)-phyllosilicates formed during Co(II) and Ni(II) sorption onto amorphous SiO_2 and quartz at near-neutral to alkaline pH.[20,42,43] Due to the substantial error associated with the coordination numbers of second shell Fe and Si, the structure and composition of these Fe(II) phases are poorly constrained by the EXAFS data fitting results.

The EXAFS results of the clay sorption samples suggest an important role of pH in controlling the type of secondary Fe(II) precipitates formed during reaction of Fe(II) with this substrate. The EXAFS data of the pH 7.5 and the 15-month pH 7.0 samples are similar, although not identical, to those of nikischerite and the Fe(II)-Al(III)-LDH phases formed during Fe(II) sorption onto γ-Al_2O_3 (Figure A1.2a; Table 2.1). Of note is the truncated oscillation at 7−8 $Å^{-1}$ in the k^3-weighted χ spectra of the pH 7.5 Fe(II)-clay sorption samples, which is also present in the nikischerite and the Fe(II)-γAl_2O_3 sorption spectra (Figure A1.2a), and has been identified as a signature feature for the presence of Al in the octahedral $Me^{II}(OH)_2$ sheets formed by divalent Ni, Zn, Co, and Fe, allowing distinction of Me(II)−Al(III)−LDH precipitates from Me(II)$(OH)_2$ and Me(II)-phyllosilicate phases.[17,21] Its presence in the pH 7.0 and 7.5 Fe(II)-clay sorption χ data thus demonstrates formation of Fe(II)-Al(III)-LDH in these samples.

The EXAFS data and fitting results of the pH 8.0 clay sorption samples point to the formation of Fe(II)-phyllosilicate with a structure very similar to the Fe(II)-phyllosilicates formed in the amorphous SiO_2 suspensions (Figure 2.3; Table 2.1; Figure A1.2b), and notably different from the Fe(II)-Al(III)-LDH phases formed in the clay suspensions at pH 7.0 and 7.5. Macroscopic evidence for the difference in Fe(II) sorption

products formed at pH 7.5 *versus* pH 8.0 is presented in Figure A1.4, which compares the concentration of dissolved silica in Fe(II)-clay sorption samples reacted at pH 7.5 and 8.0 to those of control samples made up of suspensions identical to the sorption samples but without added Fe(II). At pH 8.0, distinct depletion of dissolved Si occurs in the Fe(II)-clay suspension over the 15 d time period monitored, whereas dissolved Si in the pH 7.5 Fe(II)-clay suspension increases similar to the control sample (Figure A1.4). These results demonstrate association of Si with the secondary Fe(II)-precipitates formed at pH 8.0, consistent with Fe(II)-phyllosilicate formation. Based on these results, we conclude that the mechanism of Fe(II) sorption in the clay suspensions transitions from predominant formation of Fe(II)-Al(III)-LDH at pH 7.0 and 7.5 to precipitation of Fe(II)-phyllosilicate at pH 8.0.

2.3.3 Influence of precipitate formation on Fe(II) sorption trends

The formation of secondary Fe(II) precipitates evident from the EXAFS data explains the pH and kinetic trends observed in the macroscopic data presented in Figures 2.1 and 2.2. Precipitation of Fe(II) phases is correlated to the steep increases in Fe(II) removal seen in the pH edges at pH > 7 (Figure 2.1), and these therefore in effect define the pH thresholds where Fe(II) precipitation commences during sorption. In the blank samples (with no sorbent present), Fe(II) precipitates as β-$Fe(OH)_2$ at pH > 8.2 (Figure 2.1, 2.3). The higher solubility of β-$Fe(OH)_2$ relative to Fe(II)-Al(III)-LDH and Fe(II)-phyllosilicates is reflected in the 1.0-1.5 pH unit shift to higher values of the pH edge of the blank samples compared to the other edges (Figure 2.1).

Slow Fe(II) sorption observed in the kinetic experiments at pH >7 (Figure 2.2) can similarly be attributed to precipitation of secondary Fe(II) phases. This is well

illustrated by the data obtained at pH 7.0 for Fe(II) sorption onto γ-Al_2O_3, where continued Fe(II) sorption at reaction times beyond 1 d is accompanied by a distinct increase in the intensity of second shell scattering from Fe and Al neighbors (Figure 2.3b) consistent with a process of slow nucleation and precipitate growth. At pH 7.5 and 8.0, secondary Fe(II) precipitates dominate the Fe(II) speciation in the γ-Al_2O_3, clay, and amorphous SiO_2 suspensions after sorption times as short as 1 d, so that additional precipitate growth over longer sorption times does not change the average Fe speciation and causes no further change in the Fe EXAFS (Figure 2.3). We note that, although precipitation of Fe(II)-Al(III)-LDH in the γ-Al_2O_3 suspensions continues over the course of several weeks, formation of these phases commences in the early stages of sorption as evidenced by the appearance of Fe(II)-Al(III)-LDH within 2 h at pH 7.5 (Figure 2.3), making Fe(II)-Al(III)-LDH precipitation a Fe(II) sorption process relevant to both short- and long-term reaction times in these samples.

Sorbent type and pH represent major controls on the kinetics of Fe(II) precipitation. For all three sorbents, the kinetics of Fe(II) sorption at pH > 7 (where precipitation occurs) increase distinctly as pH is raised (Figure 2.2). However, the kinetics are much slower in the clay suspensions than in the γ-Al_2O_3 and amorphous SiO_2 suspensions of equivalent pH, with no evidence of sorption equilibrium attained in the Fe(II)-clay suspensions after 80 days, while the Fe(II)-γAl_2O_3 and Fe(II)-SiO_2 samples do reach equilibrium in this time frame (Figure 2.2). At pH 7.0, Fe(II)-Al(III)-LDH precipitates are observed in the clay suspension only after 15 months of reaction, whereas nucleation of these phases occurs within 1 month in the pH 7.0 γ-Al_2O_3 sorption samples (Figure 2.3). Scheidegger et al.[40] proposed that formation of Me(II)-Al(III)-LDH phases

during long-term metal sorption onto Al-bearing substrates is rate-limited by the dissolution of Al from the mineral sorbent. The slow kinetics of Fe(II)-Al(III)-LDH precipitation in the pH 7.0 and 7.5 clay suspensions relative to γ-Al_2O_3 thus suggest slower release of Al from the clay than from the γ-Al_2O_3 substrate at these pHs. Similarly, the slower kinetics of Fe(II)-phyllosilicate precipitation in the clay samples at pH 8.0 relative to the SiO_2 suspensions of the same pH (Figure 2.2) may be attributed to much slower release of Si from the clay than from the amorphous SiO_2 substrate. Factors controlling Al and Si solubility include the solubility product of the clay substrate, the rate and congruency of dissolution, as well as the abundant permanent charge sites on montmorillonite particles which may present an alternative sink for Al competing with incorporation of Al into growing LDH phases.[39,40,46]

Comparison of the equilibrium Fe(II) solution concentrations attained at pH 7.5 and pH 8.0 in the Fe(II)-γAl_2O_3 and Fe(II)-SiO_2 systems shows that more Fe(II) sorption occurs in the amorphous SiO_2 suspensions than in the γ-Al_2O_3 suspensions of equivalent pH (Figure 2.2). This implies that the Fe(II)-phyllosilicates formed in the presence of amorphous SiO_2 maintain a lower Fe(II) solution concentration than the Fe(II)-Al(III)-LDH phases formed in the γ-Al_2O_3 suspensions. This result agrees with thermodynamic studies of Ni(II)-phyllosilicate and Ni(II)-Al(III)-LDH precipitation in clay and metal-oxide suspensions, which have shown that the solubility of Ni(II)-phyllosilicate is lower than that of Ni(II)-Al(III)-LDH.[26,44,45,77]

The pH threshold required to induce Fe(II)-phyllosilicate formation in the SiO_2 suspensions occurs at slightly higher pH than the threshold of Fe(II)-Al(III)-LDH precipitation in the γ-Al_2O_3 samples (Figures 2.2, 2.3), demonstrating the importance of

pH as a control on occurring precipitation processes. This is particularly true for the Fe(II)-clay systems, where Fe(II) precipitation transitions from predominant formation of Fe(II)-Al(III)-LDH at pH 7.0 and 7.5 to formation of Fe(II)-phyllosilicates at pH 8.0 (Figure 2.3, A1.2, A1.4). Previous studies have observed formation of Ni(II)-phyllosilicate phases during long-term (> 6 months) Ni(II) sorption onto pyrophyllite (a 2:1 clay) at pH 7.5, which was attributed to slow Si exchange and polymerization in the interlayer of Ni(II)-Al(III)-LDH phases,[39,44,45,77] which are equivalent to the Fe(II)-Al(III)-LDHs observed in the pH 7.0 and 7.5 clay suspensions (Figure 2.3). Slow interlayer silification of Fe(II)-Al(III)-LDH is likely to occur as well in the pH 7.0 and 7.5 clay suspensions over sorption times longer than employed here. In the pH 8.0 clay suspensions, however, precipitation of Fe(II)-phyllosilicates occurs within days, and generates Fe(II) phases very similar to those formed in the Fe(II)-SiO_2 sorption samples (Figure 2.3 and A1.2b), which suggests that these may contain no or little structural Al. Systematic investigation of the impact of Al substitution on the structure and EXAFS spectra of Fe(II)-phyllosilicates will be useful in resolving the role of Al in the precipitation of these phases during Fe(II)-clay interaction. Additional thermodynamic and kinetic studies are needed to quantify the influence of pH on the saturation state of the various Fe(II) precipitate phases, and to assess kinetic controls on their formation.

2.3.4 Thermodynamic calculations

The Fe(II)-γAl_2O_3 sorption experiments conducted at pH 7.0, 7.5 and 8.0 experiments all reach equilibrium in the 100 day time frame used in the experiments (Figure 2.2a). Moreover, the EXAFS results identify Fe(II)-Al(III)-LDH precipitates as the main Fe(II) sorption product after long-term sorption at all three pH values (Figure 2.3), suggesting

that these phases control the dissolved Fe(II) levels in these samples. The results of the Fe(II)-γAl_2O_3 sorption experiments therefore allow estimation of the solubility products (K_{sp}) of the Fe(II)-Al(III)-LDH phases formed. The EXAFS results (Figure 2.3, Table 2.1) indicate that the Fe(II)-Al(III)-LDH phases in the γ-Al_2O_3 suspensions contain octahedral metal-hydroxide sheets very similar to those of nikischerite, having a Fe(II):Al(III) ratio of 2:1 (Figure A1.3b).[17,66] Assuming that the positive structural charge of the mineral sheets is balanced by the dominant Cl^- anions of the reaction electrolyte, the chemical formula of the precipitates is $Fe(II)_{2/3}Al(III)_{1/3}(OH)_2Cl_{1/3}$. The aqueous chemical equilibrium of this phase can be expressed as: $Fe(II)_{2/3}Al(III)_{1/3}(OH)_2Cl_{1/3\,(s)} \leftrightarrow 2/3\ Fe^{2+}_{(aq)} + 1/3\ Al^{3+}_{(aq)} + 2\ OH^-_{(aq)} + 1/3\ Cl^-_{(aq)}$, yielding $K_{sp} = (Fe^{2+})^{2/3} * (Al^{3+})^{1/3} * (OH^-)^2 * (Cl^-)^{1/3}$, where brackets denote ion activities. All concentrations required to calculate K_{sp} at given pH are known, except for dissolved Al^{3+}, which was too low for detection by ICP-OES. Therefore, we calculated (Al^{3+}) assuming it was set by equilibrium with gibbsite (α-$Al(OH)_3$) or bayerite (β-$Al(OH)_3$), which are the main Al-oxide phases formed during aging of (metastable) γ-Al_2O_3 in aqueous suspensions.[78–80] Using the Davies equation to derive ion activities, K_{sp} values were calculated from the long-term (equilibrium) experimental data of the Fe(II)-γAl_2O_3 sorption experiments conducted at pH 7.0, 7.5 and 8.0 (details in section A1.9 of Appendix 1). The calculated values are very similar for the three experiments, yielding $K_{sp} = 1.18*10^{-21}$, $1.20*10^{-21}$ and $1.26*10^{-21}$ at pH 7.0, 7.5 and 8.0 when assuming gibbsite as the mineral phase controlling (Al^{3+}), and $K_{sp} = 2.35*10^{-21}$, $2.39*10^{-21}$ and $2.49*10^{-21}$ assuming bayerite controls (Al^{3+}) (Table A1.1). This suggests that similar Fe(II)-Al(III)-LDH phases form at the three pHs, which is consistent with the EXAFS data, and that dissolved Al^{3+} is controlled by the same Al-

oxide phase at all three pHs. Unfortunately, we were not able to make similar estimates of K_{sp} for the Fe(II)-phyllosilicates phases formed in the amorphous SiO_2 samples because, as noted earlier, these phases are likely to be poorly crystalline and their structure cannot be deduced conclusively from the EXAFS data. We are currently conducting Fe(II)-Al(III)-LDH and Fe(II)-phyllosilicate synthesis experiments for more detailed analysis of the solubility products of these minerals. Comparisons of the K_{sp} values determined from these synthesis experiments and from sorption studies such as conducted here will be addressed in future work.

2.4 Environmental Implications

This study reports the formation of Fe(II)-Al(III)-LDH and Fe(II)-phyllosilicate phases as the main secondary precipitation products formed during Fe(II) sorption in anoxic suspensions of clay, Al-oxide and amorphous SiO_2. The precipitation rate and the type of precipitates formed are controlled both by pH and the type of sorbent present, suggesting an important role of soil mineralogy in directing Fe(II) precipitation and the potential for considerable variability in the composition and structure of the secondary Fe(II) phases. The precipitation reactions characterized here may be of particular significance to the geochemistry of Fe(II) in anoxic and suboxic groundwaters and soils, where pH values typically are in the range 6.5-8.0[81,82] and reductive dissolution of Fe(III) may elevate aqueous Fe(II) concentrations to mM levels.[4,5,83–85] Dissolution of Al and Si from common mineral phases including Al-oxide, silica and smectite clay, may induce precipitation of Fe(II)-Al(III)-LDH and Fe(II)-phyllosilicate phases under these conditions. The formation of these secondary Fe(II) precipitates may impact the solubility of Fe(II) in reducing environments. Furthermore, these Fe(II) phases may affect the fate

of trace metals through adsorption and co-precipitation reactions, and control Fe(II) redox reactivity towards redox sensitive compounds.[86–89] Additional thermodynamic and kinetic studies are needed to assess and predict the formation of these phases in natural systems and their reactivity towards trace elements and pollutants.

2.5 Table and Figures

Table 2.1. Fe *K*-edge EXAFS fitting results of Fe(II) sorption and reference samples

		atomic shell[a]								
γ-Al2O3 sorption samples		Fe-O			Fe-Fe			Fe-Al		
pH	time	N[b]	R(Å)	σ^2(Å^{-2})	N	R(Å)	σ^2(Å^{-2})	N	R(Å)	σ^2(Å^{-2})
7.5	1 week	5.5	2.12	0.009	3.0	3.13	0.006	3.0	3.13	0.006
8.0	1 week	5.5	2.12	0.009	3.0	3.14	0.005	3.0	3.14	0.005
7.5	1 month	5.3	2.13	0.008	3.0	3.14	0.006	3.0	3.14	0.006
8.0	1 month	5.2	2.12	0.008	3.0	3.14	0.006	3.0	3.14	0.006
references										
nikischerite		5.2	2.14	0.007	3.0	3.14	0.006	3.0	3.14	0.006
$Fe(OH)_2$		5.2	2.14	0.006	6.0	3.26	0.006			
green rust (chloride)		4.7	2.09	0.014	6.0	3.21	0.013			
aqueous Fe(II)		5.3	2.12	0.009						
no sorbent										
10.0	1 week	5.3	2.14	0.008	6.0	3.26	0.008			
clay sorption samples										
7.5	1 week	6.2	2.10	0.010	3.0	3.14	0.008	3.0	3.14	0.008
7.5	1 month	5.8	2.10	0.010	3.0	3.14	0.007	3.0	3.14	0.007
clay sorption samples		Fe-O			Fe-Fe			Fe-Si		
8.0	1 week	5.7	2.11	0.009	6.0	3.20	0.010	4.0	3.25	0.010
8.0	1 month	5.5	2.10	0.010	6.0	3.20	0.010	3.9	3.25	0.010
SiO_2 sorption samples										
7.5	1 week	5.2	2.10	0.010	6.0	3.22	0.011	5.2	3.27	0.011
8.0	1 week	5.3	2.12	0.013	6.0	3.23	0.012	4.0	3.31	0.012

[a]N is coordination number, R is interatomic radial distance and σ^2 is Debye-Waller factor.

Details on fitting can be found in Appendix 1.

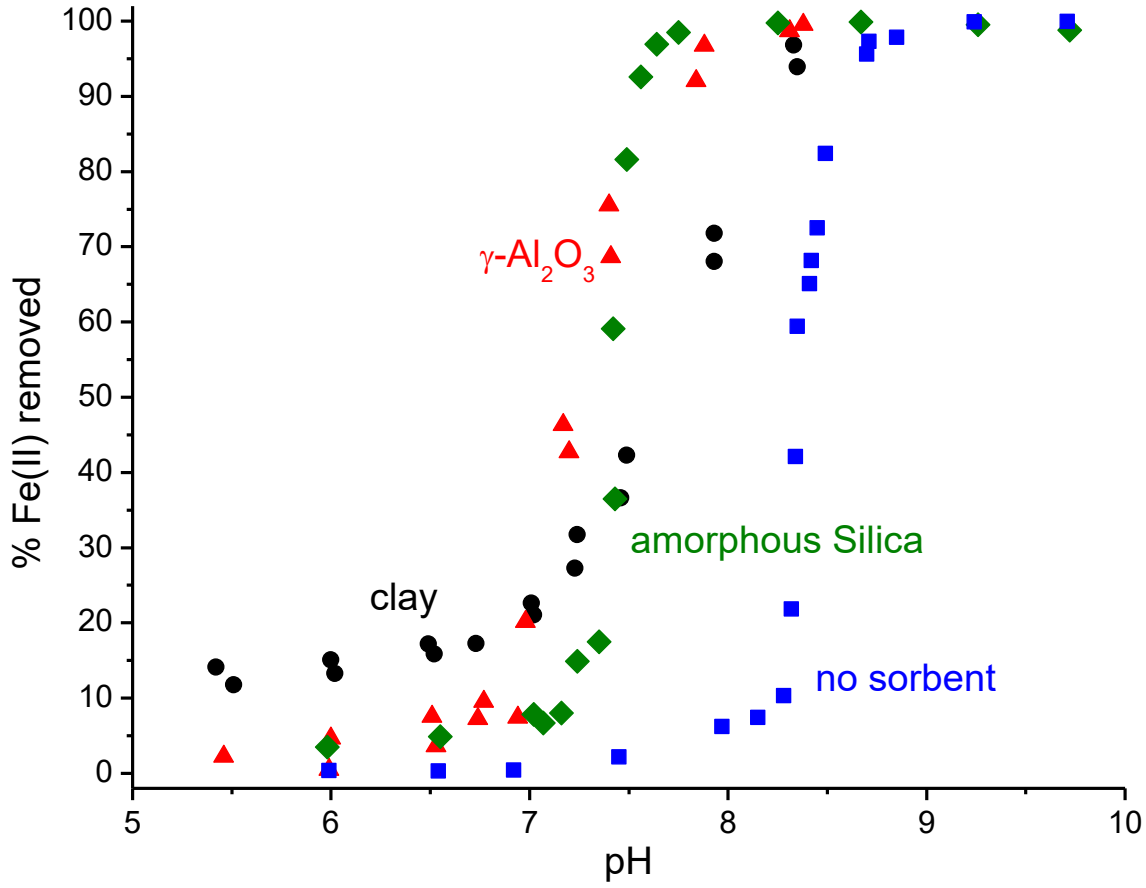

Figure 2.1. Fe(II) sorption pH edges results

Comparison of the pH edges of Fe(II) removal in anoxic γ-Al_2O_3, clay, and amorphous silica suspensions, and in experimental control samples containing no sorbent. Reaction time=7 days, $[Fe(II)]_0$= 2.7 mM, solid/solution=5g L^{-1}.

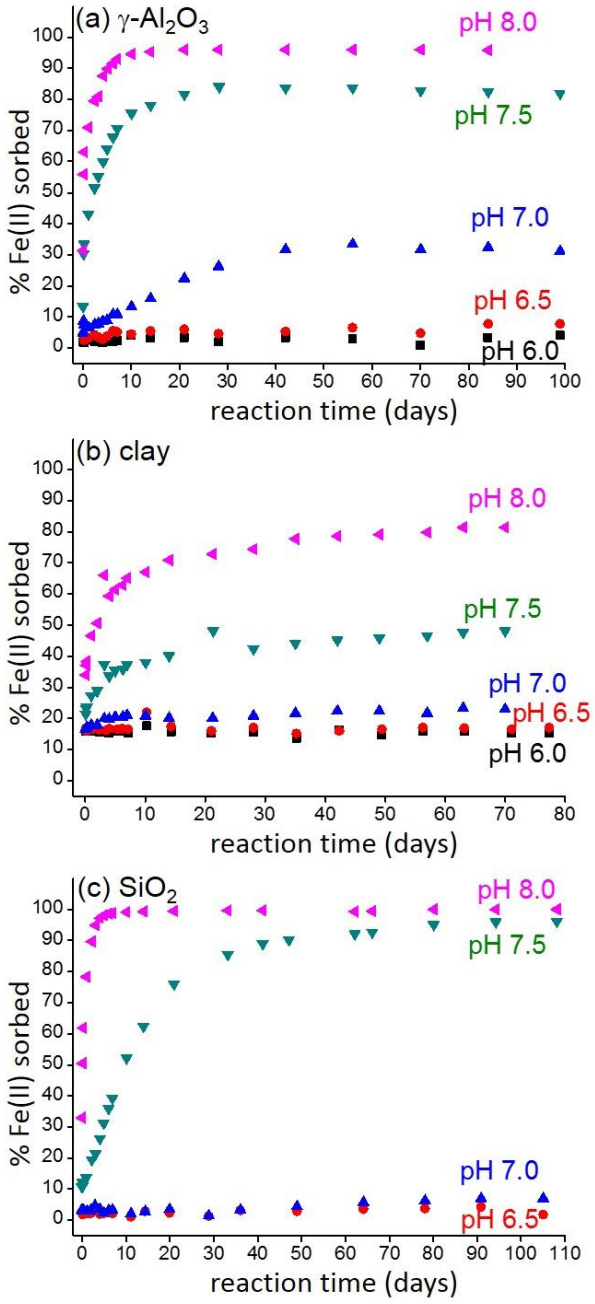

Figure 2.2. Fe(II) sorption kinetics results

Kinetics of Fe(II) sorption in anoxic suspensions of (a) γ-Al_2O_3, (b) clay and (c) amorphous silica at pH 6.0, 6.5, 7.0, 7.5 and 8.0 during reaction times up to 110 days.

The solids concentration in the experiments was 5 g L^{-1}, and the aqueous Fe(II) concentration was 2.7 mM.

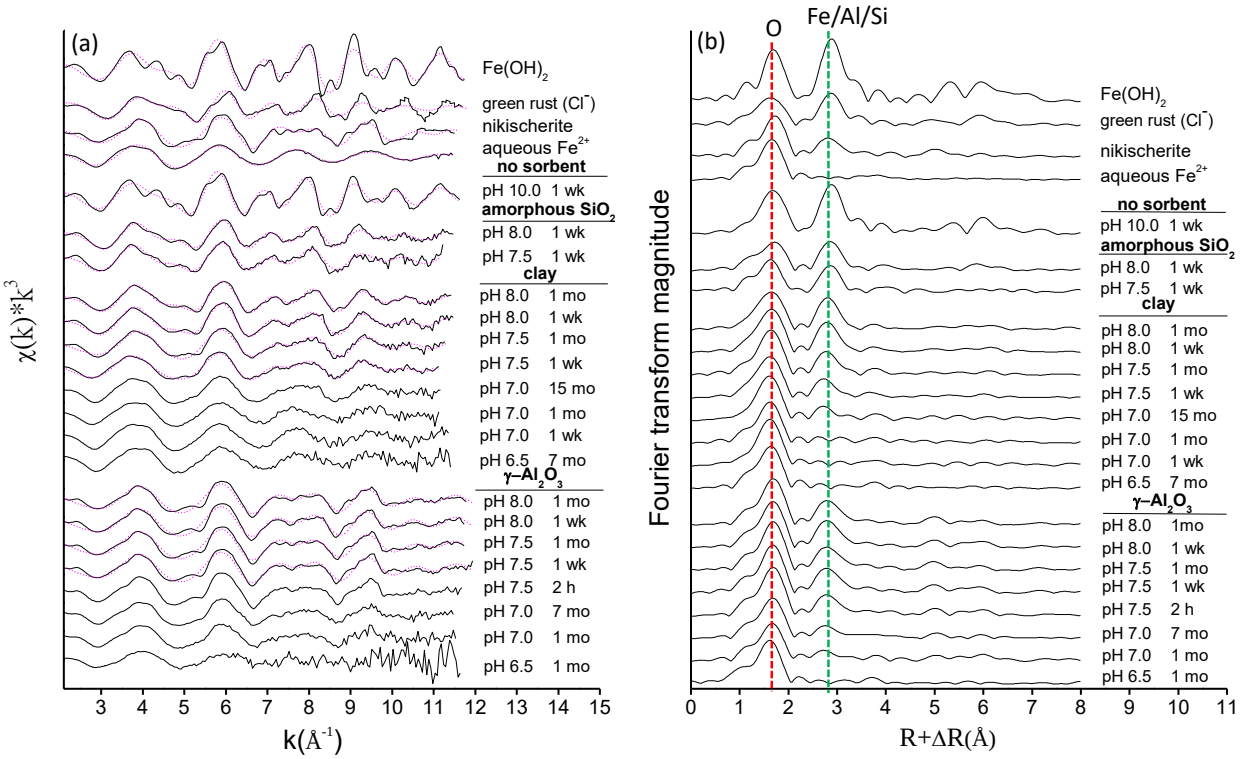

Figure 2.3. Fe *K* edge EXAFS data of sorption samples and references

(a) k^3-weighted χ spectra and (b) corresponding radial structure functions (RSFs). Solid and dotted lines in (a) represent raw and fitted spectra, respectively. Dotted lines in (b) locate the atomic neighbors indicated. Data fitting results are summarized in Table 2.1.

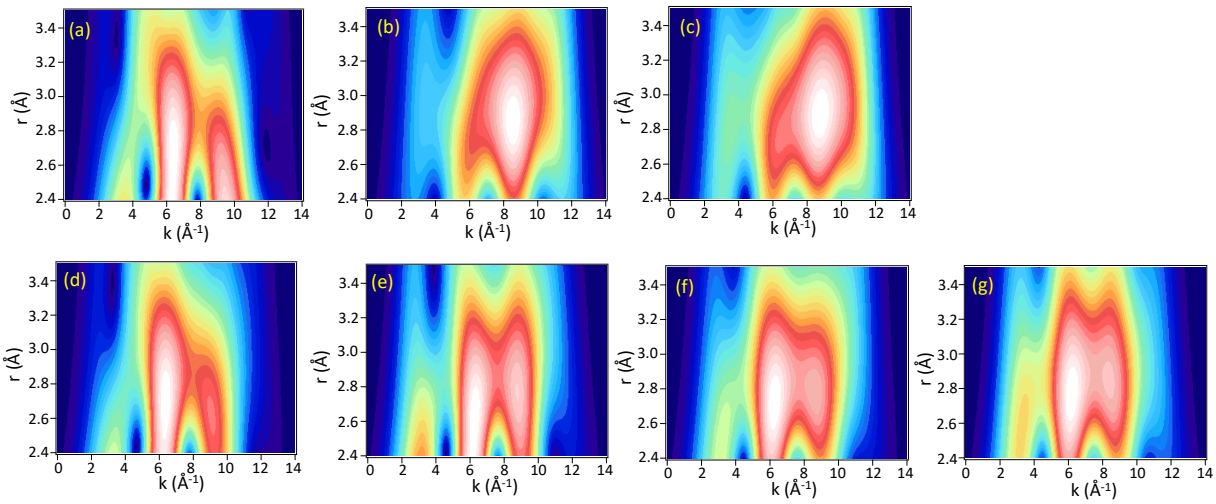

Figure 2.4. Wavelet transform results of Fe(II) references and sorption samples

Wavelet transform (WT) analyses of the second coordination shell (η=5.8, σ=1) for reference compounds: (a) nikischerite; (b) β-$Fe(OH)_2$; (c) green rust; and sorption samples: (d) Fe(II)-γAl_2O_3 (pH 8.0); (e) Fe(II)-clay (pH 7.5); (f) Fe(II)-clay (pH 8.0); and (g) Fe(II)-amorphous silica (pH 8.0). All sorption samples were reacted for 1 month, except for the Fe(II)-SiO_2 sample, which was reacted for 1 week.

Chapter 3: Macroscopic and Spectroscopic Assessment of the Cosorption of Fe(II) with As(III) and As(V) on Al-Oxide

Abstract

The co-sorption of Fe(II) with As(III) and As(V) in anoxic suspensions of γ-Al_2O_3 at pH 7.5 was investigated with batch kinetic experiments and synchrotron EXAFS analyses. Single-sorbate results showed that Fe(II) formed secondary Fe(II)-Al(III)-layered double hydroxide (LDH) phases during reaction with the Al-oxide sorbent, whereas As(III) and As(V) formed inner-sphere surface complexes. The kinetics and mechanisms of Fe(II) and As(III) sorption were identical in dual-sorbate and single-sorbate experiments, indicating that the processes involved operate independently. In contrast, As(V) and Fe(II) interacted strongly during co-sorption. Fe(II) enhanced the rate and extent of As(V) removal from solution, but did not affect the mechanism of As(V) adsorption. Conversely, As(V) hindered the formation of Fe(II)-Al(III)-LDH, slowing down precipitation at low As(V) concentrations and preventing it at high concentrations. This was attributed to interference of adsorbed As(V) with the Al supply needed for Fe(II)-Al(III)-LDH precipitation, possibly combined with enhanced surface complexation of Fe(II) cations promoted by anionic As(V) surface species. No evidence was found for redox reactions between Fe(II) and As(V) or As(III), or precipitation of Fe-arsenic phases. These results improve our understanding of the geochemistry of Fe(II) and arsenic in reducing environments, and demonstrate the utility of mechanistic studies on geochemically complex model systems.

3.1 Introduction

Sorption reactions at mineral-water interfaces have a profound impact on the solid-water partitioning of trace metal(loid)s and thus play an important role in controlling the mobility and fate of these species in soils and sediments.[52] Various studies have shown the ability of Al-bearing mineral substrates to induce the precipitation of Me(II)-Al(III)-layered double hydroxides (LDHs) during sorption of Ni(II), Zn(II) and Co(II) at near neutral pH values.[18–30,40] Our recent work has demonstrated that aqueous Fe(II) also readily precipitates during interaction with mineral sorbents, forming Fe(II)-Al(III)-LDH phases and poorly crystalline Fe(II)-phyllosilicates during sorption in anoxic suspensions of Al-oxide, smectite clay, and amorphous silica at pH values > 7.[17,90] The formation of such secondary Fe(II) phases may play an important role in determining Fe(II) sequestration and speciation in environments undergoing Fe(III) reduction, where concentrations of aqueous Fe(II) are elevated and pH values commonly are in the range 6.5-8.0.[4,5,81–85]

Reductive dissolution of Fe(III)-oxides not only leads to the build-up of high levels of aqueous Fe(II), but also releases trace metals and metalloids originally associated with these mineral sorbents.[81,83,85,91,92] The presence of dissolved trace metal(loid)s may affect the formation of secondary Fe(II) phases during Fe(II) sorption, while, conversely, the formation of Fe(II) precipitates may influence the retention of the aqueous metal(loid) species, e.g. through co-precipitation, adsorption or redox reactions. Therefore, studies of the co-sorption of Fe(II) with common trace elements are needed to obtain a better understanding of the formation of secondary Fe(II) precipitates and their impacts on trace metal(loid) solubility and speciation in suboxic and anoxic environments.

The current study focuses on the co-sorption of Fe(II) with the arsenic species arsenite, As(III) and arsenate, As(V), which are the dominant inorganic As species in groundwaters and soils,[93] using a model Al-oxide as the mineral sorbent. Previous studies have demonstrated that both As(III) and As(V) are sorbed effectively on Al-oxide substrates, but that the sorption affinities and mechanisms differ between the two As redox states. Arsenate adsorbs more extensively on Al-oxide than does arsenite under equivalent conditions, and spectroscopic work has shown that As(V) predominantly forms inner-sphere complexes at the Al-oxide surface whereas As(III) forms a mixture of outer- and inner-sphere complexes.[94–97] These differences in adsorption behavior may influence the impacts of these As species on the interaction of aqueous Fe(II) with Al-oxide sorbents.

Besides influencing the process of Fe(II)-Al(III)-LDH precipitation, the presence of arsenate and arsenite oxyanions may also affect the complexation of Fe(II) cations at the Al-oxide surface (i.e. Fe(II) adsorption). Results from past studies have indicated the potential of oxyanion co-sorbates for modifying metal adsorption through surface electrostatic effects and ternary complex formation.[98–105] Additional processes of potential importance include the precipitation of secondary Fe(II)-arsenic phases, and redox reactions between sorbed Fe(II) and As. Clearly, the geochemical complexity of dual-sorbate Fe(II)-As systems is substantially higher than those of the corresponding single-sorbate systems.

The objective of this study was to investigate the macroscopic and mechanistic aspects of the co-sorption of Fe(II) with As(III) and As(V) onto Al-oxide under anoxic conditions at pH 7.5. The experiments were conducted at conditions conducive to the

formation of Fe(II)-Al(III)-LDH in order to assess the impacts of As(III) and As(V) on the precipitation process, and to determine the influence of these secondary Fe(II) phases on As retention. Our results demonstrate notable differences in Fe(II) and arsenic sorption trends and mechanisms between single- and dual-sorbate systems, thus highlighting the need for mechanistic studies of model systems mimicking the complexity of natural environments.

3.2 Experimental Section

3.2.1 Experimental conditions and materials

All experiments were conducted under strictly anoxic conditions using a glovebox filled with 95% $N_{2(g)}$ and 5% $H_{2(g)}$, and equipped with Pd catalyst to scrub the atmosphere off trace $O_{2(g)}$. The anoxic protocols employed here are described in detail in our previous studies.[17,90] An anoxic stock solution of 1.0 M Fe(II) was prepared by dissolving $FeCl_2{\cdot}4H_2O$ (Fisher Scientific, Cat. No. I90-500) in anoxic 0.1 M HCl and filtering the resulting solute through a 0.22 μm nitrocellulose membrane. Anoxic As(III) and As(V) stock solutions of 0.1 M were prepared from $NaAsO_2$ (Fisher Scientific, Cat. No. S225I-100) and $Na_2HAsO_4{\cdot}7H_2O$ (Sigma-Aldrich, Cat. No. 455857) salts, respectively. The mineral sorbent used in this study was γ-Al_2O_3 (Alfa Aesar, Cat. No. 39812), with a specific surface area measured as 70.5 $m^2\ g^{-1}$ using the N_2-BET method.

3.2.2 Batch sorption studies

Sorption experiments were conducted with anoxic 5.0 g γ-$Al_2O_3\ L^{-1}$ suspensions maintained at pH 7.5 with 50 mM HEPES dissolved in the electrolyte background. The ionic strength was set at 0.1 M with NaCl after accounting for the buffer speciation and the addition of titrant NaOH.

Kinetic experiments were performed in a total of 9 batches comprised of 5 single-sorbate and 4 dual-sorbate systems. For the single-sorbate experiments, γ-Al_2O_3 suspensions were spiked with either Fe(II) (1 mM), As(III) (0.25 mM) or As(V) (0.10 mM, 0.25 mM or 0.50 mM). In the dual-sorbate systems, Fe(II) (1 mM) was added to the γ-Al_2O_3 suspensions simultaneously with either As(III) or As(V) at the same concentrations as used for the single-sorbate experiments. Aqueous speciation calculations using Mineql+[69] showed that the speciation of aqueous Fe(II) is dominated by non-complexed $Fe^{2+}_{(aq)}$ (97.8 %) with a minor component of $FeCl^{+}_{(aq)}$ (2.2 %), whereas aqueous As(III) consists of 97.9 % $H_3AsO_3^{0}{}_{(aq)}$ and 2.1 % $H_2AsO_3^{-}{}_{(aq)}$, and aqueous As(V) consists of 88.2 % $HAsO_4^{2-}{}_{(aq)}$ and 11.8 % $H_2AsO_4^{-}{}_{(aq)}$.

The reaction vessels were wrapped in aluminum foil to prevent light exposure, and sealed in three zip-lock bags inside the glovebox to prevent accidental exposure to O_2 during equilibration. The containers were sampled regularly over the course of 9 months to monitor the sorption of Fe(II), As(III) and As(V). Sampling involved retrieval of a 5 mL suspension aliquot which was filtered through a 0.22 μm nitrocellulose membrane inside the glovebox. The filtrates were acidified with 125 μL of 37 % HCl, and analyzed for the concentration of dissolved Fe(II) with the ferrozine method,[57] and/or for the concentration of aqueous arsenic using ICP-OES. Ion sorption was calculated as the difference between the initial and final solution concentrations.

Speciation calculations using the solubility product (K_{sp}) of symplesite ($Fe^{II}_3(As^{V}O_4)_2 \cdot 8H_2O$) reported by Johnston and Singer[106] indicated that the initial solutions of the dual-sorbate experiments with As(V) were oversaturated with respect to this phase. The saturation state of the equilibrated solutions, however, could not be

assessed, because the aqueous As(V) concentrations were below the detection limit of ICP-OES. Catalano et al.[107] showed that the K_{sp} value used in the thermodynamic calculations may under-predict symplesite solubility in dilute solutes such as used here. We therefore experimentally assessed the potential of Fe(II)-As(V) precipitation in our systems, in two ways. First, we prepared blank samples that lacked γ-Al_2O_3 but were otherwise identical to the ternary sorption examples. The solutions were filtered through 0.22 μm nitrocellulose membranes and analyzed. No removal of aqueous Fe(II) or As(V) was observed. Secondly, the XAS data of the sorption samples were compared to those of a synthetic Fe(II)-As(V) precipitate (details in the 3.3 Results section), and to those of symplesite as reported in Jönsson and Sherman.[108] These comparisons showed no evidence for Fe(II)-As(V) precipitation as discussed in the Results section below.

3.2.3 XAS studies

Samples for X-ray absorption spectroscopy (XAS) analysis were prepared under the same conditions and with the same methods as for the kinetic experiments described above, using sample volumes of 50 mL to obtain enough paste for XAS analysis. Both single-sorbate and dual-sorbate samples were prepared, at equilibration times varying from 1 day to 9 months. The anoxic protocols used for XAS sample preparation and transport were described previously.[90]

Besides the sorption samples, the following reference compounds were analyzed as well: (1) aqueous Fe(II); (2) nikischerite ($NaFe^{II}_6Al_3(SO_4)_2(OH)_{18}(H_2O)_{12}$); (3) aqueous As(III); (4) aqueous As(V); and (5) a synthetic Fe(II)-As(V) precipitate. The $Fe(II)_{(aq)}$ and nikischerite references are described in Zhu and Elzinga,[90] while the aqueous As(III) and As(V) standards were prepared as solutions of 10 mM $NaAsO_2$ and

$Na_2HAsO_4 \cdot 7H_2O$ dissolved in DDI water. The Fe(II)-As(V) precipitate was prepared per the protocol of symplesite synthesis of Jönsson and Sherman.[108] Powder X-ray diffraction analysis of the mineral product showed broad diffraction peaks indicative of a poorly crystalline solid (not shown). XAS analyses confirmed that the local coordination environments of Fe and As in the solid resembled those of symplesite, as described in more detail in Appendix 2.

Synchrotron Fe *K*-edge (7112 eV) and As *K*-edge (11,867 eV) spectra were recorded on beamline X-11A of the National Synchrotron Light Source at Brookhaven National Laboratory, and beamline 12-BMB of the Advanced Photon Source at Argonne National Laboratory. The data were collected at room temperature in fluorescence mode using a Si(111) monochromator detuned by 40 % for Fe scans and by 25 % for As scans to suppress higher order harmonics. Fe foil and Au foil (L_{III}-edge 11,919 eV) were used for energy calibration of the Fe and As K-edges, respectively. The possibility of beam damage of the Fe(II) sorption samples during analysis was checked by comparing the normalized spectra of the first and last scan of each sample, as in Elzinga[17]. No damage was observed. EXAFS data processing and fitting were performed with WINXAS 3.1,[58] combined with Feff 7.0 [59] and ARTEMIS[60]. Details of the EXAFS data fitting routines used for the sorption and reference samples are described in Appendix 2.

3.3 Results

3.3.1 Batch kinetic studies

Figure 3.1 compares the kinetics of sorption of Fe(II) (1 mM) in the absence and presence of As(III) (0.25 mM) and As(V) (0.10, 0.25 and 0.50 mM). Consistent with our earlier studies,[17,90] the Fe(II) sorption kinetics in the single-sorbate experiment are biphasic, with

fast uptake during the first hours of reaction followed by a slower sorption stage that continues until equilibrium is reached after ~30 days (Figure 3.1). Effects of arsenic depend on As oxidation state and concentration. The presence of 0.25 mM As(III) does not discernibly affect the kinetics and extent of Fe(II) sorption, indicating that As(III) has little impact on Fe(II) retention even at this relatively high concentration (Figure 3.1a). The presence of As(V), in contrast, noticeably changes the kinetics of Fe(II) sorption, although the extent of sorption is relatively unaffected with 75-85 % of Fe(II) ultimately removed under all conditions (Figure 3.1b). The kinetic impacts of As(V) vary with concentration. At the two lower As(V) additions (0.10 mM and 0.25 mM), the Fe(II) sorption kinetics slow down relative to the binary Fe(II)/γ-Al_2O_3 system, with the time required to attain apparent equilibrium increasing to ~100 days in the presence of 0.10 mM As(V), and to ~240 days in the presence of 0.25 mM As(V). At the highest level of As(V) addition (0.50 mM), on the other hand, Fe(II) sorption reaches equilibrium on a similar time scale as for the binary system, stabilizing within the first month of reaction (Figure 3.1b).

Figure 3.2 compares the sorption kinetics of As(III) and As(V) in the presence and absence of Fe(II). The retention of As(III) is not influenced by Fe(II), as shown by the similarity of the As(III) kinetic sorption patterns in the binary As(III)/γ-Al_2O_3 and ternary As(III)/Fe(II)/γ-Al_2O_3 suspensions (Figure 3.2a). This finding resembles the results of Figure 3.1a showing that As(III) does not affect the sorption of Fe(II). Combined, these observations suggest that the processes controlling the removal of aqueous Fe(II) and As(III) in the ternary samples are neither competitive nor synergistic, but operate independently under the conditions investigated here.

Contrariwise, the presence of Fe(II) enhances both the rate and extent of As(V) sorption relative to the binary As(V)/γ-Al_2O_3 systems, mediating rapid and essentially complete removal of As(V) from solution (Figure 3.2b-d). This promotive effect of Fe(II) on the sorption of As(V) contrasts with the inhibitive effect of As(V) on the sorption of Fe(II) at [As(V)]=0.10 and 0.25 mM (Figure 3.1b). These opposite impacts of co-sorption demonstrate the complexity of ternary sorption systems, where interactions between multiple processes complicate prediction of net outcomes.[98–105] Overall, the kinetic data presented in Figures 3.1 and 3.2 indicate that the arsenic oxidation state and concentration are important factors in regulating As impacts on Fe(II) sorption behavior on Al-oxide, and that the influence of Fe(II) on the sorption of arsenic depends on the As oxidation state. The mechanisms behind these macroscopic sorption trends are addressed below based on EXAFS spectroscopic results.

3.3.2 Fe K-edge EXAFS data

Figure 3.3 presents the Fe K-edge EXAFS data of the binary and ternary Fe(II) sorption samples and Fe reference compounds, with Figure 3.3a showing the raw and fitted k^3-weighted χ spectra, and Figure 3.3b the corresponding radial structure functions (RSFs) obtained from Fourier transforming the raw χ data. The fit results are summarized in Table A2.1.

The Fe EXAFS spectra of the sorption samples vary with reaction time, As oxidation state, and As concentration (Figure 3.3), indicating that these variables influence the speciation of sorbed Fe. The Fourier transforms of all samples exhibit a peak at ~1.6 Å (uncorrected for phase shift), which is due to backscattering from first-shell O ligands. This shell is fitted with 4.8-6.0 O atoms at a radial distance of 2.08-2.12

Å (Table A2.1). These results indicate that sorbed Fe is present in the divalent form and in octahedral coordination with first-shell O, as in the reference compounds Fe(II)(aq) and nikischerite.[17,66–68,90] The persistence of Fe(II) as the predominant Fe species in the ternary systems indicates that redox reactions between Fe(II) and As(V) or As(III) co-sorbates do not occur to a significant extent.

The RSFs of the binary Fe(II)/γ-Al_2O_3 sorption samples exhibit a second shell at ~2.8 Å (uncorrected for phase shift) (Figure 3.3b), which is due to backscattering from second-neighbor Fe/Al and thus indicates the formation of Fe(II) precipitates. The k^3-weighted χ spectra (Figure 3.3a) and fit results (Table A2.1) of these samples closely resemble those of the nikischerite reference (Figure 3.3a), identifying the precipitate formed as a Fe(II)-Al(III)-layered double hydroxide (LDH). These findings are consistent with our previous studies showing Fe(II)-Al(III)-LDH as the main Fe(II) sorption product of the interaction of Fe(II) with Al-oxide and clay substrates under similar conditions as used here.[17,90] These Fe(II) phases consist of brucitic $Fe(OH)_2$ layers in which 1/3 of Fe(II) has been substituted with Al(III), generating a positive structural layer charge that is neutralized by interlayer Cl^- anions derived from the background electrolyte.[17,66] In line with our previous results,[17,90] precipitation of Fe(II)-Al(III)-LDH occurs rapidly in the binary experiments, with clear evidence for the presence of these phases after 2 h (Figure 3.3, spectrum b).

The Fe EXAFS results of the ternary samples show that Fe(II)-Al(III)-LDH precipitation occurs in the presence of As as well (Figure 3.3), but that the rate and extent of precipitation are modified in dependence of the As oxidation state and concentration. In the system containing As(III), precipitation of Fe(II)-Al(III)-LDH occurs on a similar

time scale as in the binary Fe(II)/γ-Al_2O_3 system, with Fe(II)-Al(III)-LDH observed after 1 day (Figure 3.3 spectrum d). The apparent lack of interference of As(III) with the precipitation of Fe(II)-Al(III)-LDH is consistent with the macroscopic data of Figures 3.1a and 3.2a which similarly suggest that the sorption of Fe(II) and As(III) are mutually independent under the current experimental conditions.

In contrast to As(III), the presence of As(V) interferes with the precipitation of Fe(II)-Al(III)-LDH. This is demonstrated by spectra f-p in Figure 3.3, which were collected for the 1 d, 6 d, 35 d, and 8-9 mo samples of the ternary samples containing 0.10, 0.25 and 0.50 mM As(V). These data show that after 1 day of reaction, none of the ternary samples contain Fe(II)-Al(III)-LDH (Figure 3.3, spectra f, i, m). This contrasts with the As(V)-free Fe(II)/γ-Al_2O_3 system where formation of Fe(II)-Al(III)-LDH occurs within 2 hours (Figure 3.3, spectrum b). Precipitation of Fe(II)-Al(III)-LDH does ultimately occur as well in the ternary samples with 0.10 and 0.25 mM As(V), with evidence for the presence of these phases visible after 6 d and 35 d, respectively (Figure 3.3). In the ternary system containing 0.50 mM As(V), however, there is no evidence for precipitation of Fe(II)-Al(III)-LDH even after 8 months of reaction (Figure 3.3, spectrum p; Table A2.1). Use of the Fe EXAFS results for identification of the mode of Fe(II) sorption in this system is limited by the lack of well-defined scattering contributions from atomic neighbors beyond first-shell O (Figure 3.3b, spectra m-p). We do, however, note the dissimilarity of the Fe XAS data of this system to those of the reference Fe(II)-As(V) precipitate (spectrum r in Figure 3.3), and those of crystalline symplesite reported by Jönsson and Sherman.[108] This suggests that formation of secondary Fe(II)-As(V) phases is not a major process. Constraints on the mechanisms of Fe(II) retention in this system

are discussed below based on the combined Fe and As EXAFS spectroscopic data and the macroscopic sorption trends.

3.3.3 As K-edge EXAFS data

The As EXAFS data of sorption samples and reference compounds are displayed in Figure 3.4, and the fit results are presented in Table A2.2. Only the 6-day sorption samples are shown, because no changes were observed in the As XAS data over the course of the experiment (Figure A2.4-A2.7). The k^3-weighted χ spectra are dominated by the sinusoidal oscillations resulting from the backscattering of first-shell O neighbors (Figure 3.4a). The radial distance of first-shell O is fitted at 1.68 Å for the As(V) samples, and at 1.78-1.79 Å for the As(III) samples (Table A2.2), which are values consistent with the As(III)-O and As(V)-O coordination observed in previous XAS studies.[e.g. 94,105,107–112] There are no differences in the As(III)-O and As(V)-O coordination of the ternary and binary samples (Table A2.2). This indicates that the valence states of these arsenic species do not change during co-sorption with Fe(II), an observation that is consistent with the Fe EXAFS results which similarly demonstrated the absence of redox reactions between Fe(II) and As(III) or As(V) (Figure 3.3; Table A2.1).

The RSFs of the As(III) and As(V) sorption samples (Figure 3.4b) show a second coordination shell at ~3.0 Å (uncorrected for phase shift). This shell was fitted with Al atomic neighbors located at a radial distance of 3.13-3.15 Å for the As(V) samples, and 3.22-3.25 Å for the As(III) samples (Table A2.2). These results are consistent with previous XAS studies of As(III) and As(V) adsorption on Al-oxide substrates,[e.g. 94,105,109,112] and indicate the formation of inner-sphere bidentate binuclear complexes for both As(III) and As(V) at the γ-Al_2O_3 surface.

We note the strong similarity of the As(III) and As(V) XAS spectra and fit results obtained for the binary (i.e. As(III)/γ-Al_2O_3 and As(V)/γ-Al_2O_3) and the corresponding ternary sorption samples (Figures 3.4 and A2.9; Table A2.2). This indicates that any differences in the As(III) and As(V) speciation between the binary and ternary systems are minor. This is particularly noteworthy for the As(V) systems, where effects of Fe(II) on As sorption are strong (Figure 3.2), and therefore mechanistic differences in As(V) retention between binary and ternary samples might be expected. We note that the As(V) XAS data of the ternary systems do not resemble those of the reference Fe(II)-As(V) precipitate (spectrum e in Figure 3.4), and that the data fits are inconsistent with precipitation of symplesite (Table A2.2). Instead, the As(V) XAS data of the binary As(V)/γ-Al_2O_3 and ternary Fe(II)/As(V)/γ-Al_2O_3 systems are essentially identical (Figure 3.4; Table A2.2), as illustrated particularly well by the overlay of the As(V) χ spectra presented in Figure A2.9d. These results indicate that Fe(II) has no noticeable impact on the mode of As retention in our experimental systems, with As(III) and As(V) adsorbed as inner-sphere bidentate binuclear complexes at the Al-oxide surface in both the presence and absence of Fe(II).

3.4 Discussion

3.4.1 Mechanisms of Fe(II) and As(III) cosorption

The combined macroscopic and spectroscopic data presented here suggest that As(III) and Fe(II) react independently with the γ-Al_2O_3 substrate, as indicated by the identical results obtained for the ternary and binary sorption systems in terms of the rate, extent and mechanisms of Fe(II) and As(III) sorption (Figures 3.1-3.4; Tables A2.1 and A2.2). The XAS results demonstrate that As(III) coordinates as inner-sphere adsorption

complexes at the γ-Al_2O_3 surface, while Fe(II) forms secondary Fe(II)-Al(III)-LDH precipitates with Al(III) supplied by partial dissolution of the Al-oxide sorbent.

The absence of a discernable effect of Fe(II) on the adsorption of As(III) at the γ-Al_2O_3 surface indicates that the secondary Fe(II)-Al(III)-LDH precipitates formed in the ternary samples do not represent a significant sink for As(III) compared to the γ-Al_2O_3 surface. This is likely at least in part due to the relatively small amount of Fe(II) (1.0 mM) in the system compared to Al (98 mM), limiting the potential of Fe(II)-Al(III)-LDH to act as a quantitatively important sorbent relative to the γ-Al_2O_3 substrate. An additional consideration is that Fe(II)-Al(III)-LDH may not have a particularly high affinity for sorption of As(III). The surface of Fe(II)-Al(III)-LDH is dominated by positively charged basal surfaces,[17,66] whereas the dominant aqueous As(III) species in our experimental systems is charge-neutral $H_3AsO_3^0{}_{(aq)}$. The absence of favorable electrostatic interactions between $H_3AsO_3^0{}_{(aq)}$ and Fe(II)-Al(III)-LDH may limit the adsorption of aqueous As(III) onto this secondary Fe(II) phase, especially in the presence of the relatively high concentration of Cl^- anions provided by the 0.10 M NaCl background electrolyte. Studies addressing the affinity and mechanisms of As(III) interaction with Fe(II)-Al(III)-LDH are needed to assess the potential of this Fe(II) mineral phase to act as a sink of As(III).

The dominant mode of Fe(II) sorption in the ternary Fe(II)/As(III)/γ-Al_2O_3 systems is the formation of Fe(II)-Al(III)-LDH phases (Figure 3.3). However, in view of the relatively high solution pH and the fact that some Fe(II) remains in solution (Figure 3.1), adsorption of Fe(II) to the γ-Al_2O_3 surface is expected to occur as well.[17,90] Assuming that the resulting Fe(II) surface complexes are inner-sphere, as observed for the divalent metals Zn(II) and Pb(II),[41,46] the Al-oxide surface charge is expected to

increase (i.e. become more positive) in the presence of aqueous Fe(II). Since the adsorption of As(III) is not sensitive to this presumed change in the surface charge of the mineral sorbent (Figure 3.2a), we infer that the As(III) surface complexes are charge-neutral. This conclusion is consistent with the predominant occurrence of aqueous As(III) as the (uncharged) $As(OH)_3^0{}_{(aq)}$ species in our systems, and is supported by the electrophoretic mobility measurements of Arai et al.[94], who demonstrated that the surface charge of γ-Al_2O_3 is not modified by As(III) adsorption. Verification of this argument will require studies characterizing the mononuclear adsorption complexes formed by Fe(II) at the Al-oxide surface.

A final point we make from the Fe(II)-As(III) co-sorption results is that the As(III) surface complexes do not appear to affect the availability of sorbent-derived Al for formation of Fe(II)-Al(III)-LDH. We have previously proposed that the slow stage of Fe(II) sorption, which occurs between 1-30 days under the current conditions (Figure 3.1), is due to ongoing precipitation of Fe(II)-Al(III)-LDH, and is rate-controlled by the dissolution of the Al-oxide sorbent supplying the Al needed for LDH precipitation, consistent with the conclusions from other studies.[17,39,40,46,90] The identical kinetics of Fe(II) sorption in the absence and presence of As(III) (Figure 3.1a) therefore indicate that the release of Al from the surface is not affected by adsorbed As(III). This suggests that the interaction of As(III) with the Al-oxide surface is insufficiently strong to interfere with Al-oxide dissolution.

3.4.2 Mechanisms of Fe(II) and As(V) cosorption

The experiments conducted with As(V) and Fe(II) demonstrate distinctly different sorption behavior of both species in ternary versus binary systems, indicating interactions

between the two during co-sorption. The presence of Fe(II) strongly increases the sorption of As(V) (Figure 3.2). However, the As XAS data indicate that the mode of As(V) retention is not noticeably modified by the presence of Fe(II) (Figure 3.4, A2.9; Table A2.2). We therefore exclude formation of Fe(II)-As(V) precipitates and sorption of As(V) onto secondary Fe(II)-Al(III)-LDH phases as significant drivers of the observed enhancement of As(V) sorption in the presence of Fe(II). Instead, the current results suggest surface electrostatic effects as a plausible cause for the increase in As(V) sorption in the ternary experiments. In this scenario, the Al-oxide surface becomes more positively charged due to inner-sphere complexation of Fe(II) cations, and this promotes additional sorption of anionic As(V) (relative to the binary As(V)/γ-Al_2O_3 system) by lowering the electrostatic barrier for ion approach. The dominant aqueous As(V) in our experimental systems is anionic $HAsO_4^{2-}{}_{(aq)}$, and the electrophoretic mobility studies of Arai et al.[94] indicate that the inner-sphere adsorption complexes of As(V) at the Al-oxide surface carry negative charge. The electrostatics of the As(V)/γ-Al_2O_3 surface interaction thus favor increased As(V) adsorption mediated by inner-sphere surface complexation of Fe(II). As noted above, the inner-sphere coordination of Fe(II) cations and the consequent increase in Al-oxide surface charge remains to be confirmed, but is consistent with the mechanisms of Zn(II) and Pb(II) adsorption onto γ-Al_2O_3.[28,41]

Besides electrostatic effects, direct interactions between adsorbed Fe(II) and As(V) surface complexes may occur as well. Such interactions lead to the formation of ternary surface complexes exhibiting chemical or physical bonds between adsorbed Fe(II) and As(V) that increase the stability of sorption of both species. Ternary complexes have been observed in IR studies of the co-sorption of oxyanions like phosphate, sulfate and

carbonate with various divalent metals (including Fe(II)) on Fe(III)-oxide substrates,[98–104,113–115] and have been suggested to occur during co-sorption of Co(II) and Se(IV) (as the selenite oxyanion SeO_3^{2-}) onto γ-Al_2O_3.[116,117] If similar As(V)-Fe(II) ternary surface complexes are formed to a significant extent in our systems, they do not induce a major change in the interaction of As(V) with the Al-oxide surface, as shown by the As EXAFS data (Figure 3.4; Table A2.2). This suggests that they are either ligand-bridged (i.e. arranged as γAl_2O_3-As(V)-Fe(II)) or involve lateral interactions between adsorbed Fe(II) and As(V). Unfortunately, EXAFS spectroscopy is relatively insensitive towards detection of small numbers of second-neighbor atomic scatterers, especially if the coordination is relatively disordered, making identification and characterization of ternary surface complexes difficult with this technique.[98] Application of IR measurements would be useful in resolving the potential importance of ternary complexes in these systems.

The sorption of Fe(II) is slower in the ternary experiments with the two lower As(V) (0.10 and 0.25 mM) than in the binary Fe(II)/γ-Al_2O_3 experiment (Figure 3.1b), although the main mode of Fe(II) retention in the ternary systems remains the precipitation of Fe(II)-Al(III)-LDH (Figure 3.3). The Fe EXAFS data demonstrate that As(V) noticeably slows down the formation of secondary Fe(II)-Al(III)-LDH (Figure 3.3; Table A2.1), explaining the slower rate of Fe(II) sorption observed macroscopically. These results resemble those of Boyle-Wright et al.[117], who similarly observed that the precipitation of Co(II)-Al(III)-LDH during Co(II) interaction with γ-Al_2O_3 is hindered by the presence of Se(IV), a strongly sorbing oxyanion, as a co-sorbate. The inhibitive effect of As(V) on LDH precipitation may result from: (i) interaction of As(V) with growing

Fe(II)-Al(III)-LDH crystallites slowing down their growth; or (ii) interference of As(V) with the release of Al from the Al-oxide sorbent limiting the supply of Al available for Fe(II)-Al(III)-LDH precipitation. The As EXAFS data (Figure 3.4; Table A2.2) show no evidence for interaction of As(V) with Fe(II)-Al(III)-LDH in the ternary samples, but instead suggest that As(V) predominantly forms inner-sphere adsorption complexes at the Al-oxide surface. We therefore deem interference of As(V) with the Al supply required for precipitation of Fe(II)-Al(III)-LDH phases the more likely cause of their relatively slow growth in the ternary samples.

The presence of As(V) may inhibit the release of Al from the Al-oxide sorbent through two main mechanisms: (i) by blocking surface sites where Al release occurs through formation of inner-sphere surface complexes; and/or (ii) by forming As(V)-Al(III) precipitates that compete with the precipitation of Fe(II)-Al(III)-LDH phases as a sink of Al. The mechanism of surface site blocking has been demonstrated in studies with ferrihydrite, a metastable Fe(III)-oxide mineral, where the presence of adsorbed As(V) inhibited mineralogical transformation by inhibiting dissolution and re-precipitation of Fe(III).[e.g. 118–121] Boyle-Wight et al.[117] suggested scavenging of Al(III) through formation of Se(IV)-Al(III) inner-sphere complexes or precipitates as a likely cause of the inhibitive effect of Se(IV) on Co(II)-Al(III)-LDH precipitation in Co(II)/Se(IV)/γ-Al_2O_3 sorption experiments. D'Espinose de la Caillerie et al.[122] observed that γ-Al_2O_3 dissolution was promoted by reaction with Ni(II) and Co(II) at pH 7.0-8.2 forming Ni(II)- and Co(II)-Al(III)-LDH precipitates, and suggested that adsorbed divalent metal cations may weaken structural Al-O bonds thereby accelerating the dissolution of the γ-Al_2O_3 sorbent. Based on this argument, blocking of surface sites by As(V) may reduce the extent of Fe(II)

surface complexation and thereby the rate of Al release and Fe(II)-Al(III)-LDH formation. Precipitation of As(V)-Al(III) phases was proposed by Arai and Sparks[112] as an explanation for the increased resistance of As(V) to desorption during long-term aging in γ-Al_2O_3 suspensions. Our As EXAFS data show no discernable change in As(V) speciation over the duration of the experiments (Figures 3.4 and A2.4-A2.7; Table A2.2), implying that any arsenate-aluminum phases formed either are present at concentrations too low to be detected by bulk EXAFS, or have an As-Al coordination similar to that of the inner-sphere As(V) adsorption complexes on the Al-oxide surface. Resolving the mechanism of As(V) interference with Al release will require detailed additional characterization of the As(V) interaction with Al-oxide substrates, particularly with respect to the potential role of As(V)-Al(III) precipitates as a long-term sink of As(V).

Fe(II)-Al(III)-LDH phases do not form in the ternary experiment with the highest level of As(V) co-addition (0.5 mM; Figure 3.3). The Fe speciation in this system is otherwise, however, poorly constrained by the Fe EXAFS results because of the absence of well-defined scattering from second-shell atomic neighbors (Figure A2.3b). The data do not resemble that of the reference Fe(II)-As(V) precipitate (Figure A2.3), which suggests that formation of such phases does not occur. This is corroborated by the As *K*-edge EXAFS data demonstrating that arsenate is dominantly adsorbed onto the γ-Al_2O_3 surface with no evidence to suggest precipitation with Fe(II) (Figure 3.4; A2.9d). From these results, we infer that Fe(II) most likely is present as mononuclear surface species, a conclusion that is consistent with the relatively fast Fe(II) sorption kinetics observed macroscopically (Figure 3.1b). The lack of distinct second-neighbor scattering points to a disordered average local coordination around adsorbed Fe(II), suggestive of the existence

of multiple coordination environments. The concentration of Al surface sites in the system is estimated at 1.35 mM based on the specific surface area of the γ-Al_2O_3 sorbent (70.5 m^2 g^{-1}), the γ-Al_2O_3 suspension density (5.0 g L^{-1}) , and an assumed surface site density of 2.3 sites nm^{-2}.[123] This concentration is similar to the sum of the concentrations of aqueous As(V) and Fe(II) removed from solution in this ternary system, where 0.5 mM of aqueous As(V) is removed from solution (Figure 3.2d) and ~0.75 mM of aqueous Fe(II) is sorbed (Figure 3.1b). This suggests a crowded surface where ternary interactions between sorbate Fe(II) and As(V) are likely, and polynuclear species may form. We speculate that adsorbed Fe(II) may be simultaneously engaged in interactions with Al-oxide surface sites and in ternary interactions with sorbed As(V) and/or Fe(II), resulting in a mixture of different surface species. The absence of Fe(II)-Al(III)-LDH precipitation in this high [As(V)] system may be the combined result of the apparent interference of As(V) with the Al supply needed for LDH formation (as discussed above), and the favorable conditions established by adsorbed As(V) for Fe(II) surface complexation through surface electrostatic changes and ternary interactions. Clearly, additional work is required to determine the Fe(II) surface speciation in this ternary system in more detail. Despite this uncertainty, the results unambiguously demonstrate that As(V) induces a major change in the speciation of sorbed Fe(II) relative to the As(V)-free system and the ternary system with the two lower As(V) additions. Such impacts need to be understood for accurate prediction of the geochemical fate of aqueous Fe(II) and the importance of Fe(II) precipitation in suboxic and anoxic geochemical environments.

3.5 Environmental Implications

The results presented here demonstrate the potential importance of mutual interactions between released Fe(II) and As(III) or As(V) in controlling the solubility and speciation of these species in reducing environments. We show that Fe(II) promotes the adsorption of As(V) onto the Al-oxide surface, while the retention of As(III) is unaffected by the presence of Fe(II). In turn, the precipitation of secondary Fe(II)-Al(III)-LDH phases during Fe(II) sorption proceeds unaffected by the presence of As(III), but slows down at low levels of As(V), and shuts down in systems with high As(V) concentrations, where Fe(II) surface complexes are formed instead. The observed effects of As valence imply that impacts of co-sorption likely will be minimal in highly reducing environments such as deep groundwaters containing reduced As(III), whereas strong impacts are expected in suboxic systems such as riparian soils containing As(V). The mutual interactions (or lack thereof) between Fe(II) and arsenic sorbates characterized here are critical to the development of qualitative and quantitative models of the speciation and fate of these species in reducing environments. Our results suggest that other environmental factors including pH and the presence of phosphate and natural organic matter are likely to impact Fe(II) precipitation in suboxic environments. Due to the resemblance in chemical properties of arsenate and phosphate, phosphate may exert a similar influence on Fe(II) sorption as observed here for arsenate. Organic substances have a high affinity for Al complexation, and may limit Al availability for Fe(II)-Al(III)-LDH precipitation. Solution pH impacts the solubility of Fe(II)-Al(III)-LDH and Al-oxide, and affects the extent of As sorption with the Al-oxide surface, which may impact Al availability based on the current results. Additional work is needed to address these issues.

3.6 Figures

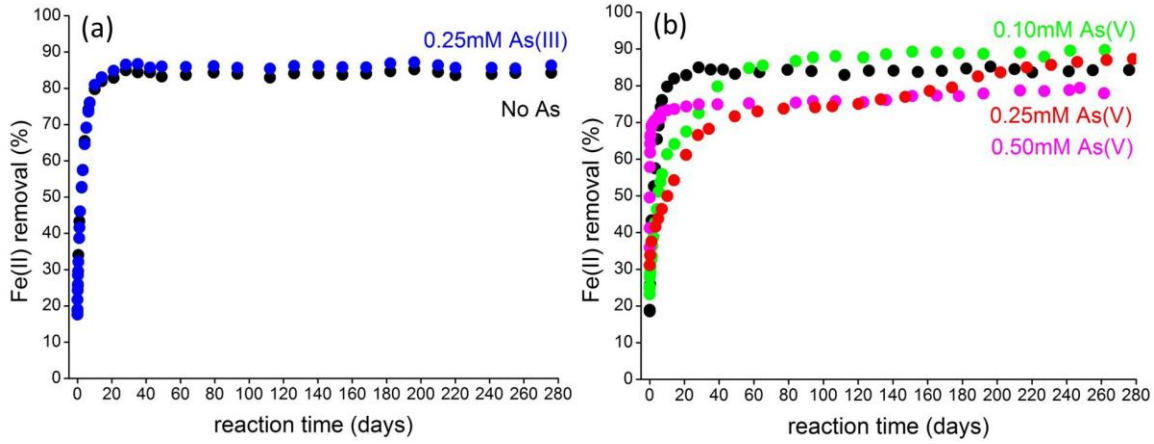

Figure 3.1. Fe(II) sorption kinetics in single-sorbate and dual sorbate experiments Kinetics of Fe(II) sorption in anoxic suspensions of 5.0 g L^{-1} γ-Al_2O_3 at pH 7.5 in single-sorbate and dual-sorbate experiments containing **(a)** As(III) and **(b)** As(V) at the concentrations indicated. The Fe(II) concentration was 1.0 mM in all systems.

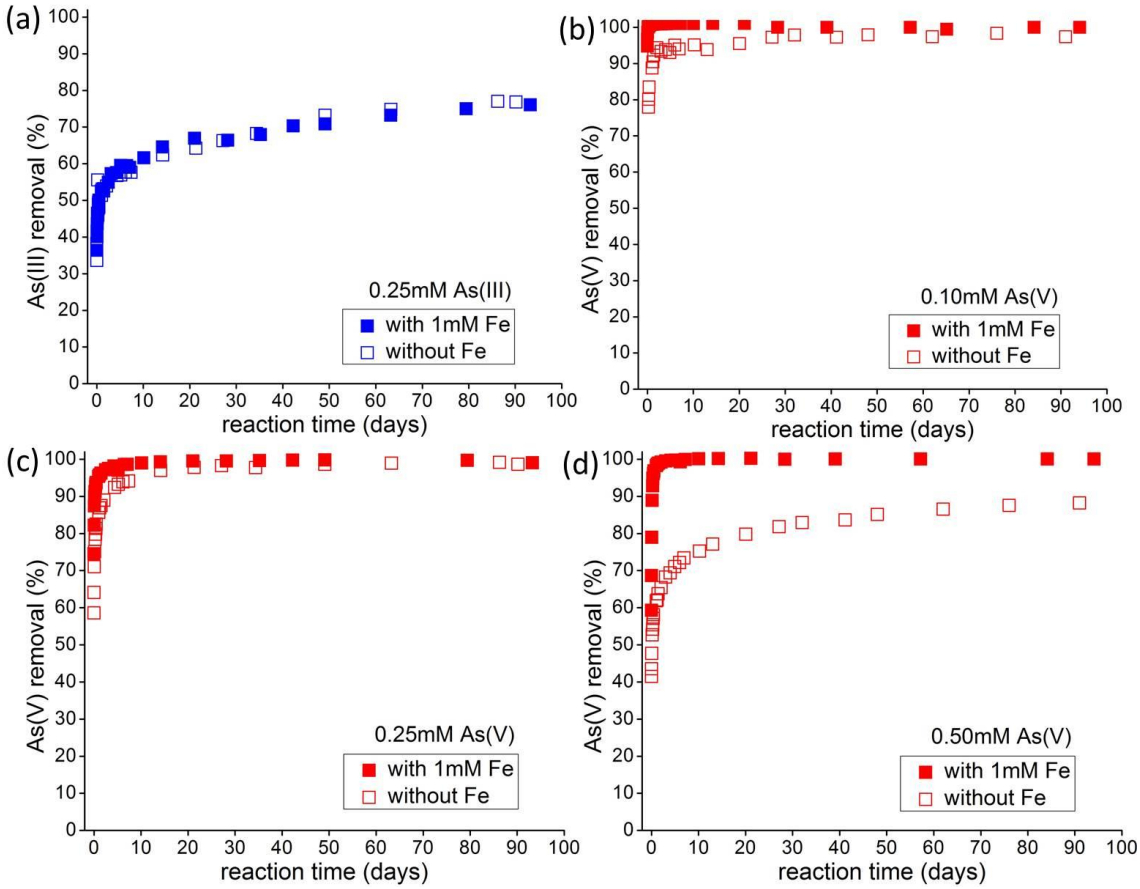

Figure 3.2. As(III/V) sorption kinetics in single-sorbate and dual sorbate experiments Kinetics of As sorption onto 5.0 g L^{-1} γ-Al_2O_3 at pH 7.5 in the presence and absence of 1.0 mM Fe(II), for **(a)** 0.25mM As(III); **(b)** 0.10 mM As(V); **(c)** 0.25 mM As(V); and **(d)** 0.50 mM As(V).

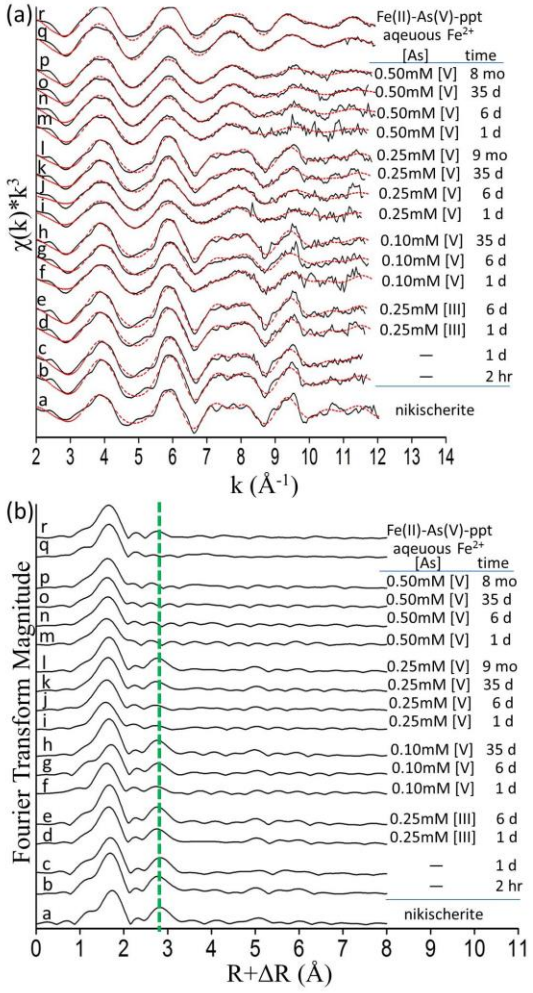

Figure 3.3. Fe *K*-edge EXAFS results of Fe references and sorption samples

Fe *K*-edge EXAFS data of Fe references and sorption samples from single-sorbate and dual-sorbate systems containing 1.0 mM Fe(II), reacted at variable As(III) and As(V) concentrations for reaction times up to 9 months: **(a)** k^3-weighted χ spectra; and **(b)** corresponding radial structure functions (RSFs). Solid and red dotted lines in panel (a) represent raw and fitted spectra, respectively. Green vertical dashed line in panel (b) locates second-shell Fe-Fe/Al backscatters in the nikischerite and Fe(II) sorption samples, and second-shell Fe-Fe/As backscatter in Fe(II)-As(V) precipitate. The fit results are summarized in Table A2.1.

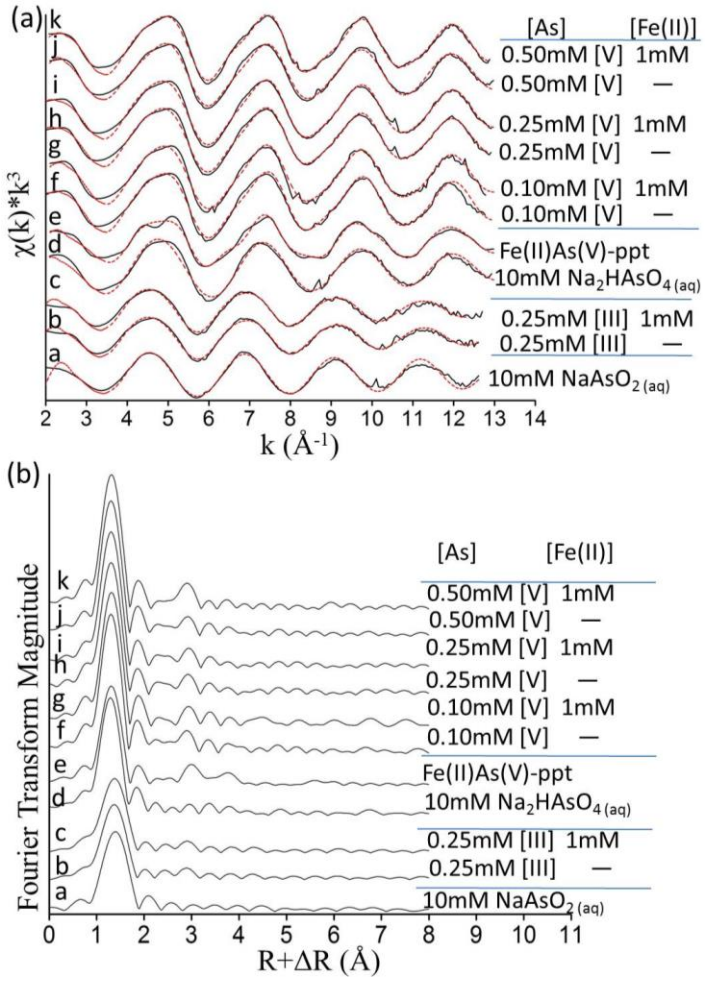

Figure 3.4. As *K*-edge EXAFS results of As references and sorption samples

As *K*-edge EXAFS spectra of As reference and sorption samples from single-sorbate systems and dual-sorbate systems containing 1.0 mM Fe(II). The reaction time of the sorption samples was 6 days. **(a)** k^3-weighted χ spectra and **(b)** corresponding radial structure functions (RSFs). Solid and red dotted lines in panel (a) represent raw and fitted spectra, respectively. The red dotted line panel b locates second-shell Al neighbors in the As(V) and As(III) sorption samples. The fit results are summarized in Table A2.2.

Chapter 4: Effects of Humic Substances on Fe(II) Sorption onto Clay and Aluminum Oxides Substrates

Abstract

Sorption of Fe(II) onto 0, 1 ,4 wt% humic acid (HA) pre-coated γ-Al_2O_3 or clay and cosorption of Fe(II) and 0, 4 wt% humic acid(HA) or fulvic acid (FA) onto γ-Al_2O_3 at pH 7.5 were studied, using batch kinetic sorption experiments and synchrotron EXAFS analyses. The impacts of humic substances(HS) on Fe(II) sorption behavior depended on sorbent types, HS type and addition sequence. In Fe(II) reacted Al-oxide systems, the presence of HS slowed down Fe(II) sorption kinetics by hindering the formation of Fe(II)-Al(III)-layered double hydroxide (LDH) phases, with greater impact observed during Fe(II)&HS cosorption experiments compared to HS pre-coated experiments. During cosorption reactions, FA exhibited larger inhibitive effects than HA on Fe(II) sorption kinetics during initial reaction stage. In Fe(II) reacted clay systems, the presence of HA coating dominantly inserted thermodynamic effects by altering main Fe(II) sorption product from Fe(II)-Al-LDH to Fe(II)-phyllosilicate. The interference of humic substances with Fe(II) sorption onto mineral substrates was associated with Al dissolution capability of mineral substrates, HS masking effect on substrate surface and HS formation of organo-Al complex limiting the Al availability to incorporate in the octahedral layer of Fe(II)-Al(III)-LDH phase. This study explores the role of humic substances on Fe(II) sequestration onto mineral substrate. The formation of secondary Fe(II) precipitates even at relatively high organic matter contents suggests the importance of these phases in determining Fe fate and transport in anoxic and suboxic soils and sediments.

4.1 Introduction

Metal-oxides and clay minerals are considered to be important sink for metal(loid)s sequestration through various sorption mechanisms, and thus affect the speciation, solubility, mobility and bioavailability of metals.[124,125] Metal sorption behavior at mineral-water interface is affected by several factors such as chemical properties of metals, sorbent type, presence of other chemical substances, reaction time, surface loading, pH and ionic strength. Compared to adsorption process, surface induced precipitation which involves (i) ion adsorption on the mineral surface, (ii) surface nucleation and (ii) crystal growth, induces slower sorption kinetic and more stable form of sequestered metals.[2,126] Thus understanding of the sorption mechanisms helps properly predict the fate of metals in geochemical environment.

The formation of secondary precipitates such as layered double hydroxides (Me(II)-Al(III)-LDH) and phyllosilicate during divalent metal sorption onto Al-bearing mineral substrates has been intensively studied and identified as a significant sequestration pathway for divalent metal ions such as Co(II), Zn(II), Ni(II) and Fe(II) at near-neutral pH.[17–30,39,40,44,45,90,127] Results from our previous work have demonstrated the formation of Fe(II)-Al(III)-LDH and poorly crystalline Fe(II)-phyllosilicate upon aqueous Fe(II) sorption on Al-oxide, clay and amorphous silica at pH >7.0.[17,90] During Fe(II) cosorption with arsenic (As(III)/ As(V)) on Al-oxide at pH 7.5, Fe(II) sorption behavior is not affected by the presence of As(III), while formation of Fe(II)-Al(III)-LDH precipitate is hindered at low As(V) concentration and inhibited at high As(V) concentration. It is suggested that the formation of secondary Fe(II) precipitate is likely to be affected by the heterogeneous components of soil and sediment environments.

Natural organic matters particularly humic substances (HSs) occur ubiquitously in all terrestrial and aquatic environments.[128] Organic compounds could potentially affect metal sorption onto mineral by forming organo-metal complexes with aqueous metal ions, adsorbing on the mineral surfaces,[128,129] and/or forming metal-bridging (Type A) and/or ligand-bridging (Type B) ternary surface complexes.[51,130,131] Previous studies have suggested that HSs (i.e. humic acids (HA) and fulvic acids (FA)) and relevant low-molecular-weight organic compounds affect divalent metal ions sorption kinetics and mechanisms onto Al-bearing minerals under various reaction conditions.[31,48–51,132] In particular, presence of organic compounds was demonstrated to slow down or inhibit the precipitate formation of Me(II)-Al(III)-LDH during divalent Zn(II) and Ni(II) ions sorption onto Al-bearing substrates at neutral to alkaline pH. [31,48–51] Surface induced Ni-Al-LDH formation was inhibited in the presence of high organic content, and Ni adsorption complexes and $Ni(OH)_2$ precipitates formed instead.[31,48,49] Li reported that addition of glyphosate (GPS) suppressed the formation of Zn-Al-LDH on γ-alumina, but the formation of GPS ligand bridging ternary surface complex was found instead.[51]

The objective of this work is to study how the presence of humic substances affects the kinetics and mechanisms of Fe(II) sorption onto Al-oxide and clay minerals under reaction condition favorable to secondary Fe(II) precipitate formation. Both Fe(II) sorption onto HS pre-coated Al-bearing minerals and Fe(II) cosorption with HS onto Al-bearing minerals experiments were conducted, in order to comprehensively study the effects of HS on the secondary Fe(II) precipitate process. The results of this study will increase our understanding of the role of natural organic matter on the formation of secondary Fe(II) precipitate under anoxic geochemical environment.

4.2 Material and Methods

4.2.1 Materials and anoxic settings

The mineral sorbents used in this study were (i) γ-Al_2O_3 (Cat. No. 39812) purchased from Alfa Aesar, and (ii) synthetic mica-montmorillonite (Syn-1 clay) purchased from Clay Minerals Repository.[55] The syn-1 clay was treated to obtain <1 μm size fraction with interlayer saturated with Na^+, through the process of sedimentation, sodium saturation, dialysis for excess salts and freeze-drying. The specific surface areas measured by N_2-BET method were 70.5 and 124.6 for γ-Al_2O_3 and clay, respectively. The organic compounds used here were Suwanee River humic acid standard II and Suwanee River fulvic acid standard obtained from International Humic Substances Society.

Due to the sensitivity of aqueous Fe(II) to oxidation at neutral pH and higher, the sorption experiments were conducted in an anaerobic glovebox using the protocols applied in our previous studies.[17,90] Anoxic background electrolyte composed of 0.1 M NaCl and buffered to pH 7.50 with 50 mM HEPES was prepared inside the glovebox using boiled and $N_{2(g)}$ purged DDI water.

4.2.2 Coating procedure

The Al-oxide and clay sorbents used for pre-coated sorption experiments were coated with humic acid (HA) at varying content of HA (1 or 4 wt % with respect to the mass of mineral) following a procedure modified from Nachtegaal and Sparks.[31] For each coated mineral sample, appropriate amount of humic acid was firstly dissolved into 60mL of 0.05M NaOH solution, followed by adjusting solution pH to 7.50 using 1.0 M HCl. The HA solution was then mixed with 0.625g mineral sorbent followed by titrating pH to 3.50. The HA-mineral mixture was placed on a reciprocal shaker for two days. The HA coated

mineral was then separated from the solution through centrifugation. The resulted paste was washed and dispersed in 10 mL prepared background electrolyte using a sonifier. The suspension was transferred inside the glovebox and brought to 125 mL using the anoxic background electrolyte mentioned above, in order to achieve 5g L^{-1} γ-Al_2O_3 or clay concentration. The HA coated mineral suspension was hydrated for 2 days prior to Fe(II) addition. Blank clay and γ-Al_2O_3 suspensions (0 wt % HA) were also prepared as the same manner but without addition of humic acid.

4.2.3 Batch kinetic experiments

Two major types of kinetic experiments were performed: (i) Fe(II) sorption onto humic acid (0, 1, 4 wt %) pre-coated mineral sorbents (clay or γ-Al_2O_3); (ii) Fe(II) and HS (4 wt % HA or FA) cosorption onto uncoated γ-Al_2O_3. Mass of mineral sorbents was 5 g L^{-1} in all reactions. For the type i experiments (denoted as Fe(II)/[γAl_2O_3-HA] and Fe(II)/[clay-HA], and referred to as "pre-coated samples"), 2.7 mM Fe(II) was injected using acidified 1 M $FeCl_2$ stock solution to 0, 1, 4 wt% HA pre-coated γ-Al_2O_3/ Clay suspensions, prepared as described above. Fe(II) reacted 0 wt% HA coated γ-Al_2O_3/ Clay samples were deemed as control samples for type i experiment. For the type ii experiments (denoted as Fe(II)&HA/[γAl_2O_3] and Fe(II)&FA/[γAl_2O_3], and referred to as the "cosorption samples"), 0.625 g γ-Al_2O_3 was directly suspended in 125 mL anoxic background electrolyte and hydrated for 2 days prior to simultaneous injection of 2.7 mM Fe(II) and 0.2 g L^{-1} (=4 wt % in respective to the mass of sorbents) HA or FA prepared by dissolving 25 mg HA or FA in 1.5 mL 0.05 M NaOH. Blank sample for type ii experiments was run by only spiking 2.7 mM Fe(II) into the anoxic suspension of γ-Al_2O_3.

The γ-Al_2O_3 reaction suspensions were sampled regularly over the course of 120 days by filtrating 5mL aliquot through a 0.22 μm nitrocellulose membrane and filtrates were collected into a polyethylene tube containing 125 μL concentrated HCl. As direct filtration could not be done, sampling of clay suspensions started with centrifugation using airtight centrifuge tube before transferring suspensions back into the glovebox for supernatant filtration. The acidified filtrates were analyzed for Fe(II) concentration using ferrozine method,[57] and the sorption level was calculated as the difference between Fe(II) initial and remaining solution concentrations.

4.2.4 XAS studies

XAS samples were prepared under the same reaction conditions as described above for the kinetic experiments. For each reaction system, samples were taken at different time points varying from 7 days to 158 days for XAS analysis. XAS sorption sample preparation involved terminating sorption reaction by separating the mineral solid from the solution by centrifugation, and sealing wet pastes into lucite sample holders with Kapton tape. Reference Fe(II) compounds for XAS analysis included: (1) aqueous Fe(II), (2) nikischerite ($NaFe^{II}_6Al_3(SO_4)_2(OH)_{18}(H_2O)_{12}$), (3) Fe(II) reacted humic acid solution, (4) Fe(II) reacted fulvic acid solution, (5) Fe(II) sorption samples on clay at pH 8.0 and on amorphous silica at pH 7.5 and 8.0. The preparation and source of $Fe(II)_{(aq)}$ and nikischerite references were described in our previous work.[90] Fe(II)-HS solutions were prepared by mixing 10 mM Fe(II) with 1500 mg L^{-1} HA or FA in the same background electrolyte as used in sorption reactions. The reference spectra of Fe(II)-reacted clay or amorphous silica sorption samples were from our previous work.[90]

Synchrotron Fe *K*-edge (7112 eV) spectra were collected on beamline X-11A of the National Synchrotron Light Source at Brookhaven National Laboratory, and beamline 12-BMB of the Advanced Photon Source at Argonne National Laboratory. The anoxic protocols used for XAS sample preparation and transport are described in our previous study.[90] The XAS data collection procedures were identical to that employed previously.[90] Potential Fe(II) oxidation in samples caused by beamline damage was not observed in this study, as checked by visual inspection and comparing the normalized first and last scans of each sample. EXAFS data analysis and fitting were conducted with WINXAS3.1[58], combined with Feff 7.0[59] and ARTEMIS.[60] Detailed information about EXAFS data fitting routines for Fe reference and sorption samples is provided in Appendix 3.

4.3 Results

4.3.1 Macroscopic kinetic experiments

Figure 4.1 presents Fe(II) sorption kinetics upon (1) Fe(II) sorption onto HA (0, 1, 4 wt%) coated γ-Al_2O_3, (2) Fe(II) and HA/FA (0, 4 wt%) cosorption onto γ-Al_2O_3, (3) Fe(II) sorption onto HA (0, 1, 4 wt%) coated clay, under anoxic reaction conditions at pH 7.5. The kinetic patterns vary distinctly with organic type, concentration, additions sequence and mineral substrate. Consistent with our previous results,[17,90] Fe(II) sorption in organic free γ-Al_2O_3 suspension shows biphasic kinetics behavior, with rapid Fe(II) uptake during the first hours of reaction followed by a slower removal stage continuing for ~40 days when equilibrium is reached (Figure 4.1a). A similar pattern is observed for the HA-coated samples; but at an overall lower extent of Fe(II) sorption over most of the experimental reaction time frame. In addition, the presence of the HA coating on the γ-

Al_2O_3 surface extends the length of the slower sorption stage to ~120 days, and appears to lower the final amount of Fe(II) sorbed in the 4% HA system (Figure 4.1a). The HA addition sequence (pre-coated on γ-Al_2O_3 vs co-sorbed with Fe(II) onto γ-Al_2O_3) has a strong effect on the Fe(II) sorption kinetics. While Fe(II) sorption in the HA pre-coated γ-Al_2O_3 system stabilizes within the time scope investigated here, Fe(II) sorption in the Fe(II)&HA/FA cosorption system is still ongoing after 120 days (Figure 4.1a). The type of humic substance added impacts the kinetic results as well. The amount of Fe(II) uptake is generally lower in the Fe(II)-FA cosorption samples than in the Fe(II)-HA cosorption samples during the first 80 days of reaction, followed by Fe(II) sorption levels merging at later reaction stage (Figure 4.1a).

In contrast to the γ-Al_2O_3 experiments, Fe(II) sorption does not reach equilibrium in any of the clay systems within the 120-day reaction time frame (Figure 4.1b). This finding is consistent with our previous study where slowly continuing Fe(II) sorption onto clay was observed under similar conditions as used here.[90] Similar to the γ-Al_2O_3 systems, the presence of a HA coating on the clay surface affects the Fe(II) sorption pattern. While no discernible impact of 1% HA coating is seen, 4% HA coating has impact on lowering the sorption extent throughout the reaction time frame up to 120 days (Figure 4.1b). In general, kinetic data shown in Figure 4.1 indicates significant impact of humic substances during Fe(II) interaction with mineral substrates. Spectroscopic data discussed below is expected to assess the mechanisms behind these macroscopic sorption trends.

4.3.2 EXAFS data

Fe K-edge EXAFS data of reference and sorption samples with varying organic content, type, addition sequence and reaction time, for γ-Al_2O_3 and clay systems are displayed in Figure 4.2 and Figure 4.3 respectively, with panel a showing the raw and fitted k^3-weighted χ spectra, and panel b showing the corresponding radial structure functions (RSFs) obtained from Fourier transformation of the raw χ data. The fit results are summarized in Table 4.1.

The RSFs of the references and sorption samples exhibit a peak at ~1.6 Å (uncorrected for phase shift), which is due to the backscattering of first-shell O neighbors (Figure 4.2b and 4.3b). This shell is fitted with 5.1-6.1 O atoms at a radial distance of 2.09-2.13 Å, consistent with octahedral coordination of Fe(II) by first-shell O atoms, as in the $Fe^{2+}_{(aq)}$, β-$Fe(OH)_2$ and nikischerite references (Table 4.1).[17,65–68] Except for $Fe^{2+}_{(aq)}$, Fe^{2+}-$HA_{(aq)}$, Fe^{2+}-$FA_{(aq)}$ references, RSFs results of other references and all sorption samples show a second peak at ~2.8 Å (uncorrected for phase shift), which is due to the backscattering of second neighbor atoms and thus indicates the formation of Fe(II) precipitate in all Fe(II) sorption samples (Figure 4.2b and 4.3b). The spectra of Fe^{2+}-$HA_{(aq)}$, Fe^{2+}-$FA_{(aq)}$ references are similar to that of aqueous Fe^{2+} (Figure 4.2, spectra m-o), with no shell observed beyond the first O shell, nor a Fe-C path fitted (Table 4.1) for these two references. The lack of distinct features in the XAS data of the Fe(II)-HS solutions complications assessment of the complexation between aqueous Fe(II) and dissolved HA and FA. Aqueous Fe(II) may not form aqueous complexes with HA/FA to a significant extent, or engage in weak outer-sphere complexation with the organic molecules. Alternatively, inner-sphere Fe(II)-HA/FA complexation may occur, but

second shell scattering may not be discernible due to the weak backscattering from (light) C, and/or a large degree of structural disorder in the coordination of Fe(II) to HA and FA molecules. Future study is needed to further investigate the extent and mechanisms of Fe(II)-HS complexation.

The k^3-weighted χ spectrum of Fe(II) reacted γ-Al_2O_3 in control system (no HA/FA) is similar to that of nikischerite (Figure 4.2a, spectra a and i), indicating Fe(II)-Al(III)-LDH as the main Fe(II) sorption product in this sample. This finding agrees with our previous results, where precipitation of Fe(II)-Al(III)-LDH was identified as the main Fe(II) sorption mechanism during interaction of Fe(II) with Al-oxide and clay substrates under similar reaction conditions as applied here.[17,90] The second-shell RSF feature is fitted using Fe-Fe and Fe-Al backscattering paths at a radial distance of 3.15 Å (Table 4.1), which is consistent with the structural data of nikischerite[66] and much shorter than the 3.26 Å Fe-Fe distance of β-$Fe(OH)_2$ due to the contraction caused by Al^{3+} substitution of Fe^{2+} in the Fe octahedral sheet (Table 4.1). The resulted precipitate of Fe(II)-Al(III)-LDH is composed of positively charged Fe/Al brucite-like sheets with 2:1 Fe to Al ratio, and the positive charge is neutralized by interlayer Cl^- anions of the background electrolyte.[17,66,90]

The EXAFS data and fitting results of Fe(II)/[γAl_2O_3-HA] sorption, Fe(II)&HA/[γAl_2O_3] and Fe(II)&FA/[γAl_2O_3] cosorption samples show the formation of Fe(II)-Al(III)-LDH in all these reaction systems (Figure 4.2, spectra b-k; Table 4.1). The rate of precipitation is however strongly affected by HA and FA. Fe(II) interaction with γ-Al_2O_3, pre-coated with HA results in the formation of a well-developed Fe(II)-Al(III)-LDH within 7-day reaction, as shown by the EXAFS results (spectra f and i in Figure

4.2a). In contrast, the resulted Fe(II)-Al(III)-LDH is still growing for the 7-day cosorption samples with 4% HA or FA addition, with increasing intensity of second shell scattering from Fe and Al neighbors observed (Figure 4.2b, spectrum b-e). The slower growth of Fe(II)-Al(III)-LDH in the cosorption systems compared with the HA precoated γ-Al_2O_3 systems agrees macroscopic data showing that the cosorption samples have much slower Fe(II) sorption than the other samples (Figure 4.1a). These findings suggest that the organic addition sequence has distinct impact on the formation rate of Fe(II)-Al(III)-LDH during Fe(II) sorption process onto Al-oxide substrate.

The presence of HA coatings on the clay surface has a significant impact not only on the kinetics of Fe(II) sorption, but also on the type of Fe(II) sorption product formed. For the Fe(II)/clay sorption sample without HA coating, the EXAFS data and fitting results are similar, though not identical, to that of nikischerite (Figure 4.3, spectra a-b; Table 4.1). In line with our previous results,[90] a truncated oscillation is seen at 7-8 $Å^{-1}$ in the k^3-weighted χ spectrum of Fe(II)/clay sorption sample(Figure 4.3, spectrum b), which has been shown to be a fingerprint feature to unequivocally identify Metal(II)-Al(III)-LDH precipitates from Metal(II) hydroxide and Metal(II)-phyllosilicate phases.[17,21,30] Additionally, attempt to fit second-shell Fe-Si backscattering to the Fe(II)/clay control sample was unsuccessful, which was used to fit other Fe(II) sorption samples onto HA pre-coated clay. These findings point to the formation of Fe(II)-Al(III)-LDH as the predominant sorption product in the HA free Fe(II)/clay system.

In contrast, the XAS spectra obtained from Fe(II)/[clay-HA] sorption samples with 1% and 4% HA content are quite similar to that obtained from Fe(II)/SiO_2 (at pH 7.5 and 8.0) and Fe(II)/clay (at pH 8.0) sorption references (Figure 4.3, spectra c-j). Based on

results from our previous study,[90] poorly crystalline Fe(II)-phyllosilicate predominantly forms in these three sorption references (Figure 4.3, spectra h to j). The fitting results show that second-shell Fe-Fe and Fe-Si radial distance of Fe/[clay-HA] sorption samples (3.19-3.20 Å and 3.25-3.30 Å) are similar to the distances observed in the three sorption references (Table 4.1) and that in minnesotaite (a 2:1 hydrous iron silicate) and greenalite (1:1).[72–74,90] Due to the substantial error associated with the coordination number derived from EXAFS analysis for second-shell Fe and Si atoms, detailed analysis of structure and composition of the formed precipitate is not possible. Based on these results, we conclude that Fe(II) sorption mechanism in the clay suspensions transitions from predominant Fe(II)-Al(III)-LDH formation in HA free systems to Fe(II)-phyllosilicate precipitation in HA coated clay system.

4.4 Discussion

4.4.1 Kinetic impacts of humic substances on Fe(II) sorption in Al-oxide system

The presence of humic substances lowers Fe(II) sorption rate and extent onto Al-oxide (Figure 4.1a), though the main Fe(II) sorption mode remains the precipitation of Fe(II)-Al(III)-LDH (Figure 4.1 and 4.2). The slower Fe(II) sorption observed in the kinetic experiments with the presence of humic substances is correlated with continuing precipitation of Fe(II)-Al(III)-LDH. The inhibitive effect of humic substances is more pronounced when HA/FA is added simultaneously with aqueous Fe(II) in cosorption system than that in Fe(II) sorptive reaction onto HA pre-coated Al-oxide (Figure 4.1a). This is well illustrated by the data obtained for Fe(II)&HA/FA cosorption sample onto γ-Al_2O_3, where continued Fe(II) uptake beyond 7 days is accompanied by distinct increase in the second-shell Fe-Fe and Fe-Al backscattering (Figure 4.2b, spectra b-e). Present

results are in good agreement with findings from previous studies where suppression of Me(II) (e.g. Ni(II) and Zn(II)) sorption kinetics and Me(II)-Al(III)-LDH precipitate is observed when organic compounds interact with the sorptive reaction. [31,48–51,132] Nachtegaal and Sparks reported that formation of Ni(II)-Al(III)-LDH was found with 1 wt% HA coated kaolinite, however was absent with high (5 wt%) HA coated kaolinite and Ni-hydroxide was formed instead. It is possible that formation of Fe(II)-Al(III)-LDH could be fully prevented with organic content being high enough in our systems. Further systematic studies investigating the threshold of organic content prohibiting Fe(II)-Al(III)-LDH formation and the resulted Fe(II) sorption end-product are needed.

The presence of organic substances predominantly affects the Fe(II) sorption kinetics onto γ-Al_2O_3, by competing with Fe(II)-Al(III)-LDH for free Al availability through forming organic complexation with Al^{3+}. This process can explain the substantial slower Fe(II) sorption rate observed in Fe(II)& 4%HA cosorption experiment than that in Fe(II) sorption experiment with 4% HA precoated Al-oxde (Figure 4.1a). In the Fe(II)&HA cosorption experiment with simultaneous addition of HA and $Fe^{2+}_{(aq)}$, formation of HA-Al complexation competes with Fe(II)-Al(III)-LDH for aluminum. Whereas in the HA pre-coated Al-oxide system, sufficient Al is released from the coated Al-oxide prior to Fe(II) injection and readily available for Fe(II)-Al(III)-LDH formation. In addition, larger inhibitive effect of FA than HA on Fe(II) sorption before 100 days (Figure 4.1a) in the cosorption experiments can be explained by possibly stronger organo-Al complex formation by FA, as FA has higher charge density and more carboxyl and phenolic content served as available surface sites for metal complexation compared to HA.[133] As more Al is complexed with FA, less Fe(II)-Al(III)-LDH forms due to the

limited Al availability in the Fe&FA cosorption system. At later reaction stage (>100 days), more Al becomes available via dissolution from Al-oxide substrate, the influence of organo-Al complexation on Al availability becomes minimum and thus the difference in Fe(II) sorption extent between the two cosorption experiments disappears (Figure 4.1a). Besides forming organo-Al complex, other inhibitive mechanism of HS on Fe(II) sorption may also exist, such as adsorbed HS masking onto mineral surface where Al releases. Schulthess and Huang suggested that organics including HA formed strong adsorption by the Al sites on the Al-oxide.[134] D'Espinose de la Caillerie et al. showed that the dissolution of γ-Al_2O_3 was promoted by reaction with Ni(II) and Co(II) forming Me(II)-Al(III)-LDH phases and suggested that adsorbed Me(II) may weaken the structural Al-O bonds thereby enhancing the γ-Al_2O_3 dissolution.[122] Here in the Fe(II) reacted HA coated γ-Al_2O_3 samples, masking of surface sites by HA coating may reduce Fe(II) forming complexes with surface Al and thereby the rate of Al release and Fe(II)-Al(III)-LDH formation. Consequently, it takes longer for Fe(II) to reach sorption equilibrium on HA precoated γ-Al_2O_3.

Due to the presence of structurally similar Fe(II)-Al(III)-LDH as the end-product in all Fe(II) reacted Al-oxide systems regardless of the presence of humic substances (Figure 4.2; Table 4.1), the Fe(II) concentrations at equilibrium are expected to be similar among all sorption samples. Assuming 2:1 Fe(II)/Al(III) ratio in the octahedral Fe/Al sheet and the positive charge of the sheet balanced by Cl^- anions from the background electrolyte, the aqueous chemical equilibrium of the Fe(II)-Al(III)-LDH phase can be expressed as: $Fe(II)_{\frac{2}{3}}Al(III)_{\frac{1}{3}}(OH)_2Cl_{\frac{1}{3}(s)} = \frac{2}{3}Fe^{2+} + \frac{1}{3}Al^{3+} + 2OH^- + \frac{1}{3}Cl^-$.[90] The pH

is fixed, and activity of Al and Cl are set by the Al-oxide sorbent and 0.1 M NaCl from background electrolyte respectively in all systems. Thus, the same endpoint of Fe(II) concentration will be ultimately reached in all systems if the formed LDH phases are not affected by the humic substances. Therefore, the Fe(II) sorption will be most likely to equilibrate at the same level as in HA/FA free Fe(II)/γ-Al_2O_3 system within a timeframe longer than applied here, though the simultaneously added HS in cosorption samples significantly slows down LDH formation during the process of reaching equilibrium. In the 1 wt% HA pre-coated γ-Al_2O_3 system, Fe(II) sorption eventually reaches same equilibrium level as in the HA/FA free system after long slower sorption stage up to 120 days (Figure 1). And in the 4 wt% HA pre-coated γ-Al_2O_3 system, the Fe(II) sorption extent is also relatively similar to that in the control sample (81% vs. 88%). The slight drop in Fe(II) sorption level at equilibrium may be due to the different thermodynamic properties of the formed secondary Fe(II)-Al(III)-LDH phase, e.g., smaller particle size or a lower structural Al content, which lead to the higher Fe(II) solubility and is difficult to be detected by the EXAFS method applied here.

4.4.2 Thermodynamic effects of humic acid on Fe(II) sorption in clay system

In contrast to Al-oxide system, the presence of HA coating on clay primarily inserts thermodynamic effects by changing the main Fe(II) sorption product from Fe(II)-Al-LDH to Fe(II)-phyllosilicate phase. The secondary Fe(II) precipitates form within 7 days in all clay systems at pH 7.5, with Fe(II)-Al(III)-LDH formed in HA free Fe(II)/clay sorption sample and poorly crystalline Fe(II)-phyllosilicate formed in Fe(II) reacted HA coated clay samples (Figure 4.3; Table 4.1). The formed Fe(II)-phyllosilicate phase is similarly observed upon Fe(II) sorption onto amorphous silica at pH 7.5 and 8.0 and onto clay at

pH 8.0, suggesting no or little structural Al in the formed Fe(II)-phyllosilicate precipitate (Figure 4.3). The presence of HA coating prevents the Fe(II)-Al(III)-LDH formation and otherwise promotes interlayer silification leading to the formation of Fe(II)-phyllosilicate, which is supposed to form at higher pH of 8.0 in the Fe(II)/clay system. Thus, the Fe(II) kinetic patterns in HA coated samples are correlated with the growth of Fe(II)-phyllosilicate. The generally lower Fe(II) sorption level observed in the 4% HA coated clay system compared to the 1% HA coated clay system (Figure 4.1b) suggests smaller amount of Fe(II)-phyllosilicate formed, which is most likely attributed to the making effect of HA coating on clay surface preventing Si dissolution and thus reducing Si availability for Fe(II)-phyllosilicate formation.

The thermodynamic effects of HA occurring in clay system instead of Al-oxide system can be associated with the differing Al solubilities between the two mineral substrates. Compared to γ-Al_2O_3, clay is relatively less soluble and thus provides less Al for LDH formation, which is the rate limiting factor leading to the much slower Fe(II) sorption kinetics in the HA free clay suspensions than in the HA free γ-Al_2O_3 suspension (Figure 4.1). In the HA coated Al-oxide suspension, even though Al availability is limited due to HA masking on mineral surface and the formation of HA-Al complex, sufficient Al dissolved from the Al-oxide substrate is still enough to thermodynamically initiate the Fe(II)-Al-LDH formation. However, in the HA coated clay suspension, Al released from less soluble clay becomes even less due to the masking effect of HA on clay surface, and the smaller amount of dissolved Al then becomes unavailable by complexing with HA. Thus, the lack of free Al leads to the formation of Fe(II)-Al(III)-LDH phase thermodynamically unfavorable. Our finding is consistent with previously reported

thermodynamic effects of organic compound altering the Me(II) sorption product onto less soluble mineral substrate. Yamaguchi et al. showed that with the presence of citrate and salicylate, the formed precipitate phase remained Ni(II)-Al-LDH on more soluble pyrophyllite, but changed to α-Ni hydroxide on less soluble gibbsite.[49] In our HA coated clay sorption samples, Fe(II) octahedral sheet with fewer or no Al substitution initially formed due to the free Al insufficiency is less contracted than the mixed Fe(II)/Al(III) sheet in Fe(II)-Al(III)-LDH. This less contracted sheet may be more compatible for Si incorporation in the interlayer, making the formation of Fe(II)-phyllosilicate both kinetically and thermodynamically favored under conditions originally suitable for Fe(II)-Al(III)-LDH formation. In addition, the secondary precipitate of Fe(II)-phyllosilicate may also ultimately form in HA free clay suspension, as a result of interlayer silification of Fe(II)-Al(III)-LDH phase over sorption time longer than employed here. Previous studies have observed that Ni(II)-phyllosicate was more stable than Ni(II)-Al(III)-LDH, and Ni(II)-phyllosilicate formed as a long-term Ni(II) sorption product onto pyrophyllite (2:1 mineral) as a result of the slow Si exchange and polymerization in the interlayer of Ni(II)-Al(III)-LDH.[39,44,45,77]

4.5 Environmental Implications

The results reported here demonstrate the potential importance of ubiquitous existence of organic substances in affecting Fe(II) sorption behavior onto Al-bearing mineral substrates in soils and sediments under reducing geochemical environment. During Fe(II) sorption onto Al-oxide, the presence of humic substances predominantly affects Fe(II) sorption kinetics, by reducing free Al availability necessary for Fe(II)-Al(III)-LDH formation. However, during Fe(II) sorption onto clay, the presence of humic acid

predominantly inserts thermodynamic impacts by changing the main sorption mode from Fe(II)-Al(III)-LDH to Fe(II)-phyllosilicate. The impacts of humic substances differ by the type of mineral substrates, suggesting an important role of soil mineralogy in directing humic substances interaction with Fe(II) sorptive reaction onto mineral substrate. In addition, our results suggest larger inhibitive effect of humic substances on the formation of Fe(II)-Al-LDH phases during Fe(II) cosorption with HS than during Fe(II) sorption onto HS pre-coated Al-oxide, which implies strong suppressive impact by organic compounds on Fe(II)-Al(III)-LDH formation under circumstances when originally adsorbed organic compounds and aqueous Fe(II) are simultaneously released during microbially reductive dissolution of Fe(III)-oxides.[81,85,135] The results shown here are needed to be considered when assessing the geochemical fate and transportation of Fe(II) in reducing field conditions.

4.6 Table and Figures

Table 4.1. Fe *K*-edge EXAFS fitting results of Fe(II) reference and sorption samples

			atomic shell								
γ-Al2O3 sorption samples			Fe-O			Fe-Fe			Fe-Al		
organic	type	time	CN[a]	R(Å)[b]	Å^{-2}	CN	R(Å)	Å^{-2}	CN	R(Å)	Å^{-2}
4% HA	pre-coat	5 mo	5.3	2.12	0.008	3.5	3.15	0.010	1.7	3.15	0.010
4% HA	pre-coat	1 mo	5.3	2.11	0.008	3.2	3.15	0.010	1.9	3.15	0.010
4% HA	pre-coat	1 wk	5.4	2.11	0.009	3.2	3.15	0.010	1.6	3.15	0.010
1% HA	pre-coat	5 mo	5.2	2.13	0.008	3.7	3.15	0.010	2.0	3.15	0.010
1% HA	pre-coat	1 mo	5.7	2.12	0.008	3.6	3.15	0.010	2.0	3.15	0.010
1% HA	pre-coat	1 wk	5.4	2.12	0.008	3.9	3.15	0.010	2.1	3.15	0.010
4% HA	co-sorb	2 mo	5.0	2.12	0.009	3.3	3.15	0.011	1.7	3.15	0.011
4% HA	co-sorb	1 wk	5.0	2.10	0.010	2.0	3.14	0.010	1.0	3.14	0.010
4% FA	co-sorb	2 mo	5.2	2.12	0.009	3.5	3.15	0.011	1.8	3.15	0.011
4% FA	co-sorb	1 wk	5.1	2.10	0.010	2.0	3.14	0.010	1.3	3.14	0.010
-	-	1 wk	5.5	2.12	0.008	4.1	3.15	0.010	1.7	3.15	0.010
references (I)											
Nikischerite			5.4	2.14	0.007	3.9	3.15	0.009	2.1	3.15	0.009
Fe(OH)2			5.2	2.14	0.006	6.0	3.26	0.006			
$Fe^{II}_{(aq)}$			5.3	2.12	0.009						
Fe^{II}-$FA_{(aq)}$			5.5	2.09	0.009						
Fe^{II}-$HA_{(aq)}$			5.4	2.09	0.009						
clay sorption samples											
-	-	1 wk	5.9	2.10	0.010	3.9	3.15	0.012	1.8	3.15	0.012
clay sorption samples			Fe-O			Fe-Fe			Fe-Si		
4% HA	pre-coat	5 mo	5.4	2.11	0.010	6.0	3.19	0.012	3.8	3.27	0.012
4% HA	pre-coat	1 mo	5.1	2.10	0.009	6.0	3.20	0.012	4.6	3.30	0.012
4% HA	pre-coat	1 wk	5.4	2.10	0.01	6.0	3.19	0.012	3.8	3.25	0.012
1% HA	pre-coat	1 mo	5.4	2.10	0.011	6.0	3.19	0.012	3.9	3.25	0.012
1% HA	pre-coat	1 wk	5.6	2.10	0.010	6.0	3.19	0.012	4.3	3.26	0.012
references (II)											
Fe(II)/clay @pH 8.0			6.1	2.11	0.010	6.0	3.20	0.012	3.4	3.28	0.012
Fe(II)/SiO_2 @pH 8.0			5.3	2.12	0.013	6.0	3.23	0.012	4.0	3.31	0.012
Fe(II)/SiO_2 @pH 7.5			5.2	2.10	0.013	6.0	3.23	0.012	4.0	3.31	0.012

[a]CN is coordination number, [b]R is interatomic radial distance, and [c]σ^2 is Debye-Waller factor. Error estimates for CN ± 25%; first-shell R ±0.02 Å; second shell R ±0.04 Å. Details on fitting procedure is provided in Appendix 3.

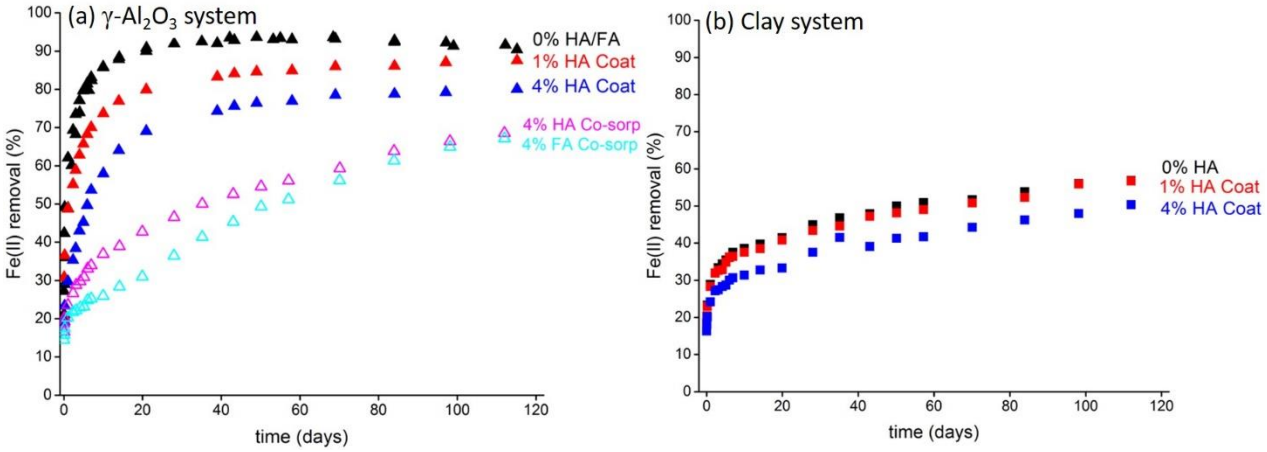

Figure 4.1. Fe(II) sorption kinetics results

Fe(II) sorption kinetics upon (a) Fe(II) sorption onto 5.0 g L^{-1} HA (0%, 1%, 4%) pre-coated γ-Al_2O_3; Fe(II) and HA/FA (0%, 4%) cosorption onto 5.0 g L^{-1} γ-Al_2O_3; (b) Fe(II) sorption onto 5.0 g L^{-1} HA (0%, 1%, 4%) pre-coated clay at pH 7.5 for reaction time up to 120 days. The initial aqueous Fe(II) concentration was 2.7 mM in all systems. The sorption kinetics of 0% HA/FA in panel a is the combined results from control samples of Fe(II) sorption onto 0% HA pre-coated γ-Al_2O_3 and Fe(II) sorption onto γ-Al_2O_3 with 0% HA added simultaneously. (Note: The identical sorption trends between these two samples suggest pH drop to 3.5 during HA coating process does not dissolve significant amount of γ-Al_2O_3)

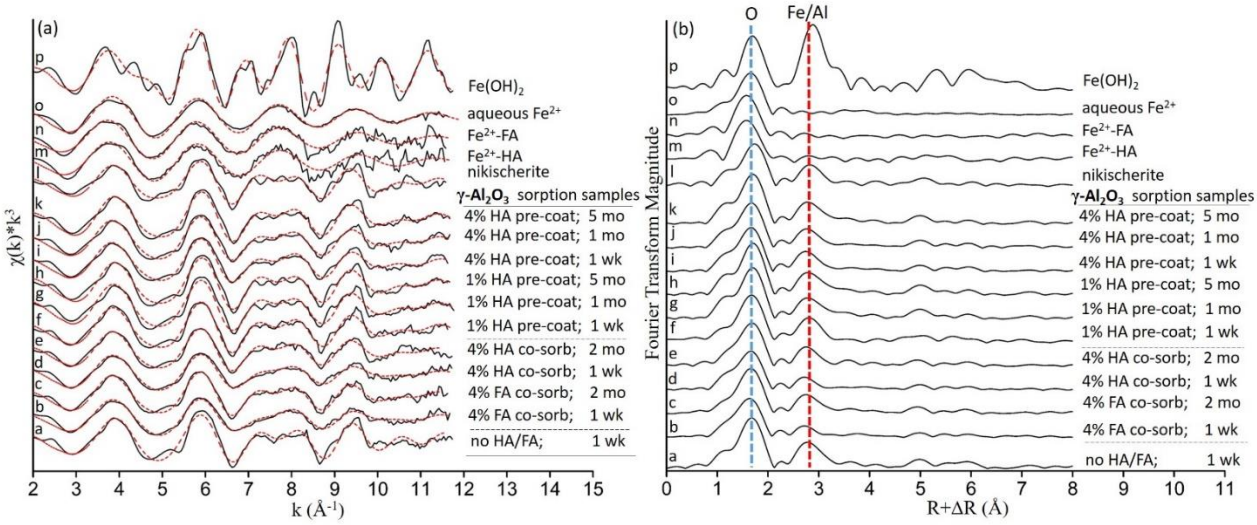

Figure 4.2. Fe *K*-edge EXAFS results in γ-Al_2O_3 systems

Fe *K*-edge EXAFS data of Fe references and sorption samples in γ-Al_2O_3 systems containing 2.7mM Fe(II), and variable HA/FA concentrations for reaction times up to 5 months: (a) k^3-weighted χ spectra; and (b) corresponding radial structure functions (RSFs). Solid and red dotted lines in panel (a) represent raw and fitted spectra, respectively. Vertical dashed line in panel (b) indicates atomic neighbors. The fit results are summarized in Table 4.1.

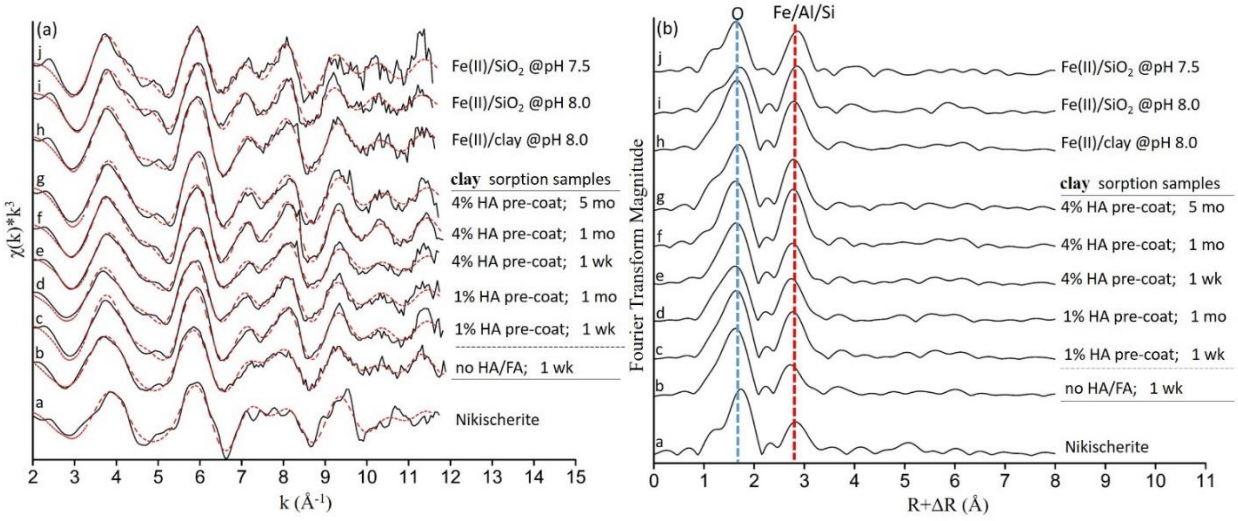

Figure 4.3. Fe *K*-edge EXAFS results in γ-Al_2O_3 systems

Fe *K*-edge EXAFS data of Fe references and sorption samples in HA pre-coated clay systems containing 2.7mM Fe(II), and variable HA concentrations for reaction times up to 5 months: (a) k^3-weighted χ spectra; and (b) corresponding radial structure functions (RSFs). Solid and red dotted lines in panel (a) represent raw and fitted spectra, respectively. Vertical dashed line in panel (b) indicates atomic neighbors. The fit results are summarized in Table 4.1.

Chapter 5: Conclusions

5.1 General Conclusions

The results from this thesis work suggest that secondary Fe(II) layered hydroxides such as Fe(II)-Al(III)-LDH and Fe(II)-phyllosilicate form rapidly and extensively during aqueous Fe(II) sorption onto mineral substrates under lab-based experimental conditions, simulating anoxic or suboxic geochemical environments. A series of environmental factors (i.e. pH, reaction time, sorbent type and the presence of foreign elements) were found to be related with the kinetics and thermodynamics of the formed Fe(II) precipitates onto mineral substrates.

In Chapter 1, solution pH and sorbent type play important role in determining the sorption kinetics and products during Fe(II) sorptive reactions. The secondary Fe(II) layered hydroxides form at pH > 7.0 with the formation rate and extent increasing with pH in all systems with the presence of various mineral sorbents. Compared to the blank system, the presence of mineral substrates moves the pH threshold for commencing Fe(II) precipitate to lower value and altered the β-$Fe(OH)_2$ precipitate to other forms of Fe(II) layered hydroxides. The formation of Fe(II)-Al(III)-LDH was observed in Fe(II)/Al-oxide system at pH ≥ 7.0 and in Fe(II)/clay system at pH 7.0 and 7.5. Fast formation (<2 hours) of Fe(II)-Al(III)-LDH phases upon Fe(II) sorption onto Al-oxide at pH 7.5 indicates the formation of such phases is both kinetically and thermodynamically favored. On the other hand, the formation of poorly crystalline trioctahedral Fe(II)-phyllosilicate was observed in Fe(II)/amorphous silica system at pH ≥ 7.5 and in Fe(II)/clay system at pH 8.0. The substantial effects of pH and sorbent type involved suggest the important

role of soil mineralogy in directing the form of Fe(II) sequestration and further influencing the Fe solubility under reducing soil environment.

The potential effects from foreign elements on secondary Fe(II) precipitates are also addressed in this dissertation. The presence of arsenic (Chapter 3) and humic substances (Chapter 4) could affect the kinetics and mechanisms of Fe(II) sorption, with effects depending on the speciation, concentration (Chapter 3 and 4) and addition sequence (Chapter 4) of the foreign elements present, and/or sorbent type (Chapter 4). The precipitation of Fe(II)-Al(III)-LDH during Fe(II) sorption onto Al-oxide is unaffected by As(III), however slows down at low concentrations of As(V), and fully shuts down at high As(V) concentration, where the surface Fe(II) adsorption occurs instead (Chapter 3). In Chapter 4, the presence of humic substances (i.e. humic acid (HA) and fluvic acid (FA)) in Fe(II)/Al-oxde system slows down Fe(II)-Al(III)-LDH formation kinetics. But the presence of HA coating in Fe(II)/clay system predominantly alters the main Fe(II) sorption product from Fe(II)-Al-LDH to Fe(II)-phyllosilicate. The different effects of HA coating on Al-oxide compared to clay (kinetic vs. thermodynamic) further demonstrate the importance of sorbent reactivity and solubility in directing the Fe(II) precipitates formation. The results from Chapter 3 and Chapter 4 suggest that some geochemical elements such as As(V) and organic compounds constituting the heterogeneous soil environments can act as potential inhibitors of the Fe(II)-Al(III)-LDH precipitate.

It is noteworthy that the availability of Al and/or Si is closely associated with the kinetics and types of secondary Fe(II) precipitates formation. As shown in Chapter 2, mineral substrates serve as the source of Al and Si supply for Fe(II)-Al(III)-LDH and

Fe(II)-phyllosilicate formation. The dissolved Al from Al-oxide and clay can incorporate in the octahedral layer of Fe(II)-hydroxide sheets, and the dissolved Si from amorphous silica and clay can form tetrahedral Si layers to link Fe(II)-hydroxide sheets. The dissolution rate of Al and Si from the mineral substrates is the rate-limiting factor influencing the formation kinetics of Fe(II)-Al-LDH and poorly crystalline Fe(II)-phyllosilicate. The slower kinetics of Fe(II) precipitates formation in the clay suspension compared to γ-Al_2O_3 and amorphous SiO_2 suspensions are associated with the slower release of Al and Si from clay substrate than γ-Al_2O_3 and amorphous SiO_2 (Chapter 2). Strong interaction between foreign elements and Al supply inserts inhibitive effects on the formation of Fe(II)-Al(III)-LDH. In Chapter 3, adsorbed As(V) hinders the precipitate of Fe(II)-Al(III)-LDH by interaction with the Al supply. In Chapter 4, humic substances exhibit impacts on Fe(II) sorption kinetics and/or mechanisms onto Al-oxide and clay, by HS forming organo-Al complexes and masking on substrate surfaces limiting Al needed to form Fe(II)-Al(III)-LDH and Si needed to form Fe(II)-phyllosilicate. These results suggest important role of Al and/or Si availability in regulating Fe(II) speciation and solubility under reducing environments.

5.2 Environmental Significance

This dissertation work emphasizes the potential importance of Fe(II) precipitates under anoxic and suboxic environments such as rapirian soils and sediments, and investigates the geochemical factors affecting the precipitation rate and the type of the precipitates formed. The Fe(II) precipitates characterized here (Fe(II)-Al(III)-LDH and amorphous Fe(II)-phyllosilicate) are likely to form under anoxic and suboxic groundwaters and soils with near-neutral pH ranges of 6.5-8.0,[81,82] where sufficient Fe(II) is available due to the

reductive dissolution of Fe(III) bearing minerals.[4,5,83–85] Our results suggest that the availability of Al and/or Si which could incorporate in the structure of Fe(II) precipitates affects the formation kinetics and thermodynamics of the precipitates onto mineral substrates. In Chapter 3 and 4, it is shown that the existence of foreign elements such as As(V) and organic compounds inhibits the Fe(II)-Al(III)-LDH formation by interacting with Al supply in various ways. Thus, the secondary Fe(II) precipitates are more likely to form under conditions in which the other constitutes have less interference with free Al and/or Si available for precipitates formation. In addition, the formation of Fe(II) precipitates may also affect the solubility and speciation of other elements through adsorption, coprecipitation and redox sensitive reactions. The results reported here may be considered in development of qualitative and quantitative models of the speciation and fate of Fe under anoxic geochemical systems.

5.3 Recommendations for Future Research

Future studies may focus on investigating the formation kinetics and thermodynamics of Fe(II) precipitates in various systems with more complexity and heterogeneity resembling the natural environments, and assessing the reactivity of Fe(II) precipitates (e.g., Fe(II)-Al(III)-LDH) toward redox sensitive trace elements. The following topics are recommended for future research:

1. Examine Fe(II) sorption products and kinetics under multi-sorbent systems, further investigating the importance of sorbent reactivity on the rate and form of Fe(II) sequestration under reducing conditions.
2. Investigate the interaction of Fe(II) and other divalent such as Ni(II), Zn(II), Co(II) and Mn(II) during cosorption reactions onto Al bearing mineral substrates.

3. Study the redox reactivity of structural Fe(II) in Fe(II)-Al(III)-LDH towards redox sensitive trace elements such as Cr(VI) and U(VI).

References

(1) Horne, R. A. *The Chemistry of Our Environment*; Wiley: New York, NY, 1978.

(2) Stumm, W.; Morgan, J. J. *Aquatic chemistry: chemical equilibria and rates in natural waters*, 3rd ed.; Wiley: New York, NY, 1996.

(3) Hooda, P. *Trace Elements in Soils*; John Wiley & Sons, Ltd: Chichester, U.K., 2010.

(4) Weber, K. A.; Achenbach, L. A.; Coates, J. D. Microorganisms pumping iron: anaerobic microbial iron oxidation and reduction. *Nat. Rev. Microbiol.* **2006**, *4*, 752–764.

(5) Lovley, D. R.; Phillips, E. J. P. Organic matter mineralization with reduction of ferric iron in anaerobic sediments. *Appl. Environ. Microbiol.* **1986**, *51* (4), 683–689.

(6) Jaisi, D. P.; Liu, C.; Dong, H.; Blake, R. E.; Fein, J. B. Fe^{2+} sorption onto nontronite (NAu-2). *Geochim. Cosmochim. Acta* **2008**, *72*, 5361–5371.

(7) Jeon, B.; Dempsey, B. A.; Burgos, W. D. Kinetics and mechanisms for reactions of Fe(II) with iron(III) oxides. *Environ. Sci. Technol.* **2003**, *37* (15), 3309–3315.

(8) Larese-Casanova, P.; Scherer, M. M. Fe(II) sorption on hematite: new insights based on spectroscopic measurements. *Environ. Sci. Technol.* **2007**, *41* (2), 471–477.

(9) Merola, R. B.; Fournier, E. D.; McGuire, M. M. Spectroscopic investigations of Fe^{2+} complexation on nontronite clay. *Langmuir* **2007**, *23* (3), 1223–1226.

(10) Schaefer, M. V.; Gorski, C. A.; Scherer, M. M. Spectroscopic evidence for interfacial Fe(II)-Fe(III) electron transfer in a clay mineral. *Environ. Sci. Technol.* **2011**, *45* (2), 540–545.

(11) Williams, A. G. B.; Scherer, M. M. Spectroscopic evidence for Fe(II)-Fe(III) electron transfer at the iron oxide-water interface. *Environ. Sci. Technol.* **2004**, *38* (18), 4782–4790.

(12) Tanwar, K. S.; Petitto, S. C.; Ghose, S. K.; Eng, P. J.; Trainor, T. P. Structural study of Fe(II) adsorption on hematite. *Geochim. Cosmochim. Acta* **2008**, *72* (14), 3311–3325.

(13) Tanwar, K. S.; Petitto, S. C.; Ghose, S. K.; Eng, P. J.; Trainor, T. P. Fe(II) adsorption on hematite (0001). *Geochim. Cosmochim. Acta* **2009**, *73* (15), 4346–4365.

(14) Handler, R. M.; Beard, B. L.; Johnson, C. M.; Scherer, M. M. Atom exchange between aqueous Fe(II) and goethite: an Fe isotope tracer study. *Environ. Sci. Technol.* **2009**, *43* (4), 1102–1107.

(15) Yee, N. The rate of ferrihydrite transformation to goethite via the Fe(II) pathway. *Am. Mineral.* **2006**, *91* (1), 92–96.

(16) Hansel, C. M.; Benner, S. G.; Fendorf, S. Competing Fe (II)-induced mineralization pathways of ferrihydrite. *Environ. Sci. Technol.* **2005**, *39* (18), 7147–7153.

(17) Elzinga, E. J. Formation of layered Fe(II)-Al(III)-hydroxides during reaction of Fe(II) with aluminum oxide. *Environ. Sci. Technol.* **2012**, *46* (9), 4894–4901.

(18) Thompson, H. A.; Parks, G. A.; Brown, G. E. Dynamic interactions of dissolution, surface adsorption, and precipitation in an aging cobalt(II)-clay-water system. *Geochim. Cosmochim. Acta* **1999**, *63* (11–12), 1767–1779.

(19) Ford, R. G.; Sparks, D. L. The nature of Zn precipitates formed in the presence of pyrophyllite. *Environ. Sci. Technol.* **2000**, *34*, 2479–2483.

(20) Scheckel, K. G.; Sparks, D. L. Kinetics of the formation and dissolution of Ni precipitates in a gibbsite/amorphous silica mixture. *J. Colloid Interface Sci.* **2000**, *229*, 222–229.

(21) Scheinost, A. C.; Sparks, D. L. Formation of layered single- and double-metal hydroxide precipitates at the mineral/water interface: a multiple-scattering XAFS analysis. *J. Colloid Interface Sci.* **2000**, *223*, 167–178.

(22) Scheidegger, A. M.; Sparks, D. L. Kinetics of the formation and the dissolution of nickel surface precipitates on pyrophyllite. *Chem. Geol.* **1996**, *132*, 157–164.

(23) Roberts, D. R.; Scheidegger, A. M.; Sparks, D. L. Kinetics of mixed Ni-Al precipitate formation on a soil clay fraction. *Environ. Sci. Technol.* **1999**, *33* (21), 3749–3754.

(24) Towle, S. N.; Bargar, J. R.; Brown, G. E.; Parks, G. A. Surface precipitation of Co (II) (aq) on Al_2O_3. *J. Colloid Interface Sci.* **1997**, *187*, 62–82.

(25) Elzinga, E. J.; Sparks, D. L. Reaction condition effects on nickel sorption mechanisms in illite–water suspensions. *Soil Sci. Soc. Am. J.* **2001**, *65*, 94–101.

(26) Peltier, E.; Allada, R.; Navrotsky, A.; Sparks, D. L. Nickel solubility and precipitation in soils: a thermodynamic study. *Clays Clay Miner.* **2006**, *54* (2), 153–164.

(27) Elzinga, E. J.; Sparks, D. L. Nickel sorption mechanisms in a pyrophyllite-

montmorillonite mixture. *J. Colloid Interface Sci.* **1999**, *213*, 506–512.

(28) Roberts, D. R.; Ford, R. G.; Sparks, D. L. Kinetics and mechanisms of Zn complexation on metal oxides using EXAFS spectroscopy. *J. Colloid Interface Sci.* **2003**, *263*, 364–376.

(29) Trainor, T. P.; Brown, G. E.; Parks, G. A. Adsorption and precipitation of aqueous Zn(II) on alumina powders. *J. Colloid Interface Sci.* **2000**, *231*, 359–372.

(30) Scheidegger, A. M.; Lamble, G. M.; Sparks, D. L. Spectroscopic evidence for the formation of mixed-cation hydroxide phases upon metal sorption on clays and aluminum oxides. *J. Colloid Interface Sci.* **1997**, *186*, 118–128.

(31) Nachtegaal, M.; Sparks, D. L. Nickel sequestration in a kaolinite-humic acid complex. *Environ. Sci. Technol.* **2003**, *37* (3), 529–534.

(32) Peltier, E.; Lelie, D. Van Der; Sparks, D. L. Formation and stability of Ni-Al hydroxide phases in soils. *Environ. Sci. Technol.* **2010**, *44*, 302–308.

(33) McNear, D. H.; Chaney, R. L.; Sparks, D. L. The effects of soil type and chemical treatment on nickel speciation in refinery enriched soils: A multi-technique investigation. *Geochim. Cosmochim. Acta* **2007**, *71*, 2190–2208.

(34) Voegelin, A.; Kretzschmar, R. Formation and dissolution of single and mixed Zn and Ni precipitates in soil: evidence from column experiments and extended X-ray absorption fine structure spectroscopy. *Environ. Sci. Technol.* **2005**, *39*, 5311–5318.

(35) Nachtegaal, M.; Marcus, M. A.; Sonke, J. E.; Vangronsveld, J.; Livi, K. J. T.; Lelie, D. V. D.; Sparks, D. L. Effects of in situ remediation on the speciation and bioavailability of zinc in a smelter contaminated soil. *Geochim. Cosmochim. Acta* **2005**, *69* (19), 4649–4664.

(36) Jacquat, O.; Voegelin, A.; Villard, A.; Marcus, M. A.; Kretzschmar, R. Formation of Zn-rich phyllosilicate, Zn-layered double hydroxide and hydrozincite in contaminated calcareous soils. *Geochim. Cosmochim. Acta* **2008**, *72*, 5037–5054.

(37) Juillot, F.; Morin, G.; Ildefonse, P.; Trainor, T. P.; Benedetti, M.; Galoisy, L.; Calas, G.; Brown, G. E. Occurrence of Zn/Al hydrotalcite in smelter-impacted soils from northern France : Evidence from EXAFS spectroscopy and chemical extractions. *Am. Miner.* **2003**, *88*, 509–526.

(38) Johnson, C. A.; Glasser, F. P. Hydrotalcite-like minerals ($M_2Al(OH)_6(CO_3)_{0.5}$. XH_2O, where M = Mg, Zn, Co, Ni) in the environment : synthesis , characterization and thermodynamic stability. *Clays Clay Miner.* **2003**, *51* (1), 1–8.

(39) Scheinost, A. C.; Ford, R. G.; Sparks, D. L. The role of Al in the formation of secondary Ni precipitates on pyrophyllite, gibbsite, talc, and amorphous silica: A DRS study. *Geochim. Cosmochim. Acta* **1999**, *63*, 3193–3203.

(40) Scheidegger, A. M.; Strawn, D. G.; Lamble, G. M.; Sparks, D. L. The kinetics of mixed Ni-Al hydroxide formation on clay and aluminum oxide minerals: A time-resolved XAFS study. *Geochim. Cosmochim. Acta* **1998**, *62* (13), 2233–2245.

(41) Strawn, D. G.; Scheidegger, A. M.; Sparks, D. L. Kinetics and mechanisms of Pb(II) sorption and desorption at the aluminum oxide - water interface. *Environ. Sci. Technol.* **1998**, *32*, 2596–2601.

(42) Manceau, A.; Schlegel, M.; Nagy, K. L.; Charlet, L. Evidence for the formation of trioctahedral clay upon sorption of Co(2+) on quartz. *J. Colloid Interface Sci.* **1999**, *220*, 181–197.

(43) Charlet, L.; Manceau, A. Evidence for the neoformation of clays upon sorption of Co(II) and Ni(II) on silicates. *Geochim. Cosmochim. Acta* **1994**, *58*, 2577–2582.

(44) Ford, R. G.; Scheinost, A. C.; Scheckel, K. G.; Sparks, D. L. The link between clay mineral weathering and the stabilization of Ni surface precipitates. *Environ. Sci. Technol.* **1999**, *33*, 3140–3144.

(45) Scheckel, K. G.; Scheinost, A. C.; Ford, R. G.; Sparks, D. L. Stability of layered Ni hydroxide surface precipitates — A dissolution kinetics study. *Geochim. Cosmochim. Acta* **2000**, *64* (16), 2727–2735.

(46) Li, W.; Livi, K. J. T.; Xu, W.; Siebecker, M. G.; Wang, Y.; Phillips, B. L.; Sparks, D. L. Formation of crystalline Zn-Al layered double hydroxide precipitates on γ-alumina: the role of mineral dissolution. *Environ. Sci. Technol.* **2012**, *46* (21), 11670–11677.

(47) Papelis, C.; Hayes, K. F. Distinguishing between interlayer and external sorption sites of clay minerals using X-ray absorption spectroscopy. *Colloids Surf. A* **1996**, *107*, 89–96.

(48) Yamaguchi, N. U.; Scheinost, A. C.; Sparks, D. L. Influence of gibbsite surface area and citrate on Ni sorption mechanisms at pH 7.5. *Clays Clay Miner.* **2002**, *50* (6), 784–790.

(49) Yamaguchi, N. U.; Scheinost, A. C.; Sparks, D. L. Surface-induced nickel hydroxide precipitation in the presence of citrate and salicylate. *Soil Sci. Soc. Am. J.* **2001**, *65*, 729–736.

(50) Stietiya, M. H.; Wang, J. J.; Roy, A. Macroscopic and Extended X-ray Absorption Fine Structure Spectroscopic Investigation of Ligand Effect on Zinc Adsorption to

Kaolinite as a Function of pH. *Soil Sci.* **2011**, *176* (9), 464–471.

(51) Li, W.; Wang, Y. J.; Zhu, M.; Fan, T. T.; Zhou, D. M.; Phillips, B. L.; Sparks, D. L. Inhibition mechanisms of Zn precipitation on aluminum oxide by glyphosate: A ^{31}P NMR and Zn EXAFS study. *Environ. Sci. Technol.* **2013**, *47* (9), 4211–4219.

(52) Sparks, D. L. *Environmental Soil Chemistry*, 2nd ed.; Academic Press: Boston, MA, U.S.A., 2002.

(53) Dahn, R.; Scheidegger, A. M.; Manceau, A.; Schlegel, M. L.; Baeyens, B.; Bradbury, M. H.; Morales, M. Neoformation of Ni phyllosilicate upon Ni uptake on montmorillonite : A kinetics study by powder and polarized extended X-ray absorption fine structure spectroscopy. *Geochim. Cosmochim. Acta* **2002**, *66* (13), 2335–2347.

(54) Soltermann, D.; Fernandes, M. M.; Baeyens, B.; Dähn, R.; Miehé-Brendlé, J.; Wehrli, B.; Bradbury, M. H. Fe(II) sorption on a synthetic montmorillonite. A combined macroscopic and spectroscopic study. *Environ. Sci. Technol.* **2013**, *47* (13), 6978–6986.

(55) Mermut, A. R.; Cano, A. F. Baseline studies of the clay minerals society source clays: chemical analyses of major elements. *Clays Clay Miner.* **2001**, *49* (5), 381–386.

(56) Klute, A. *Methods of Soil Analysis: Physical and Mineralogical Methods*; American Society of Agronomy, Inc.: Madison, WI, U.S.A., 1986.

(57) Stookey, L. L. Ferrozine - a new spectrophotometric reagent for iron. *Anal. Chem.* **1970**, *42* (7), 779–781.

(58) Ressler, T. WinXAS : a new software package not only for the analysis of energy-dispersive XAS data. *J. Phys. IV Fr.* **1997**, *7* (C2), C2-269.

(59) Ankudinov, A. L.; Rehr, J. J. Relativistic calculations of spin-dependent x-ray-absorption spectra. *Phys. Rev. B* **1997**, *56* (4), R1712–R1715.

(60) Ravel, B.; Newville, M. ATHENA, ARTEMIS, HEPHAESTUS: data analysis for X-ray absorption spectroscopy using IFEFFIT. *J. Synchrotron Radiat.* **2005**, *12* (4), 537–541.

(61) Funke, H.; Scheinost, A. C.; Chukalina, M. Wavelet analysis of extended x-ray absorption fine structure data. *Phys. Rev. B* **2005**, *71* (9), 94110.

(62) Nano, G. V.; Strathmann, T. J. Ferrous iron sorption by hydrous metal oxides. *J. Colloid Interface Sci.* **2006**, *297*, 443–454.

(63) Hiemstra, T.; van Riemsdijk, W. H. Adsorption and surface oxidation of Fe(II) on

metal (hydr)oxides. *Geochim. Cosmochim. Acta* **2007**, *71*, 5913–5933.

(64) Schultz, C.; Grundl, T. pH dependence of ferrous sorption onto two smectite clays. *Chemosphere* **2004**, *57*, 1301–1306.

(65) Shannon, R. D. Revised effective ionic radii and systematic studies of interatomic distances in halides and chalcogenides. *Acta Crystallogr., Sect. A* **1976**, *32* (5), 751–767.

(66) Huminicki, D. M. C.; Hawthorne, F. C. The crystal structure of nikischerite, Na $Fe^{2+}_6 Al_3(SO_4)_2 (OH)_{18}(H_2O)_{12}$, a mineral of the shigaite group. *Can. Mineral.* **2003**, *41*, 79–82.

(67) Olszewski, W.; Szymański, K.; Zaleski, P.; Zając, D. A. X-ray absorption near edge structure and extended X-ray absorption fine structure analysis of Fe(II) aqueous and acetone solutions. *J. Phys. Chem. A* **2011**, *115*, 13420–13424.

(68) Parise, J. B.; Marshall, W. G.; Smith, R. I.; Lutz, H. D.; MÖller, H. The nuclear and magnetic structure of "white rust"— Fe $(OH_{0.86}D_{0.14})_2$. *Am. Mineral.* **2000**, *85*, 189–193.

(69) Schecher, W.; McAvoy, D. MINEQL+[4.6]. Environmental Research Software: Hallowell, ME, U.S.A. 2003.

(70) Siebecker, M. Environmental speciation, chemistry, stability and kinetics of nickel in soils, mineral systems, and plants. Ph.D. Dissertation, University of Delaware, Newark, DE, 2013.

(71) Christiansen, B. C.; Balic-Zunic, T.; Petit, P.-O.; Frandsen, C.; Mørup, S.; Geckeis, H.; Katerinopoulou, A.; Stipp, S. L. S. Composition and structure of an iron-bearing, layered double hydroxide (LDH) – Green rust sodium sulphate. *Geochim. Cosmochim. Acta* **2009**, *73*, 3579–3592.

(72) Manceau, A.; Ildefonse, P.; Hazemann, J.-L.; Flank, A.-M.; Gallup, D. Crystal chemistry of hydrous iron silicate scale deposits at the salton sea geothermal field. *Clays Clay Miner.* **1995**, *43* (3), 304–317.

(73) Guggenheim, S.; Eggleton, R. A. Structural modulations in iron-rich and magnesium-rich minnesotaite. *Can. Miner.* **1986**, *24*, 479497.

(74) Guggenheim, S.; Bailey, S. W.; Eggleton, R. A.; Wilkes, P. Structural aspects of greenalite and related minerals. *Can. Miner.* **1982**, *20*, 1–18.

(75) Brindley, G. W.; Brown, G. *Crystal Structures of Clay Minerals and Their X-ray Identification*; Monograph / Mineralogical Society; Mineralogical Society: London U.K., 1980.

(76) Bailey, S. W. Crystal chemistry of the true micas. *Rev. Miner. Geochem.* **1984**, *13* (1), 13–60.

(77) Scheckel, K. G.; Sparks, D. L. Dissolution kinetics of nickel surface precipitates on clay mineral and oxide surfaces. *Soil Sci. Soc. Am. J.* **2001**, *65*, 685–694.

(78) Tang, Y.; Reeder, R. J. Uranyl and arsenate cosorption on aluminum oxide surface. *Geochim. Cosmochim. Acta* **2009**, *73*, 2727–2743.

(79) Wijnja, H.; Schulthess, C. P. ATR–FTIR and DRIFT spectroscopy of carbonate species at the aged γ-Al_2O_3/water interface. *Spectrochim. Acta Part A Mol. Biomol. Spectrosc.* **1999**, *55*, 861–872.

(80) Carrier, X.; Marceau, E.; Lambert, J.; Che, M. Transformations of γ-alumina in aqueous suspensions 1. Alumina chemical weathering studied as a function of pH. *J. Colloid Interface Sci.* **2007**, *308*, 429–437.

(81) Ponnamperuma, F. N. The chemistry of submerged soils. *Adv. Agron.* **1972**, *24*, 29–96.

(82) Hem, J. D. *Study and interpretation of the chemical characteristics of natural water*, 3rd ed.; United States Government Printing Office: Washington DC, 1985.

(83) Borch, T.; Kretzschmar, R.; Kappler, A.; Cappellen, P. Van; Ginder-Vogel, M.; Voegelin, A.; Campbell, K. Biogeochemical redox processes and their impact on contaminant dynamics. *Environ. Sci. Technol.* **2010**, *44*, 15–23.

(84) Baedecker, M. J.; Cozzarelli, I. M. The determination and fate of unstable constituents of contaminated groundwater. In *Groundwater contamination and analysis at hazardous waste sites*; Lesage, S., Jackson, R. E., Eds.; Marcel Dekker, Inc.: New York, 1992; pp 425–461.

(85) Kirk, G. *The Biogeochemistry of Submerged Soils*; John Wiley & Sons, Ltd: Chichester, U.K., 2004.

(86) Li, F.; Tao, L.; Feng, C.; Li, X.; Sun, K. Electrochemical evidences for promoted interfacial reactions: the role of Fe(II) adsorbed onto γ-Al_2O_3 and TiO_2 in reductive transformation of 2-Nitrophenol. *Environ. Sci. Technol.* **2009**, *43*, 3656–3661.

(87) Jaisi, D. P.; Dong, H.; Morton, J. P. Partitioning of Fe(II) in reduced nontronite (NAu-2) to reactive sites: reactivity in terms of Tc(VII) reduction. *Clays Clay Miner.* **2008**, *56* (2), 175–189.

(88) Larese-Casanova, P.; Cwiertny, D. M.; Scherer, M. M. Nanogoethite formation from oxidation of Fe(II) sorbed on aluminum oxide: implications for contaminant reduction. *Environ. Sci. Technol.* **2010**, *44* (10), 3765–3771.

(89) Hofstetter, T. B.; Schwarzenbach, R. P.; Haderlein, S. B. Reactivity of Fe(II) species associated with clay minerals. *Environ. Sci. Technol.* **2003**, *37*, 519–528.

(90) Zhu, Y.; Elzinga, E. J. Formation of layered Fe(II)-hydroxides during Fe(II) sorption onto clay and metal-oxide substrates. *Environ. Sci. Technol.* **2014**, *48*, 4937–4945.

(91) Gambrell, R. P. Trace and toxic metals in wetlands—a review. *J. Environ. Qual.* **1994**, *23*, 883–891.

(92) Weber, F. A.; Voegelin, A.; Kretzschmar, R. Multi-metal contaminant dynamics in temporarily flooded soil under sulfate limitation. *Geochim. Cosmochim. Acta* **2009**, *73* (19), 5513–5527.

(93) Smedley, P. L.; Kinniburgh, D. G. A review of the source, behaviour and distribution of arsenic in natural waters. *Appl. Geochem.* **2002**, *17* (5), 517–568.

(94) Arai, Y.; Elzinga, E. J.; Sparks, D. L. X-ray absorption spectroscopic investigation of arsenite and arsenate adsorption at the aluminum oxide-water interface. *J. Colloid Interface Sci.* **2001**, *235* (1), 80–88.

(95) Goldberg, S.; Johnston, C. T. Mechanisms of arsenic adsorption on amorphous oxides evaluated using macroscopic measurements, vibrational spectroscopy, and surface complexation modeling. *J. Colloid Interface Sci.* **2001**, *234* (1), 204–216.

(96) Goldberg, S. Competitive adsorption of arsenate and arsenite on oxides and clay minerals. *Soil Sci. Soc. Am. J.* **2002**, *66*, 413–421.

(97) Frankenberger, W. T. *Environmental chemistry of arsenic*; Marcel Dekker, Inc.: New York, 2002.

(98) Elzinga, E. J.; Kretzschmar, R. In situ ATR-FTIR spectroscopic analysis of the co-adsorption of orthophosphate and Cd(II) onto hematite. *Geochim. Cosmochim. Acta* **2013**, *117*, 53–64.

(99) Bargar, J. R.; Brown, G. E.; Parks, G. A. Surface complexation of Pb(II) at oxide-water interfaces : III. XAFS determination of Pb(II) and Pb(II) -chloro adsorption complexes on goethite and alumina. *Geochim. Acta* **1998**, *62* (2), 193–207.

(100) Weesner, F. J.; Bleam, W. F. Binding characteristics of Pb^{2+} on anion-modified and pristine hydrous oxide surfaces studied by electrophoretic mobility and X-ray absorption spectroscopy. *J. Colloid Interface Sci.* **1998**, *205*, 380–389.

(101) Ostergren, J. D.; Trainor, T. P.; Bargar, J. R.; Brown, G. E.; Parks, G. A. Inorganic ligand effects on Pb(II) sorption to goethite (alpha-FeOOH) I. Carbonate. *J. Colloid Interface Sci.* **2000**, *225* (2), 466–482.

(102) Ostergren, J. D.; Brown, G. E.; Parks, G. A.; Persson, P. Inorganic ligand effects on Pb(II) sorption to goethite (alpha-FeOOH) II. Sulphate. *J. Colloid Interface Sci.* **2000**, *225*, 483–493.

(103) Elzinga, E. J.; Peak, D.; Sparks, D. L. Spectroscopic studies of Pb(II)-sulfate interactions at the goethite-water interface. *Geochim. Cosmochim. Acta* **2001**, *65* (14), 2219–2230.

(104) Zhang, G. Y.; Peak, D. Studies of Cd(II)-sulfate interactions at the goethite-water interface by ATR-FTIR spectroscopy. *Geochim. Cosmochim. Acta* **2007**, *71*, 2158–2169.

(105) Tang, Y.; McDonald, J.; Reeder, R. J. Enhanced uranium sorption on aluminum oxide pretreated with arsenate. Part II: Spectroscopic studies. *Environ. Sci. Technol.* **2009**, *43* (12), 4452–4458.

(106) Johnston, R. B.; Singer, P. C. Solubility of symplesite (ferrous arsenate): implications for reduced groundwaters and other geochemical environments. *Soil Sci. Soc. Am. J.* **2007**, *71* (1), 101–107.

(107) Catalano, J. G.; Luo, Y.; Otemuyiwa, B. Effect of aqueous Fe(II) on arsenate sorption on goethite and hematite. *Environ. Sci. Technol.* **2011**, *45* (20), 8826–8833.

(108) Jönsson, J.; Sherman, D. M. Sorption of As(III) and As(V) to siderite, green rust (fougerite) and magnetite: implications for arsenic release in anoxic groundwaters. *Chem. Geol.* **2008**, *255*, 173–181.

(109) Voegelin, A.; Weber, F. A.; Kretzschmar, R. Distribution and speciation of arsenic around roots in a contaminated riparian floodplain soil: Micro-XRF element mapping and EXAFS spectroscopy. *Geochim. Cosmochim. Acta* **2007**, *71* (23), 5804–5820.

(110) Manning, B. A.; Fendorf, S. E.; Bostick, B.; Suarez, D. L. Arsenic(III) oxidation and arsenic(V) adsorption reactions on synthetic birnessite. *Environ. Sci. Technol.* **2002**, *36* (5), 976–981.

(111) Makris, K. C.; Sarkar, D.; Parsons, J. G.; Datta, R.; Gardea-Torresdey, J. L. X-ray absorption spectroscopy as a tool investigating arsenic(III) and arsenic(V) sorption by an aluminum-based drinking-water treatment residual. *J. Hazard. Mater.* **2009**, *171* (1–3), 980–986.

(112) Arai, Y.; Sparks, D. L. Residence time effects on arsenate surface speciation at the aluminum oxide-water interface. *Soil Sci.* **2002**, *167* (5), 303–314.

(113) Tang, Y.; Reeder, R. J. Enhanced uranium sorption on aluminum oxide pretreated

with arsenate. Part I: Batch uptake behavior. *Environ. Sci. Technol.* **2009**, *43* (12), 4446–4451.

(114) Ali, M. A.; Dzombak, D. A. Interactions of copper, organic acids, and sulfate in goethite suspensions. *Geochim. Cosmochim. Acta* **1996**, *60* (24), 5045–5053.

(115) Hinkle, M. A. G.; Wang, Z.; Giammar, D. E.; Catalano, J. G. Interaction of Fe(II) with phosphate and sulfate on iron oxide surfaces. *Geochim. Cosmochim. Acta* **2015**, *158*, 130–146.

(116) Boyle-Wight, E. J.; Katz, L. E.; Hayes, K. F. Macroscopic studies of the effects of selenate and selenite on cobalt sorption to γ-Al_2O_3. *Environ. Sci. Technol.* **2002**, *36* (6), 1212–1218.

(117) Boyle-Wight, E. J.; Katz, L. E.; Hayes, K. F. Spectroscopic studies of the effects of selenate and selenite on cobalt sorption to γ-Al_2O_3. *Environ. Sci. Technol.* **2002**, *36* (6), 1219–1225.

(118) Erbs, J. J.; Berquó, T. S.; Reinsch, B. C.; Lowry, G. V.; Banerjee, S. K.; Penn, R. L. Reductive dissolution of arsenic-bearing ferrihydrite. *Geochim. Cosmochim. Acta* **2010**, *74* (12), 3382–3395.

(119) Gomez, M. A.; Hendry, M. J.; Hossain, A.; Das, S.; Elouatik, S. Abiotic reduction of 2-line ferrihydrite: effects on adsorbed arsenate, molybdate, and nickel. *RSC Adv.* **2013**, *3* (48), 25812–25822.

(120) Masue-Slowey, Y.; Loeppert, R. H.; Fendorf, S. Alteration of ferrihydrite reductive dissolution and transformation by adsorbed As and structural Al: Implications for As retention. *Geochim. Cosmochim. Acta* **2011**, *75* (3), 870–886.

(121) Manceau, A. The mechanism of anion adsorption on iron oxides: Evidence for the bonding of arsenate tetrahedra on free $Fe(O, OH)_6$ edges. *Geochim. Cosmochim. Acta* **1995**, *59* (17), 3647–3653.

(122) d'Espinose de la Caillerie, J.-B.; Kermarec, M.; Clause, O. Impregnation of y-Alumina with Ni (II) or Co (II) ions at neutral pH : hydrotalcite-type coprecipitate formation and characterization. *J. Am. Chem. Soc.* **1995**, *117*, 11471–11481.

(123) Davis, J. A.; Kent, D. B. Surface complexation modeling in aqueous geochemistry. *Rev. Miner. Geochem.* **1990**, *23* (1), 177–260.

(124) Sparks, D. L. Toxic metals in the environment: the role of surfaces. *Elements* **2005**, *1*, 193–197.

(125) Wieder, R. K.; Novák, M.; Vile, M. A.; Eds. *Biogeochemical Investigations of Terrestrial, Freshwater, and Wetland Ecosystems Across the Globe.*; Kluwer

Academic Publishers: Dordrecht, The Netherlands, 2004.

(126) Selim, H. M.; Iskandar, I. . K.; Ed. *Fate and Transport of Heavy Metals in the Vadose Zone*; CRC Press: Boca Raton, FL, 1999.

(127) Voegelin, A.; Pfister, S.; Scheinost, A. C.; Marcus, M. A.; Kretzschmar, R. Changes in zinc speciation in field soil after contamination with zinc oxide. *Environ. Sci. Technol.* **2005**, *39* (17), 6616–6623.

(128) Aiken, G. R.; Mcknight, D. M.; Wershaw, R. L.; Maccarthy, P.; Ed. *Humus Substances in Soil, Sediment, and Water*; John Wiley & Sons, Inc.: New York, NY, 1985.

(129) Stevenson, F. J. *Humus Chemistry: Gnesis, Composition, Reaction*, 2nd Ed.; John Wiley & Sons, Inc.: New York, NY, 1994.

(130) Fein, J. B. The effects of ternary surface complexes on the adsorption of metal cations and organic acids onto mineral surfaces. In *Water–Rock Interactions, Ore Deposits, and Environmental Geochemistry*; Hellmann, R., Wood, S. A., Eds.; Geochemical Society: St. Louis, MO, 2002.

(131) Strathmann, T. I.; Myneni, S. C. B. Effect of soil fulvic acid on nickel(II) sorption and bonding at the aqueous-boehmite (γ-AIOOH) interface. *Environ. Sci. Technol.* **2005**, *39* (11), 4027–4034.

(132) Yang, S.; Sheng, G.; Tan, X.; Hu, J.; Du, J.; Montavon, G.; Wang, X. Determination of Ni(II) uptake mechanisms on mordenite surfaces: A combined macroscopic and microscopic approach. *Geochim. Cosmochim. Acta* **2011**, *75* (21), 6520–6534.

(133) Ritchie, J. D.; Purdue, E. M. Proton-binding study of standard and reference fulvic acids, humic acids, and naturalorganic matter. *Geochim. Cosmochim. Acta* **2003**, *67* (1), 85–96.

(134) Schulthess, C. P.; Huang, C. P. Humic and fulvic acid adsorption by silicon and aluminum oxide surfaces on clay minerals. *Soil Sci. Soc. Am. J.* **1991**, *55*, 34–42.

(135) Huang, P. M.; Li, Y.; Sumner, M. E. *Handbook of Soil Sciences: Resource Management and Environmental Impacts, 2nd Ed.*; Handbook of Soil Science; CRC Press: Boca Raton, FL, 2011.

(136) Schwertmann, U.; Cambier, P.; Murad, E. Properties of goethites of varying crystallinity. *Clays Clay Miner.* **1985**, *33* (5), 369–378.

(137) Brechbühl, Y.; Christl, I.; Elzinga, E. J.; Kretzschmar, R. Competitive sorption of carbonate and arsenic to hematite: combined ATR-FTIR and batch experiments. *J.*

Colloid Interface Sci. **2012**, *377* (1), 313–321.

(138) Refait, P.; Géhin, A.; Abdelmoula, M.; Génin, J.-M. R. Coprecipitation thermodynamics of iron(II–III) hydroxysulphate green rust from Fe(II) and Fe(III) salts. *Corros. Sci.* **2003**, *45* (4), 659–676.

(139) Mellini, M.; Viti, C. Crystal structure of lizardite-1T from Elba, Italy. *Am. Miner.* **1994**, *79* (11–12), 1194–1198.

(140) Wilke Max; François, F.; Petit, P.-E.; Brown, G.; Martin, F. Oxidation state and coordination of Fe in minerals: An Fe K-XANES spectroscopic study. *Am. Mineral.* 2001, pp 714–730.

(141) Heinrich, C. A.; Seward, T. . M. A spectrophotometric study of aqueous iron (II) chloride complexing from 25 to 200°C. *Geochim. Cosmochim. Acta* **1990**, *54* (8), 2207–2221.

(142) Verdes, G.; Gout, R.; Castet, S. Thermodynamic properties of the aluminate ion and of bayerite, boehmite, diaspore and gibbsite. *Eur. J. Miner.* **1992**, *4*, 767–792.

(143) Benjamin, M. M. *Water Chemistry*; Waveland Press: Long Grove, U.S.A., 2010.

(144) Kitahama, K.; Kiriyama, R.; Baba, Y. Refinement of the Crystal Structure of Scorodite. *Acta Cryst.* **1975**, *B31*, 322–324.

(145) Mikutta, C.; Frommer, J.; Voegelin, A.; Kaegi, R.; Kretzschmar, R. Effect of citrate on the local Fe coordination in ferrihydrite, arsenate binding, and ternary arsenate complex formation. *Geochim. Cosmochim. Acta* **2010**, *74* (19), 5574–5592.

(146) Mori, H.; Ito, T. The structure of vivianite and symplesite. *Acta Cryst.* **1950**, *3*, 1–6.

(147) Alexandratos, V. G.; Elzinga, E. J.; Reeder, R. J. Arsenate uptake by calcite: macroscopic and spectroscopic characterization of adsorption and incorporation mechanisms. *Geochim. Cosmochim. Acta* **2007**, *71* (17), 4172–4187.

(148) Graf, D. L. Crystallographic tables for the rhombohedral carbonates. *Am. Miner.* **1961**, *46* (11–2), 1283–1316.

Appendices

Appendix 1: Supporting Information for Chapter 2

A1.1 Protocols used to ensure anoxic conditions during sample preparation and analysis

The sensitivity of Fe(II) towards oxidation by O_2 necessitated all batch sorption experiments and XAS sample preparation to be conducted under strictly anoxic conditions. Sample preparation and equilibration were done inside an anaerobic glovebox with an atmosphere composed of 95% N_2 and 5% H_2, and equipped with palladium catalyst (Coy Laboratories) attached to a fan box to scavenge trace O_2, and with an O_2-H_2 meter (Coy Laboratories) to monitor the glovebox atmosphere. The O_2 meter reading remained at 0 during the entire experimental period. Water used for sample and reagent preparation was boiled and purged with pure nitrogen gas for at least 1 hour outside the glovebox, and then transferred inside to cool down and degas for at least 48 hours before use. All sample containers were wrapped in aluminum foil and sealed in 3 ziplock bags during equilibration to minimize any possibility of oxidation. All labware used in the experiments, including bottles, tubes, filters, syringes and pipette tips, were brought into glovebox at least one day before use to degas any oxygen. A description of the preparation and transport of the XAS samples is provided below in section A1.3.

A1.2 Fe reference compounds

Goethite (α-$Fe^{III}OOH$) was synthesized according to the procedure described in Schwertmann et al.[136], whereas hematite (α-$Fe^{III}_2O_3$) was prepared as described in Brechbühl et al.[137] Magnetite ($Fe^{III}_2Fe^{II}O_4$) was obtained from Alfa Aesar (catalogue #

12962); green rust ($[Fe^{II}_{(1-x)}Fe^{III}_{x}(OH)_2]^{x+}[x\ Cl^- \cdot m{\times}H_2O]^{x-}$) was prepared by the coprecipitation method from Refait et al.[138], substituting SO_4^{2-} for Cl^-. Nikischerite ($NaFe^{II}_6Al_3(SO_4)_2(OH)_{18}(H_2O)_{12}$), a Fe(II)-Al(III)-layered double hydroxide with interlayer sulfate anions, was kindly provided by Tony Nikischer from the Excalibur Mineral Corporation, Peekskill, NY, and "white rust" (β-$Fe^{II}(OH)_2$) was prepared by adding 50 mL of 1 M NaOH to 50 mL of 0.25 M aqueous $FeCl_2$ under anoxic conditions. The aqueous Fe^{2+} standard was prepared by dissolving 10 mM $FeCl_2$ in 0.1M HCl.

A1.3 Preparation of Fe(II) sorption samples for XAS analysis

A total of 20 XAS sorption samples were prepared using the reaction conditions described in Chapter 2. A sample volume of 35 mL was used to ensure enough material for EXAFS analysis. The suspensions were centrifuged following reaction, and the wet pastes were loaded into lucite sample holders inside the glovebox and sealed with Kapton tape. The sealed samples were placed in four individually sealed ziplock bags for transport to the synchrotron facility, where each Kapton-sealed sample was taken out of the anoxic bags just prior to analysis. All samples were analyzed within 24 h of preparation. Each sample was checked carefully for any signs of oxidation before and immediately after analysis, which were not observed in any case.

A1.4 Synchrotron XAS data collection

Synchrotron XAS data were collected at beamline X-11A of the National Synchrotron Light Source at Brookhaven National Laboratory, and beamline 12-BMB of the Advanced Photon Source at Argonne National Laboratory. Scanning was done at the Fe *K* absorption edge (7112 eV) using a Si(111) monochromator detuned by 30% to suppress higher order harmonics and calibrated by assigning the first inflection in the *K*

absorption edge of an iron metal foil to 7112 eV. All spectra were recorded at room temperature in fluorescence mode using a stern-Heald type Lytle detector (X11A) or a Canberra 13-element solid state detector (12 BMB). Three to five scans were collected per sample to improve data quality.

A1.5 EXAFS data analyses of the sorption samples

Shell-by-shell fitting of the XAS data was done in R-space using WinXAS 3.1.[58] Theoretical back-scattering paths were calculated using ARTEMIS[60] and Feff 7.0[59] based on the crystal structures of nikischerite (Fe(II)-Al(III)-LDH, characterized in Huminicki and Hawthorne 2003 [66]) and lizardite (a 1:1 hydrous Mg silicate described in Mellini and Viti 1994 [139], with a structure similar to greenalite[74]) with Fe substituted for Mg in octahedral positions. Central Fe(II) in these structures is surrounded by six first-shell O atoms, and by three Fe and three Al second-shell atomic neighbors positioned at the same radial distance in nikischerite, and by second shell Fe (CN=6) and Si (CN=2) located at $R_{Fe\text{-}Fe}$ = 3.20 Å and $R_{Fe\text{-}Si}$ = 3.29 Å from central Fe in Fe-substituted lizardite. For fitting, the amplitude reaction factor was fixed at 1, and a single E_0 shift value was allowed to vary during optimization. The EXAFS data of Fe(II)-Al(III)-LDH phases (i.e., the nikischerite reference, the pH 7.5 and 8.0 Fe(II)- γAl_2O_3 sorption samples, and the pH 7.5 Fe(II)-clay sorption samples) were fitted with three paths: first-shell Fe-O, second shell Fe-Fe and second shell Fe-Al. The coordination number was fixed at 3 for second-shell Fe and Al, consistent with the structure of nikischerite[66]. The radial distance (R) and Debye-Waller factors (σ^2) of second-shell Fe-Fe and Fe-Al were constrained to be same to further reduce the number of free parameters, while all other parameters were allowed to vary.

For the Fe(II)-clay sorption samples reacted at pH 8.0 and the Fe(II)-SiO_2 reacted at pH 7.5 and 8.0, the parameters associated with first shell O were allowed to vary. Fitting of the second shell was done with Fe-Fe and Fe-Si scattering paths, consistent with the formation of tri-octahedral Fe(II)-phyllosilicates in these samples as described in Chapter 2. The coordination number of second-shell of Fe-Fe was fixed at 6 consistent with tri-octahedral $Fe(OH)_2$ sheets, whereas coordination number of Fe-Si atoms was allowed to vary. We constrained the Debye-Waller factors (σ^2) of second-shell Fe-Fe and Fe-Si to be the same to further reduce the number of free parameters.

Wavelet transform (WT) analysis was employed here to visualize differences in the coordination environment of Fe of the second coordination shell in RSFs. The WT analysis was performed with the Igor Pro script developed by Funke et al.[61] Non-phase shift corrected k^3 weighted χ spectra were analyzed in the Igor program using Morlet wavelet with parameters η=5.8 and σ=1 at distance of 2.4-3.6 Å. The Morlet parameters were chosen to optimize the best resolution in both *k* and R space based on the results in Funke et al.[61]

A1.6 Comparison of Fe *K* edge XAS data of reference compounds and Fe(II) sorption samples

Analyses of the XANES data of the Fe(II) sorption samples are presented in Figure A1.1. Figure A1.1a compares the normalized Fe *K* near-edge spectra of representative sorption samples and Fe reference compounds, whereas Figure A1.1b compares the corresponding pre-edge features occurring approximately 15 eV before the main edge, which are indicative of Fe valence state.[140] The positions of both the main Fe *K* edge and the pre-edge features of the sorption samples are consistent with a 2+ valence state of sorbed Fe,

indicating that no oxidation of Fe(II) occurred during sorption or XAS data collection. This agrees with the results of our previous work[17] showing the absence of Fe(II) oxidation in samples prepared and analyzed with identical procedures and protocols as employed here (described above in section A1.1 and A1.3).

Figure A1.2 provides a direct comparison of the k^3-weighted χ spectra of Fe(II)-clay and Fe(II)-γAl_2O_3 sorption samples. Figure A1.2a demonstrates that the χ function of the pH 7.5 Fe(II)-clay sorption sample is similar to the χ spectra of nikischerite and the pH 7.5 Fe(II)-γAl_2O_3 sorption samples, suggesting precipitation of Fe(II)-Al(III)-LDH in the clay suspension at this pH value. At pH 8.0, sorption of Fe(II) onto the clay results in the precipitation of Fe(II)- phyllosilicate based on the data presented in Figure A1.2b, which shows that the pH 8.0 Fe(II)-clay sorption spectrum is similar to that of the pH 8.0 Fe(II)-SiO_2 sorption sample.

A1.7 Structure of β-$Fe(OH)_2$, nikischerite, greenalite and minnesotaite

Figure A1.3 shows the mineralogical structure of the main Fe(II) minerals discussed in Chapter 2. In β-$Fe(0H)_2$, central Fe^{2+} atoms is octahedrally coordinated with hydroxyl groups in the first coordination shell, and with Fe in the second coordination shell.[68] Substitution of Al^{3+} for Fe^{2+} in the $Fe(OH)_2$ sheets of the Fe(II)-Al(III)-LDH phase nikischerite ($NaFe^{II}_6Al_3(SO_4)_2(OH)_{18}(H_2O)_{12}$), generates a positive structural charge in the octahedral sheet, which is neutralized by negatively charged sulphate anions in the interlayer (not shown); for the Fe(II)-Al(III)-LDH phases formed in the current study the charge balancing anion is Cl^- derived from the reaction electrolyte. Greenalite and minnesotaite are 1:1 and 2:1 hydrous iron silicates, respectively, where brucitic (tri-

octahedral) $Fe(OH)_2$ sheets are coordinated to one (greenalite) or two (minnesotaite) sheets of tetrahedral Si through corner sharing bonds to the Fe(II) octahedral sheet. Central Fe has a similar distance to its nearest octahedral Fe and tetrahedral Si neighbors.

A1.8 Macroscopic Si concentration in clay and amorphous SiO_2 system

Figure A1.4 compares the dissolved silica concentrations of Fe(II)-clay and Fe(II)-SiO_2 kinetic samples to those of control samples made up of identical suspensions but without added Fe(II) at pH 6.5, 7.5 and 8.0 monitored for a reaction time up to 15 days. The dissolved Si concentrations are the same for the Fe(II) sorption samples and control samples at pH 6.5 and 7.5 in the clay system (Figures A1.4a and b), as well as at pH 6.5 in the amorphous SiO_2 system (Figure A1.4d), whereas distinct depletion of Si is observed in the pH 8.0 Fe(II)-clay and the pH 7.5 and 8.0 Fe(II)-SiO_2 sorption samples relative to their respective controls (Figures A1.4c, e, f). We observe precipitation of secondary Fe(II) phases within the 15 d experimental time frame considered here at pH 7.5 and 8.0 in both the Fe(II)-clay and Fe(II)- SiO_2 sorption systems (see Figure 2.3). The results presented in Figure A1.4 point to association of Si with the Fe(II) precipitates formed in the amorphous silica suspensions at pH 7.5 and 8.0, consistent with the formation of Fe(II)-phyllosilicate phases in these systems. In the Fe(II)-clay sorption samples, Si interaction with secondary Fe(II) precipitate is observed at pH 8.0 but not at pH 7.5 (Figure A1.4b, c), suggesting formation of Fe(II)-phyllosilicate at pH 8.0 but not at the lower pH value. This pH dependent difference in the Fe(II) precipitates formed during Fe(II)-clay sorption, as suggested by the dissolved Si trends of Figure A1.4, is corroborated by the difference in the EXAFS data of the pH 7.5 and 8.0 Fe(II)-clay

sorption samples demonstrating precipitation of Fe(II)-Al(III)-LDH at pH 7.5 and formation of Fe(II)-phyllosilicates at pH 8.0 (Figure A1.2, and Table 2.1 and Figure 2.3).

A1.9 Calculation of the solubility product (K_{sp}) of Fe(II)-Al(III)-LDH phases formed in the Fe(II)-γAl_2O_3 sorption samples

As described in Chapter 2, the chemical formula of the Fe(II)-Al(III) layered double hydroxide (LDH) formed in the γAl_2O_3 samples at pH ≥ 7.0 is assumed to be $Fe(II)_{\frac{2}{3}}Al(III)_{\frac{1}{3}}(OH)_2Cl_{\frac{1}{3}}$. The aqueous equilibrium of these phases can be expressed as:

$$Fe(II)_{\frac{2}{3}}Al(III)_{\frac{1}{3}}(OH)_2Cl_{\frac{1}{3}(s)} = \frac{2}{3}Fe^{2+} + \frac{1}{3}Al^{3+} + 2OH^- + \frac{1}{3}Cl^- \quad (1)$$

The corresponding solubility product K_{sp} is:

$$K_{sp} = (Fe^{2+})^{2/3} * (Al^{3+})^{1/3} * (OH^-)^2 * (Cl^-)^{1/3} \quad (2)$$

where round brackets denote solution activities. The activity coefficient γ for each component was calculated using the Davies equation:

$$log\ \gamma = -0.509 * Z^2(\frac{I^{0.5}}{I^{0.5}+1} - 0.2I) \quad (3)$$

where Z is the ion valence, and I is ionic strength calculated according to:

$$I = 0.5 \sum_{all\ ions} C_i {Z_i}^2 \quad (4)$$

with *C* and *Z* representing the concentration and valence state of each dissolved component, respectively.

The solubility products of $Fe(II)_{\frac{2}{3}}Al(III)_{\frac{1}{3}}(OH)_2Cl_{\frac{1}{3}}$ were estimated for each of the three kinetic experiments presented in Figure 2.2a of Chapter 2 where formation of Fe(II)-Al(III)-LDH was observed in the EXAFS measurements (i.e. at pH 7.0, 7.5 and 8.0). All equilibrium concentrations required to calculate K_{sp} at given pH are known, except for dissolved Al^{3+}, which was too low for detection by ICP-OES. The total dissolved Fe(II) concentrations, $[Fe(II)]_{tot}$, were calculated as the average aqueous Fe(II) concentration of the last 3 measurements, where equilibrium was attained (see Figure 2.2 of Chapter 2). Complexation of aqueous Fe(II) with Cl-(aq) was accounted for based on the following aqueous equilibrium:[141]

$$Fe^{2+} + Cl^{-} = FeCl^{+} \qquad \log\beta = -0.16 \tag{5}$$

where β represents the equilibrium constant for reaction (5). Thus, the formation of $FeCl^+$ can be written as $(FeCl^+) = \beta(Fe^{2+})(Cl^-)$. Consequently, (Fe^{2+}) was calculated by expressing $[Fe(II)]_{tot}$ with (Fe^{2+}), the activity coefficient γ, and (Cl^-), where only (Fe^{2+}) was unknown. The OH^- activity was determined based on the final pH measured at the end of each kinetic experiment, and $[Cl^-]$ was equal to the NaCl concentration used for ionic strength control. Concentrations were converted to activities by multiplying with the activity coefficient γ. Table A1.1 summarizes the various concentrations and activities used for these calculations.

The activity of dissolved Al^{3+}, (Al^{3+}), was calculated for two scenarios: one assuming it set by equilibrium with gibbsite, α-$Al(OH)_3$, and the other assuming it was controlled by bayerite, β-$Al(OH)_3$. The selection of gibbsite and bayerite as the

controlling phases of Al solubility is based on studies demonstrating that these are the main Al phases that form during aging of (metastable) γ-Al_2O_3 in aqueous suspensions.[78–80] The Al^{3+} activities were calculated based on the following dissolution-precipitation reaction:

$$Al(OH)_{3(s)} = Al^{3+} + 3OH^- \quad (6)$$

according to $(Al^{3+}) = \frac{K'_{sp}}{\{OH^-\}^3}$, where K'_{sp} is the equilibrium constant of the $Al(OH)_3$ polymorph of interest (i.e. gibbsite or bayerite). The solubility products of gibbsite and bayerite were calculated from the standard Gibbs free energy of reaction (ΔG_R^0) for reaction (6), according to:

$$K'_{sp} = e^{\frac{\Delta G_R^0}{-RT}} \quad (7)$$

The ΔG_R^0 values were calculated from the Gibbs free energies of formation (ΔG_f^0) of bayerite and gibbsite (-1149.8 kJ/mol and -1154.9 kJ/mol, respectively,[142] at 298.15 K) and those of $Al^{3+}_{(aq)}$ ($\Delta G^0_{f(298.15\ K)}$=-489.4 kJ/mol[143]) and $OH^-_{(aq)}$ (ΔG_f^0 =-157.3 kJ/mol[143]). Based on these data we calculated K'_{sp}=$10^{-33.042}$ and $10^{-33.936}$ for bayerite and gibbsite, respectively, for the expression of K'_{sp} in equation (7). The calculated K'_{sp} value for gibssite is similar to the value of K'_{sp}=$10^{-33.709}$ in the MINEQL+ database.[69] The (Al^{3+}) levels calculated at the experimental pH values assuming gibbsite or bayerite as the mineral phases controlling Al solubility are tabulated in Table A1.1. The corresponding estimates of the K_{sp} solubility product of the Fe(II)-Al(III)-LDH phases formed at pH 7.0, 7.5 and 8.0 in the γ-Al_2O_3 sorption systems are listed as well. The K_{sp} estimates differ

substantially depending on whether gibbsite or bayerite is assumed to control $\{Al^{3+}\}$, but are remarkably similar at the three pH values assuming either gibbsite or bayerite (Table A1.1), indicating that the Fe(II)-Al(III)-LDH phases formed in these samples have similar structure and solubility.

A1.10 Supporting information table and figures

Table A1.1. Thermodynamic calculations of the formed Fe(II)-Al(III)-LDH phases

Ion concentrations, activities and calculation results of K_{sp} for the Fe(II)-Al(III)-LDH phases formed in the Fe(II)-γAl_2O_3 sorption systems at pH 7.0, 7.5 and 8.0.

pH[f] / calculation results[a]	7.0	7.5	8.0
$[Fe(II)]_{tot}$ (mol L^{-1})	$1.82*10^{-3}$	$4.69*10^{-4}$	$1.11*10^{-5}$
$[Fe^{2+}]$ (mol L^{-1})	$1.78*10^{-3}$	$4.64*10^{-4}$	$1.10*10^{-5}$
$[FeCl^{+}]$ (mol L^{-1})	$3.81*10^{-5}$	$8.46*10^{-6}$	$1.67*10^{-6}$
pH[b]	6.91	7.33	7.79
$[Cl^{-}]$ (mol L^{-1})[c]	$8.80*10^{-2}$	$7.50*10^{-2}$	$6.20*10^{-2}$
$[Na^{+}]$ (mol L^{-1})[d]	0.10	0.10	0.10
ionic strength (mol L^{-1})	0.01	0.01	0.01
activity coefficient (γ) for univalent ions	0.77	0.77	0.77
activity coefficient (γ) for divalent ions	0.35	0.35	0.35
$(Al^{3+})_{gibbsite}$ (mol L^{-1})[e]	$2.16*10^{-13}$	$1.19*10^{-14}$	$4.94*10^{-16}$
$(Al^{3+})_{bayerite}$ (mol L^{-1})	$1.69*10^{-12}$	$9.28*10^{-14}$	$3.87*10^{-15}$
$K_{sp\ (gibbsite)}$	$1.18*10^{-21}$	$1.20*10^{-21}$	$1.26*10^{-21}$
$K_{sp\ (bayerite)}$	$2.35*10^{-21}$	$2.39*10^{-21}$	$2.49*10^{-21}$

[a] [ ] and ( ) represent concentration and activity, respectively; [ ]*γ=( )

[b] pH measured at equilibrium

[c] $[Cl^{-}]$ equal to the NaCl concentration used for ionic strength control after accounting for the addition of titrant NaOH to achieve pH of interest

[d] $[Na^{+}]$ derived from addition of NaOH titrant and NaCl background salt

[e] (Al^{3+}) in equilibrium with the final hydration product of γ-Al_2O_3; Calculated K_{sp} based on different (Al^{3+}) values

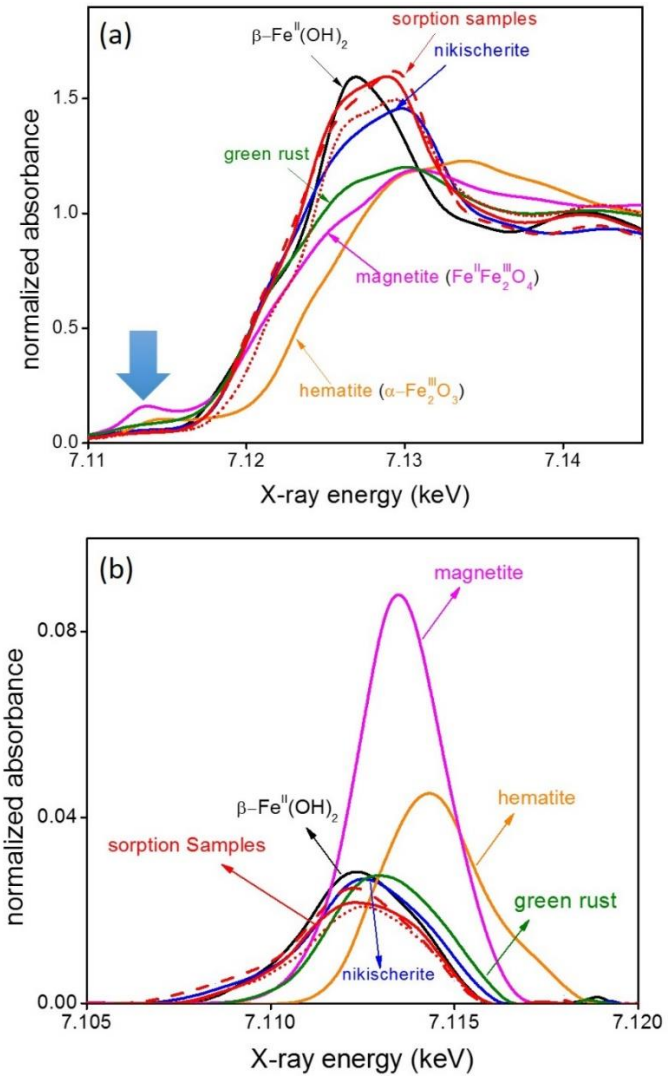

Figure A1.1. Fe *K* near-edge and pre-edge results of references and sorption samples **(a)** Normalized Fe *K* near-edge XAS spectra of representative Fe(II) sorption samples and Fe(II)- and Fe(III)-reference compounds; **(b)** Pre-edge features located approximately 15 eV before the main edge (pointed out by arrow in a), isolated by fitting a spline function through the pre-edge region of the normalized Fe *K* edge spectra.[17,140] The sorption samples were Fe(II)-reacted clay (red solid line), γ-Al_2O_3 (red dashed line) and amorphous silica (red dotted line) prepared at a Fe(II) concentration of 2.7 mM, a pH of 8.0, and a reaction time of 1month.

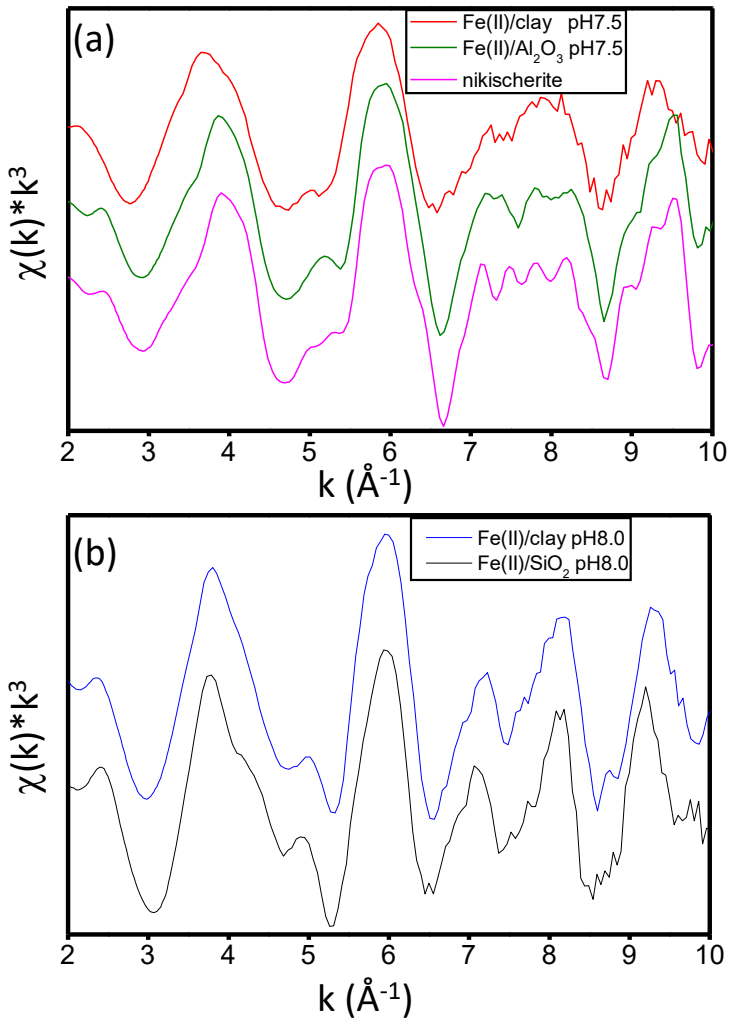

Figure A1.2. Comparison of the k^3-weighted χ spectra

(a) nikischerite and the Fe(II)-clay and Fe(II)-γAl_2O_3 sorption samples reacted at pH 7.5;

(b) the Fe(II)-clay and Fe(II)-SiO_2 sorption samples reacted at pH 8.0.

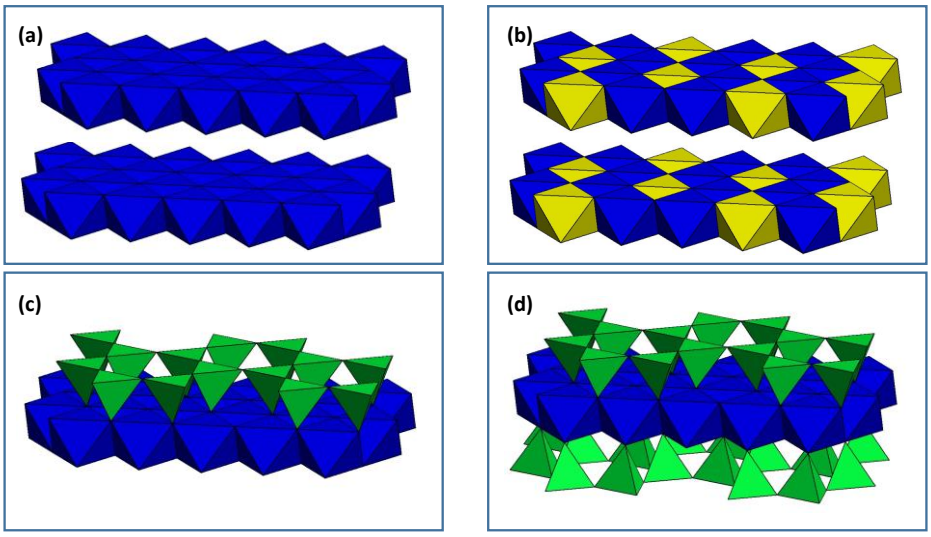

Figure A1.3. Structures of reference Fe(II) minerals

(a) white rust (β-$Fe(OH)_2$); (b) nikischerite (Fe(II)-Al(III) LDH); (c) greenalite (1:1 hydrous iron silicate, $Fe_3Si_2O_5(OH)_4$); and (d) minnesotaite (2:1 hydrous iron silicate, $Fe_3Si_4O_{10}(OH)_2$). Blue and yellow octahedra represent, respectively, Fe(II) and Al(III) cations in octahedral coordination with hydroxyl groups. Green tetrahedra in c and d represent Si tetrahedra arranged in sheets that coordinate to the octahedral $Fe(OH)_2$ sheets through corner sharing O bonds.

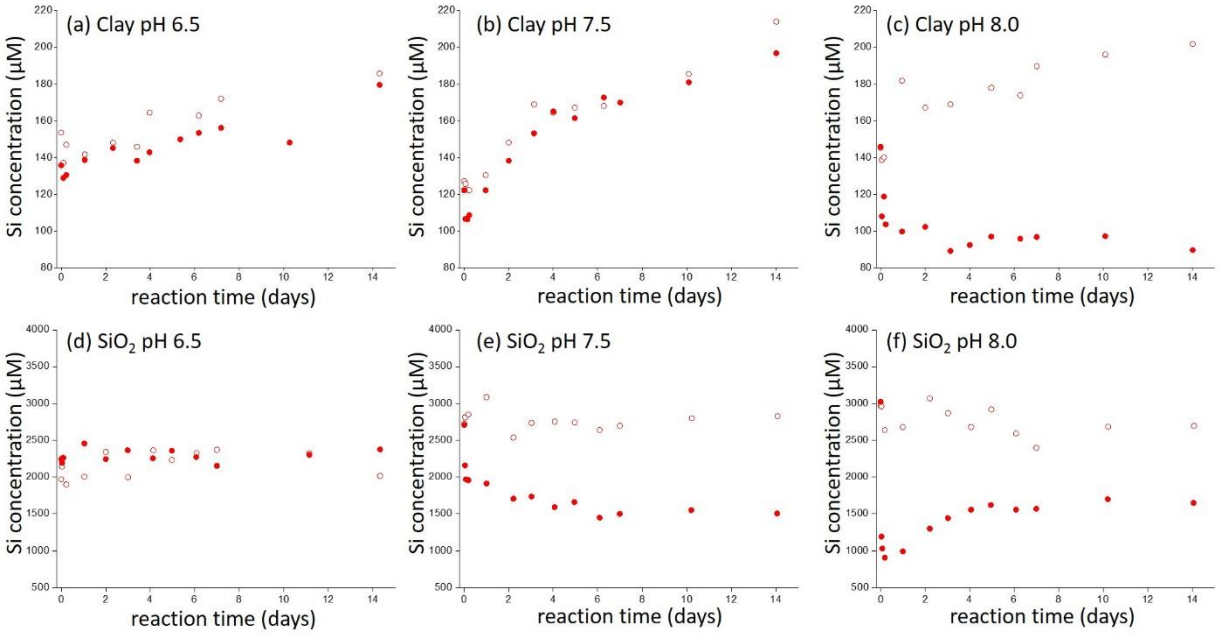

Figure A1.4. Dissolved Si concentrations

Dissolved Si concentrations in the Fe(II)-clay (a, b, c) and Fe(II)-amorphous silica (d, e, f) kinetic sorption experiments conducted at pH 6.5, 7.5 and 8.0 and in control samples consisting of identical suspensions without added Fe(II). The closed (●) and open (○) symbols denote Si concentrations in the suspensions with and without Fe(II) treatment, respectively.

Appendix 2: Supporting Information for Chapter 3

A2.1 EXAFS data analyses of the sorption samples and reference compounds

EXAFS data fitting of the spectra was done on Fourier transformed k^3 weighed χ spectra in R-space using WinXAS 3.1.[58] Theoretical backscattering paths of Fe-O, Fe-Fe and Fe-Al were calculated with the FEFF 7.0 code,[59] based on the structure of nikischerite (a Fe(II)-Al(III)-LDH with chemical formula $NaFe^{II}_6\ Al_3(SO_4)_2(OH)_{18}\ (H_2O)_{12}$, characterized in Huminicki and Hawthorne 2003 [66]), whereas Fe-As, As-O, As-Fe single scattering and three multiple scattering (MS) within the As(V) centered tetrahedron was calculated based on the structure of scorodite ($Fe(III)As(V)O_4 \cdot 2H_2O$, characterized in Kitahama et al. 1975 [144]). Theoretical As-Al scattering paths were obtained by replacing Fe with Al in octahedral positions of scorodite. The amplitude reduction factor was set at 0.9 for the Fe fits, and at 1.0 for the As fits. A single E_0 shift value was allowed to vary during optimization.

The Fe *K*-edge EXAFS data of samples containing Fe(II)-Al(III)-LDH were fitted with three paths: first-shell Fe-O, and second-shell Fe-Fe and Fe-Al, based on the crystal structure of nikischerite.[66] In this structure, Fe(II) is surrounded by six first-shell O atoms, and three Fe and three Al second-shell neighbors that are located at the same radial distance (Figure A2.1). To reduce the number of free parameters, the radial distances and Debye-Waller factors (σ^2) of second-shell Fe-Fe and Fe-Al were constrained to be the same, while all other factors were allowed to vary. For the aqueous Fe(II) reference and the dual-sorbate samples containing 0.5 mM As(V), only first-shell Fe-O was fitted due to the lack of apparent second-neighbor backscattering as observed in the RSFs (Figure

3.3 of Chapter 3). The spectrum of the Fe(II)-As(V) precipitate was fitted with first-shell Fe-O and second-shell Fe-Fe and Fe-As paths.

The As *K*-edge EXAFS data of all the sorption samples were fitted with first-shell O backscatters and second-shell Al backscatters. For As(V) sorption samples in both binary and ternary systems, three fully restrained MS paths within the As(V) centered tetrahedron were also employed in the fitting, in addition to As-O and As-Al paths alone (results not shown), following the MS fitting scheme of Mikutta et al.[145] and Voegelin et al.[109] The inclusion of MS slightly improved the fitting quality without inducing substantial changes in the major parameters of As-O and As-Al distances, which agrees with the findings of Voegelin et al.[109] Because of the minor impacts of MS on our fitting results and data interpretation, only the single-shell fits are presented in Table A2.1, consistent with other studies [e.g. 94]. For the As data of the ternary sorption samples, we also tested data fits assuming As-Fe instead of As-Al second-neighbor scattering. This yielded distinctly worse fit quality relative to fits with second-neighbor As-Al scattering, regardless of the inclusion of MS paths. This confirms our interpretation of As being present as adsorption complexes at the Al-oxide surface in both the presence and absence of Fe(II), as discussed in Chapter 3. For the aqueous arsenite and arsenate references, only first-shell O was fitted, while for the Fe(II)-As(V) precipitate reference, first-shell As-O and second-shell As-Fe paths were fitted (Table A2.1).

Error estimates of the optimized XAS fitting parameters are ±0.02 Å for the radial distance (R) of the first coordination shells, and ±0.04 Å for the radial distances of longer shells. For coordination numbers (CN), which are correlated to the Debye-Waller factor,

the estimated error is ± 25 %. These error estimates of the fitting parameters are based on fits of reference compounds and previous relevant XAS studies.[17,25,28,30,94]

A2.2 Comparison of structural information of symplesite and EXAFS fit results of the Fe(II)-As(V) reference precipitate

Figure A2.2 shows the mineralogical structure of symplesite ($Fe_3(AsO_4)_2 \cdot 8H_2O$), which is crystallographically similar to vivianite ($Fe_3(PO_4)_2 \cdot 8H_2O$),[146] reflecting the chemical similarity of arsenate and phosphate. The structure of symplesite contains single $Fe^{II}O_6$ octahedra and pairs of edge sharing Fe(II) octahedra (double Fe(II) octahedra), which are linked by arsenate groups (Figure A2.2). The structural arrangement of Fe(II) and As(V) is further resolved in Figure A2.3. Based on experimental distance of Fe-O (2.10-2.14 Å) and As-O (1.68-1.69 Å), and Fe-O-As angles provided in Figure A2.3, theoretical bond distance of Fe-As was estimated to be 3.43-3.56 Å.

Our EXAFS data fitting results (Table A2.1) of the Fe(II)-As(V) precipitate indicate that it is structurally similar to symplesite. The Fe *K*-edge EXAFS fitting results of Fe(II)-As(V)-precipitate (Table A2.1), the first shell is fitted with 5.3 O atoms at a radial distance of 2.11 Å, in agreement with an octahedral arrangement of O atoms around central Fe(II). The second-shell $R_{Fe\text{-}Fe}$=3.25 Å is very close to the Fe-Fe distance (3.26 Å) in $Fe(OH)_2$,[68] consistent with the edge-sharing octahedron configuration for double Fe(II) groups present in symplesite (Figure A2.2 and A2.3b, A2.3c). In addition, the average $R_{Fe\text{-}As}$=3.45 Å are within the range of estimated Fe-As distance in symplesite, as shown above. The As *K*-edge EXAFS fitting results show first-shell $CN_{As\text{-}O}$= 3.3(±30%) for Fe(II)-As(V) precipitate at an average distance of R = 1.68 Å, suggesting that As(V) is coordinated by O atoms in tetrahedral configuration [94,110,111,147]. The second-shell $R_{As\text{-}Fe}$ =

3.41 Å is consistent with the average R_{Fe-As} obtained from Fe *K*-edge EXAFS results, given the large error of ±0.04 Å correlated with R values of second-shell fitting. This result is also within the range of As-Fe distance of 3.31-3.55A reported in Jönsson and Sherman (2008).[108]

Although the fitting results suggest similarity between structure of Fe(II)-As(V) bulk precipitate and symplesite, we could not completely confirm the formation of symplesite and exclude the existence of impurities solely based EXAFS measurement.

A2.3 As *K*-edge EXAFS data of sorption samples and As reference compounds

Figures A2.4 - A2.7 present the entire set of As *K*-edge EXAFS data collected for this study; the fit results are presented in Table A2.2. The first peak in the RSFs represents the first-shell O atoms surrounding central As(V) and As(III). The second shells visible in the RSFs of the sorption samples represent second-shell Al neighbors in the coordination sphere of sorbed As(III) and As(V), consistent with inner-sphere coordination of both arsenic species at the Al-oxide surface.

The spectral comparison presented in Figure A2.8 illustrates that the dominant As(V) sorption mechanism on γ-Al_2O_3 remains the same, irrespective of the initial As(V) concentrations. The comparison displayed in Figure A2.9 shows the similarity of the speciation of As(III) and As(V) in single- and dual-sorbate systems. This demonstrates that Fe(II) has no noticeable impact on the mode of As retention in our experimental systems, with both As(III) and As(V) coordinated predominantly as bidentate binuclear adsorption complexes at the surface of the Al-oxide sorbent in both the presence and absence of Fe(II).

A2.4 Supporting information tables and figures

Table A2.1. Fe *K*-edge EXAFS fitting results of Fe(II) sorption and reference samples

sorption samples				Fe-O			Fe-Fe			Fe-Al			Fe-As		
$[Fe]_0$	$[As]_0$	time	Γ^d	CN[a]	R (Å)[b]	σ^2 (Å^2)[c]	CN	R (Å)	σ^2 (Å^2)	CN	R (Å)	σ^2 (Å^2)	CN	R (Å)	σ^2 (Å^2)
1mM	0.50mM V	8 mo	1.96	5.8	2.10	0.010									
1mM	0.50mM V	35 d	2.36	5.3	2.09	0.010									
1mM	0.50mM V	6 d	1.76	5.4	2.10	0.010									
1mM	0.50mM V	1 d	1.70	6.0	2.09	0.012									
1mM	0.25mM V	9 mo	2.19	5.7	2.11	0.009	3.6	3.14	0.010	2.9	3.14	0.010			
1mM	0.25mM V	35 d	1.53	5.5	2.10	0.009	2.6	3.13	0.010	2.3	3.13	0.010			
1mM	0.25mM V	6 d	0.95	5.0	2.09	0.009									
1mM	0.25mM V	1 d	0.83	4.8	2.08	0.010									
1mM	0.10mM V	35 d	1.97	6.0	2.11	0.009	4.2	3.14	0.010	2.9	3.14	0.010			
1mM	0.10mM V	6 d	1.33	5.2	2.11	0.009	3.0	3.15	0.010	2.4	3.15	0.010			
1mM	0.10mM V	1 d	0.80	5.0	2.08	0.009									
1mM	0.25mM III	6 d	1.81	6.0	2.11	0.008	4.0	3.14	0.009	2.6	3.14	0.009			
1mM	0.25mM III	1 d	1.02	5.7	2.1	0.008	3.7	3.13	0.009	2.8	3.13	0.009			
1mM	—	6 d	1.83	5.8	2.12	0.008	4.8	3.15	0.010	2.0	3.15	0.010			
1mM	—	1 d	1.07	6.0	2.12	0.009	4.0	3.15	0.010	2.3	3.15	0.010			
1mM	—	2 hr	0.50	6.0	2.12	0.009	4.2	3.15	0.010	2.4	3.15	0.010			
Fe references															
Nikischerite				5.5	2.13	0.007	4.0	3.15	0.009	2.3	3.15	0.009			
aqueous Fe^{2+}				5.7	2.11	0.010									
Fe(II)As(V)-precipitate				5.4	2.11	0.008	0.9	3.25	0.015				3.5	3.45	0.015

[a]CN is coordination number, [b]R is interatomic radial distance, and [c]σ^2 is Debye-Waller factor. Error estimates and details on fitting procedure are described above in section 1 of the SI. [d]Γ is the Fe(II) sorption density (μmol/m^2) calculated based on the N_2-BET surface area.

Table A2.2. **As *K*-edge EXAFS fitting results of As sorption and reference samples**

sorption samples				As-O			As-Al			As-Fe		
$[Fe]_0$	$[As]_0$	time	Γ^d	CN[a]	R (Å)[b]	σ^2 (Å^2)[c]	CN	R (Å)	σ^2 (Å^2)	CN	R (Å)	σ^2 (Å^2)
1mM	0.50mM V	8 mo	1.42	4.1	1.68	0.002	3.3	3.14	0.006			
1mM	0.50mM V	35 d	1.42	4.1	1.69	0.002	3.2	3.15	0.006			
1mM	0.50mM V	6 d	1.41	4.2	1.69	0.002	3.2	3.14	0.006			
1mM	0.50mM V	1 d	1.39	4.3	1.69	0.002	2.7	3.14	0.006			
	0.50mM V	6 d	1.04	4.1	1.68	0.002	2.6	3.12	0.006			
1mM	0.25mM V	9 mo	0.71	4.4	1.68	0.002	2.8	3.14	0.006			
1mM	0.25mM V	35 d	0.71	4.1	1.69	0.002	2.5	3.15	0.006			
1mM	0.25mM V	6 d	0.70	4.3	1.68	0.002	2.4	3.13	0.006			
1mM	0.25mM V	1 d	0.68	4.5	1.68	0.003	2.5	3.13	0.006			
	0.25mM V	6 d	0.67	4.4	1.68	0.002	2.6	3.14	0.006			
1mM	0.10mM V	35 d	0.28	4.3	1.68	0.002	2.5	3.15	0.006			
1mM	0.10mM V	6 d	028	4.1	1.68	0.002	2.4	3.15	0.006			
1mM	0.10mM V	1 d	0.28	4.2	1.68	0.002	2.5	3.15	0.006			
	0.10mM V	6 d	0.26	4.2	1.68	0.002	2.7	3.13	0.006			
1mM	0.25mM III	35 d	0.48	3.2	1.77	0.004	1.6	3.22	0.009			
1mM	0.25mM III	6 d	0.42	3.5	1.78	0.004	1.3	3.24	0.009			
1mM	0.25mM III	1 d	0.38	3.2	1.77	0.004	1.6	3.22	0.009			
	0.25mM III	6 d	0.41	3.4	1.78	0.004	1.3	3.23	0.009			
As references												
10mM $Na_2HAs(V)O_{4(aq)}$				4.2	1.68	0.003						
10mM $NaHAs(III)O_{2(aq)}$				3.0	1.79	0.002						
Fe(II)-As(V)-precipitate				3.3	1.68	0.002				4.1	3.41	0.015

[a]CN is coordination number, [b]R is interatomic radial distance, and [c]σ^2 is Debye-Waller factor. [d]Γ is the As(III/V) sorption density (μmol/m^2) calculated based on the N_2-BET surface area.

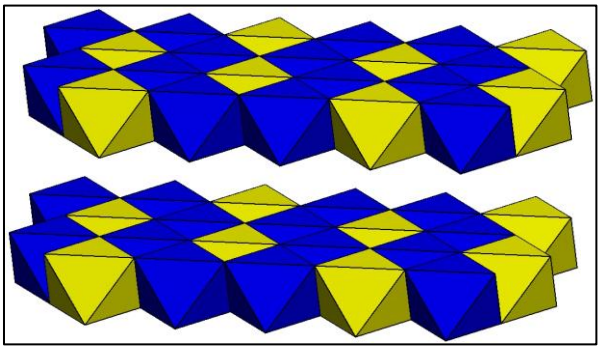

Figure A2.1. Mineralogical structure of nikischerite

Mineralogical sheet structure of nikischerite (a Fe(II)-Al(III)-LDH mineral with chemical formula $NaFe^{II}_6\ Al_3(SO_4)_2(OH)_{18}\ (H_2O)_{12}$). Blue and yellow octahedron represent Fe(II) and Al(III) cations in octahedral coordination with hydroxyl groups respectively. The octahedral layers have a positive structural charge, which is balanced by sulfate anions in the interlayer (not shown).

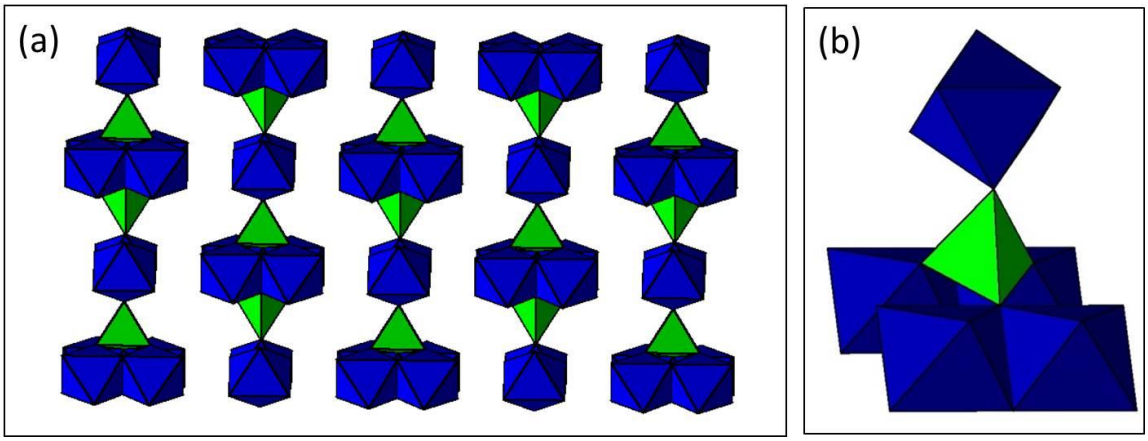

Figure A2.2. Mineralogical structure of symplesite ($Fe_3(AsO_4)_2{\cdot}8H_2O$)

(a) Sructure of symplesite ($Fe_3(AsO_4)_2{\cdot}8H_2O$);[146] (b) arsenate tetrahedron coordinated with 1 single Fe(II) octrahedron and 2 pairs of double Fe(II) octrahedra. Blue octahedra and green tetrahedra represent octahedral Fe(II) and tetrahedral As(V), respectively.

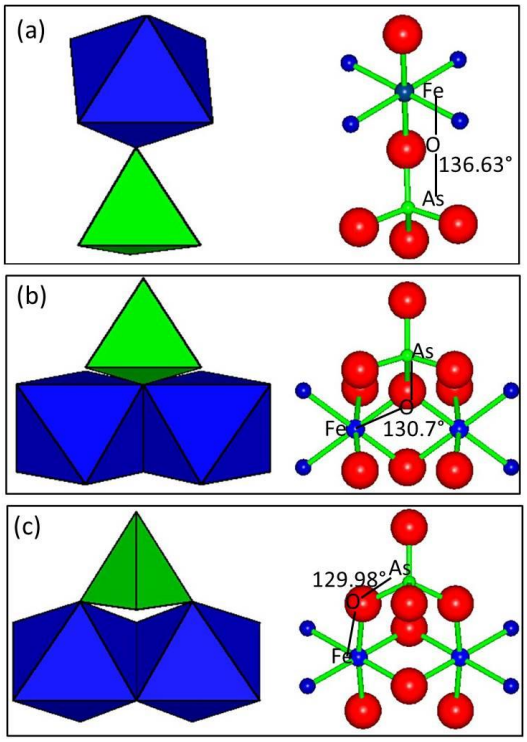

Figure A2.3. Detailed arrangement of As(V) and Fe(II) within the symplesite structure Arrangement of As(V) and Fe(II) within the symplesite structure presented by polyhedra (left) and atomic spheres (right): (a) As(V) tetrahedron coordinated with a single Fe(II) octahedron; (b)(c) As tetrahedron link with a double Fe(II) octahedral unit. Red, green, big blue and small blue atomic spheres in the right represent oxygen, As, Fe and water, respectively. Fe-O-As angles[146] used for distance calculation are indicated in each figure.

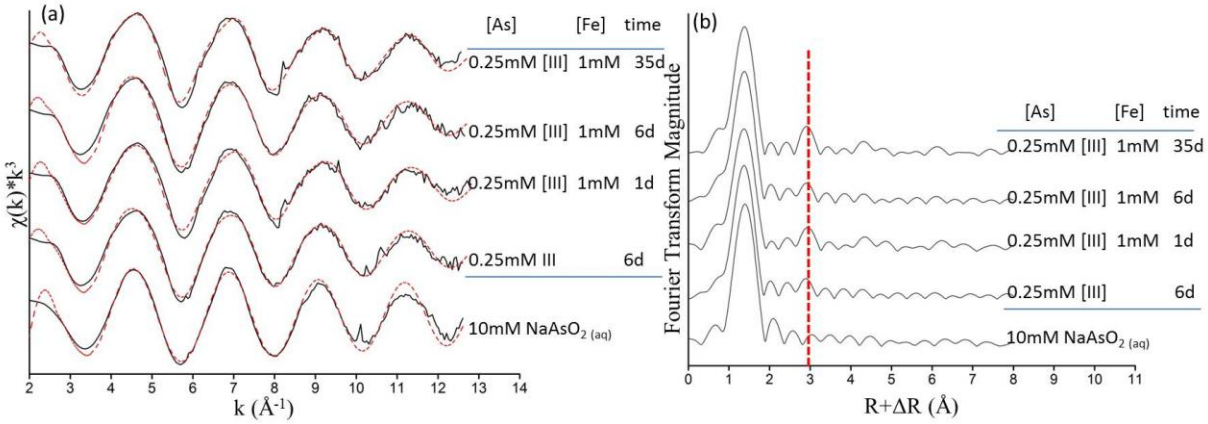

Figure A2.4. As K-edge EXAFS results of As(III) sorption references and samples

As *K*-edge EXAFS spectra of aqueous As(III) and As(III)/γ-Al_2O_3 sorption samples in single-sorbate reaction and dual-sorbate reactions with 1mM Fe(II) addition (a) k^3-weighted χ spectra and (b) corresponding radial structure functions (RSFs). Solid and red dotted lines in panel (a) represent raw and fitted spectra, respectively. The red vertical dashed line in panel (b) locates the second-shell Al neighbors in the sorption samples.

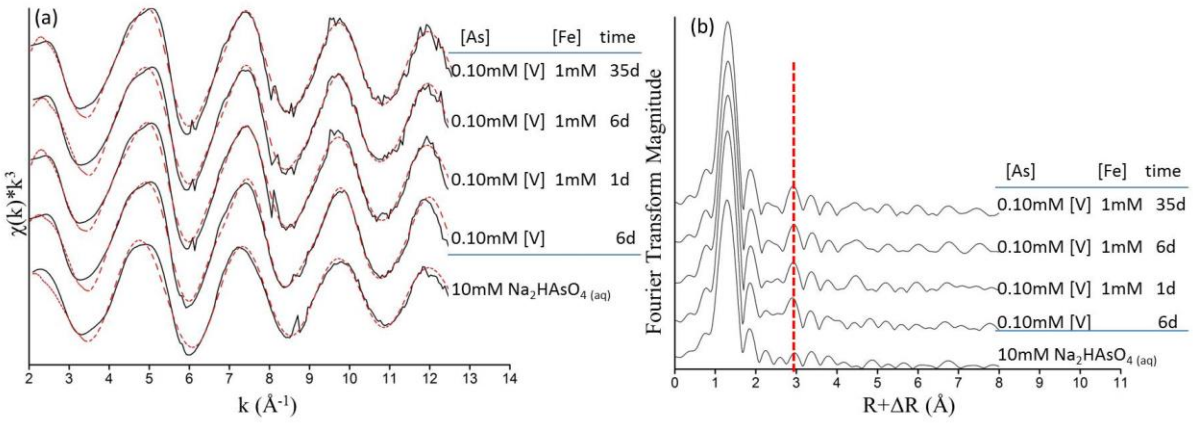

Figure A2.5. As K-edge EXAFS results of 0.1mM As(V) sorption references and samples As *K*-edge EXAFS spectra of aqueous As(V) and 0.1mM As(V)/γ-Al_2O_3 sorption products in single-sorbate reaction and dual-sorbate reactions with 1mM Fe(II) addition (a) k^3-weighted χ spectra and (b) corresponding radial structure functions (RSFs). Solid and red dotted lines in panel (a) represent raw and fitted spectra, respectively. Red vertical dashed line in panel (b) indicates second-shell As-Al backscatters in the sorption samples.

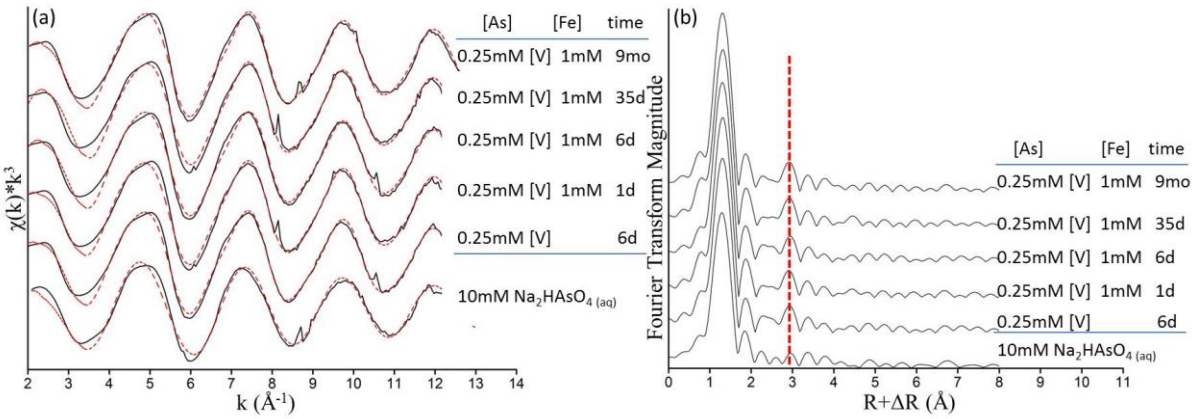

Figure A2.6. As K-edge EXAFS results of 0.25mM As(V) sorption references and samples

As *K*-edge EXAFS spectra of aqueous As(V) and 0.25mM As(V)/γ-Al_2O_3 sorption products in single-sorbate reaction and dual-sorbate reactions with 1mM Fe(II) addition (a) k^3-weighted χ spectra and (b) corresponding radial structure functions (RSFs). Solid and red dotted lines in panel (a) represent raw and fitted spectra, respectively. Red vertical dashed line in panel (b) indicates second-shell As-Al backscatters in the sorption samples.

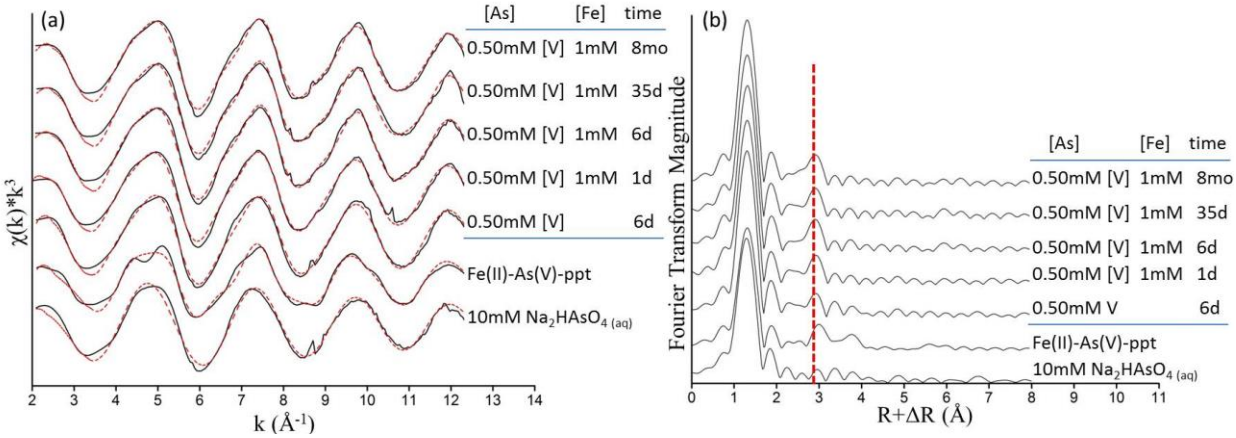

Figure A2.7. As K-edge EXAFS results of 0.50mM As(V) sorption references and samples

As *K*-edge EXAFS spectra of aqueous As(V) and 0.50mM As(V)/γ-Al_2O_3 sorption products in single-sorbate reaction and dual-sorbate reactions with 1mM Fe(II) addition (a) k^3-weighted χ spectra and (b) corresponding radial structure functions (RSFs). Solid and red dotted lines in panel (a) represent raw and fitted spectra, respectively. Red vertical dashed line in panel (b) indicates second-shell As-Al backscatters in the sorption samples.

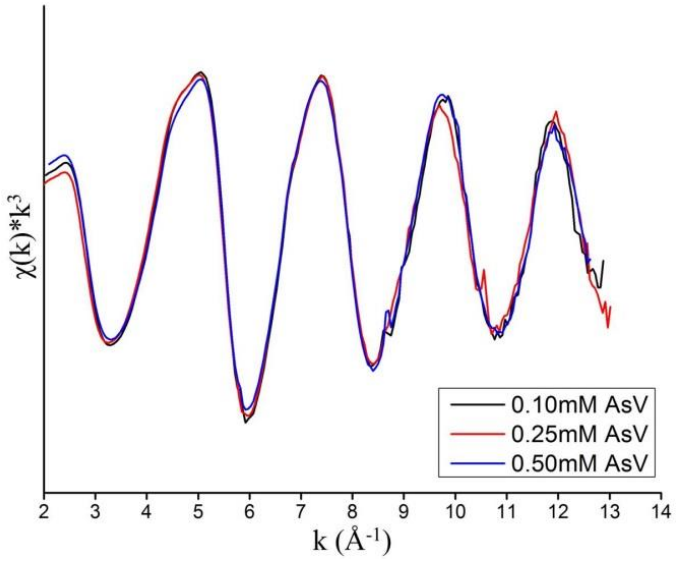

Figure A2.8. k^3-weighted χ spectra of As(V)/γ-Al_2O_3 sorption samples

Comparison of the k^3-weighted χ spectra of As(V) reacted γ-Al_2O_3 single-sorbate sorption samples with various As(V) concentration for a reaction time of 6 days.

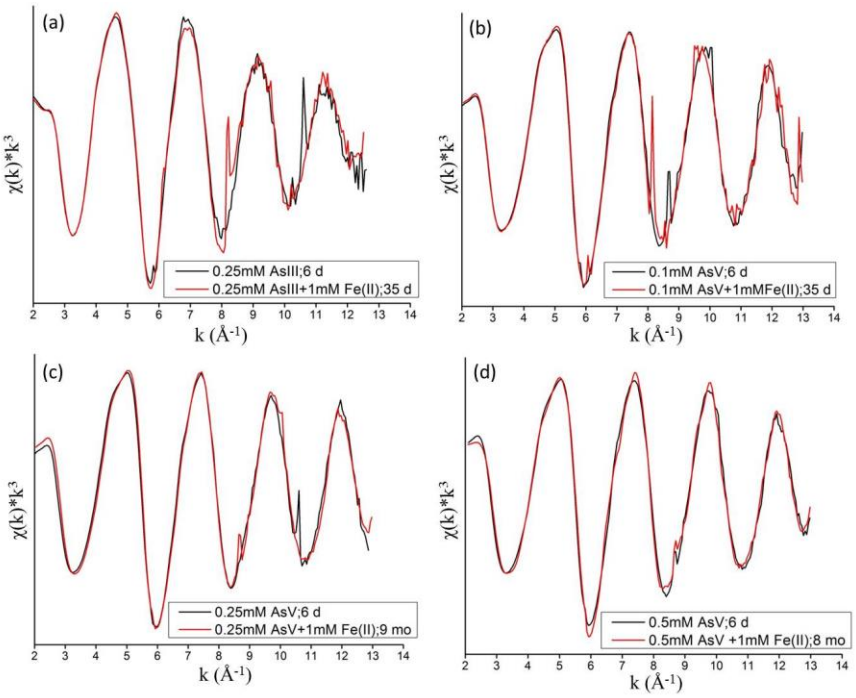

Figure A2.9. As k^3-weighted χ spectra comparison of As/γ-Al_2O_3 single-sorbate and dual-sorbate sorption samples

Comparison of the k^3-weighted As χ spectra of As reacted γ-Al_2O_3 single-sorbate and dual-sorbate sorption samples, with different As speciation and concentrations: (a) 0.25mM As(III); (b) 0.10mM As(V); (c) 0.25mM As(V); (d) 0.50mM As(V).

Appendix 3: Supporting Information for Chapter 4

A3.1 EXAFS data analyses of the sorption samples and reference compounds

EXAFS data fitting was conducted on Fourier transformed k^3 weighed χ spectra in R-space using WinXAS 3.1.[58] Theoretical backscattering paths of Fe-O, Fe-Fe, Fe-Al, Fe-Si and Fe-C were calculated using ARTEMIS[60] and Feff 7.0[59] code, based on the crystal structures of nikischerite (a Fe(II)-Al(III)-LDH, with chemical formula $NaFe^{II}_6Al_3(SO_4)_2(OH)_{18}(H_2O)_{12}$, characterized in Huminicki and Hawthorne 2003 [66]), lizardite (a 1:1 hydrous Mg silicate, characterized in Mellini and Viti 1994 [139], with a structure similar to greenalite (1:1 hydrous iron silicate)[74]) with Fe replacing Mg in octahedral positions, and siderite ($FeCO_3$, characterized in Graf 1961[148]). The amplitude reduction factor was set at 1, and a single E_0 shift value was allowed to vary during optimization. For $Fe^{2+}_{(aq)}$, Fe^{2+}-$HA_{(aq)}$, Fe^{2+}-$FA_{(aq)}$ references, only first-shell Fe-O path was used for fit due to the deficiency of second peak in the RSFs (Figure 4.2b of Chapter 4). Attempt was made to fit the spectra of Fe^{2+}-$HA_{(aq)}$, Fe^{2+}-$FA_{(aq)}$ references with additional Fe-C path, however unsuccessful. The $Fe(OH)_2$ reference was fitted with first-shell Fe-O and second-shell Fe-Fe paths, based on the structure of Fe(II)-hydroxide,[68] where central Fe(II) is surrounded with six first-shell O atoms and six second-shell Fe atoms. For the EXAFS data of Fe(II)-Al(III)-LDH phases, including nikischerite reference, all Fe(II) sorption samples on γAl_2O_3, three paths were used: first-shell Fe-O, and second-shell Fe-Fe and Fe-Al. This fitting scheme corresponds to the structure of nikischerite,[66] where Fe(II) is surrounded by six first-shell O atoms, and three Fe and three Al second-shell atoms located at the same radial distances. The radial distances (R) and Debye-Waller factors (σ^2) of second-shell Fe-Fe and Fe-Al were constrained to be the same, in order to

reduce the number of free parameters, while other factors were allowed to vary. For EXAFS data of samples containing Fe(II)-phyllosilicate (i.e., Fe(II) sorption samples on clay and references(II) listed in Table 4.1), fitting was performed using first-shell Fe-O and second-shell Fe-Fe and Fe-Si scattering paths, based on the structure of possibly formed hydrous iron silicate minnesotaite (2:1) and greenalite (1:1).[73,74] The coordination number of second-shell of Fe atoms was fixed at 6 consistent with tri-octahedral $Fe(OH)_2$ sheets, and the Debye-Waller factors (σ^2) of second-shell Fe-Fe and Fe-Si were constrained to be the same to reduce the number of free parameters.